Spring 4-13-2021

A Spectroscopic and Computational Study of Diacetyl and Water Clusters

Margaret Baldwin

A Spectroscopic and Computational Study of Diacetyl and Water Clusters

By: Margaret Baldwin

A thesis submitted to the faculty of The University of Mississippi in partial fulfillment of the requirements of the Sally McDonnell Barksdale Honors College.

Oxford, MS
April 2021

Approved by:

_____
Advisor: Dr. Nathan I. Hammer

_____
Reader: Dr. Gerald Rowland

_____
Reader: Dr. Steven Davis

ACKNOWLEDGEMENTS

There have been many people who have supported me in my time here at the University of Mississippi and in the completion of this thesis. First and foremost, I would like to thank my family and friends for encouraging me and helping me to make the most out of my four years here. I also owe an enormous amount of gratitude to the faculty in the Department of Chemistry and Biochemistry for assisting me in my undergraduate studies and research. Most notably, I would like to thank Dr. Nathan Hammer for his belief in me and the support he has offered me not only in research but throughout my studies over the past four years. I also would like to thank the members of the Hammer Lab that have guided me in my research and encouraged me to ask questions. I especially want to thank Ashley Williams, as she has been monumental in my computational chemistry education and has been a friend and mentor to me throughout my entire time here. Outside of my research group, I would like to thank Drs. Gerald and Emily Rowland. With their continual support, I have been able to flourish in my coursework and have had wonderful opportunities to teach and tutor students, a skill I believe has assisted me in this thesis and will continue to be an asset in my future profession. Finally, I would like to thank the faculty and students of the Sally McDonnell Barksdale Honors College. The funding and community they have provided me in my education at the University of Mississippi has made my experience something on which I will look back fondly. My time at this university has helped me grow, and I thank every person who has helped me to reach the point I am at today.

ABSTRACT

MARGARET BALDWIN: A Spectroscopic and Computational Study of Diacetyl and Water Clusters
(Under the direction of Dr. Nathan Hammer)

Diacetyl, otherwise known as 1,2-butadione or biacetyl, is a flavor additive used in microwave popcorn, and more importantly as of late, e-cigarettes. The compound is known to cause lung disease for those who have been exposed to a large quantity of the buttery smelling molecule. As such, the characterization of diacetyl's vibrational modes when it interacts with water are pivotal to understanding the effects it has on human lung tissue. In this research, the intermolecular interactions between water and diacetyl and the effects they have on one another's vibrational modes are explored. While some experimental data is presented, the spectra obtained are not sufficient for extensive comparison to theoretical computations. Therefore, the focus of this work is on the theoretical optimization and simulated spectra of diacetyl and water complexes ranging from 1/1 to 1/5 Diacetyl/Water ratios, with the increase in water molecules assisting in the understanding of how diacetyl behaves when it is solvated in the human body. By using the B3LYP and MP2 methods with aug-cc-pVTZ basis set and tight convergence, a total of three 1/1, ten 1/2, twelve 1/3, twenty-three 1/4, and thirty-nine 1/5 Diacetyl/Water complexes were optimized. Use of rCCSD(T) single-point energy calculations, as well as B3LYP-D3, M06-2X, M06-2X-D3, and ω-B97XD methods, the energetics of the lowest energy structures were confirmed. The simulated spectra of the lowest energy structures were investigated, and trends were gathered for the lowest energy structures from the one to five water complexes. These simulated spectra showed that the carbonyl stretching frequency of diacetyl shifted to lower energy and increased in the splitting between the symmetric and asymmetric motions as the number of water molecules increased. The stretching motions of the methyl group also increased in the range of frequencies that described their motions.

TABLE OF CONTENTS

LIST OF FIGURES

LIST OF TABLES

CHAPTER 1: INTRODUCTION

1.1 BACKGROUND OF DIACETYL

Diacetyl, otherwise known as 1,2-butanedione or biacetyl, has been studied in many contexts as a result of its biological relevance. Diacetyl appears as a yellowish liquid at room temperature. The highly symmetric four-carbon organic compound with two adjacent carbonyl groups, is of low molecular weight and is readily vaporized at temperatures typically used within microwave popcorn production, where the α-diketone creates a buttery odor and flavor for food[1,2]. The adjacent carbonyl groups are able to engage in electron sharing, making the compound particularly reactive[3].

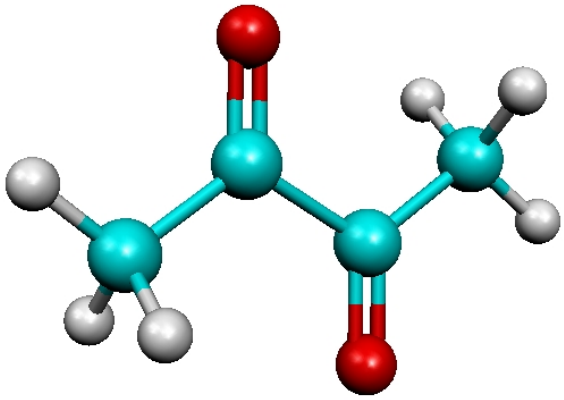

Figure 1.1: The optimized geometry of Diacetyl is shown.

Ecologically, diacetyl is an intermediate in the photolytic degradation of volatile organic compounds (VOCs) that contribute to the chemical makeup of the atmosphere[4]**.** Biomass burning can also contribute to the release of diacetyl into the atmosphere, as this process releases terpenes that can undergo ozonolysis to form glyoxal, methylglyoxal, and diacetyl[4]. Once in the atmosphere, diacetyl can easily become hydrated, and as a result the

interactions between and within clusters with water could provide further insight into the chemistry of the atmosphere[5].

More directly relevant to human health, diacetyl has been shown to form Schiff bases in vivo, and the molecule has been shown to cause protein cross-linking via Maillard reaction in vitro[6,7]. It is also a minor metabolite that arises from the metabolism of alcohol in the body and is believed to induce toxic responses like Alzheimer's disease, mutagenesis, and carcinogenesis[9,10]. Further, diacetyl was shown to be included in a class of reactive carbonyl species that are generated from oxidation of sugars, lipids, and amino acids that are known to cause cellular damage by increasing oxidative stress[3,10]. It is clear that diacetyl is involved in many physiological processes, and research of the interactions between diacetyl and water could elucidate further insight into these processes.

The study of these diacetyl/water clusters could also provide important insight for current health policy makers, specifically for the issue of e-cigarette usage. Diacetyl has been used within the food industry, and in recent years, e-cigarette juices, for creating buttery flavor. However, diacetyl is known to cause adverse health effects. Bronchiolitis obliterans, nicknamed "popcorn lung," has been shown to result from diacetyl exposure after factory workers in a microwave popcorn production facility were discovered to have an especially high incidence of the disease[11]. In a later study that exposed rats to vapors containing 203 ppm - 371 ppm of butter flavoring mixture, which included diacetyl, the rats were demonstrated to have nasal and intrapulmonary airway damage[12]. The head space above heated butter flavoring in vats within microwave production facilities have been reported to reach peak diacetyl concentrations of 1230 ppm[11,13].

Researchers have proposed that diacetyl damages epithelial tissue, alters ion transport, and creates blockage in the lungs, leading to the obstruction of small airways and epithelial necrosis that are typical symptoms of bronchiolitis obliterans[14,15]. In e-cigarettes, diacetyl has been used in fruit-, cocktail-, and candy-flavored juices[16]. A study in 2014 on middle school, high school, and college students showed that 43.8% of those surveyed were led to experiment with e-cigarettes because of these flavor options[17]. Of the 19.6% of high school students that were reported to currently use e-cigarettes in the Spring of 2020, 84.7% said they used flavored e-cigarettes[18]. The prevalence of e-cigarette use, and the role of flavors like those created with diacetyl in attracting new e-cigarette users, illustrates the importance of understanding the interactions diacetyl has with the human body. By understanding the interactions of diacetyl and water in clusters of increasing size, the effects of diacetyl as a result of e-cigarette use can be further understood.

1.2 SPECTROSCOPIC METHODS

Spectroscopy is the study of the interaction between light and matter. Different types of spectroscopy are used to understand different aspects of chemical species. Some methods are more useful for the identification or characterization of a species, such as confirming the identity of a molecule through the use of Mass Spectrometry, while others are used to gather information about the chemical properties of atoms and molecules, like the use of Infrared Spectroscopy (IR) to understand the vibrational transitions of a molecule. Nevertheless, each spectroscopic method utilizes Electromagnetic Radiation, which will be explained further in the section below.

1.2.1 ELECTROMAGNETIC RADIATION

Electromagnetic Radiation (EMR), or light, exhibits behavior that illustrates properties that are both wave-like and particle-like. This double faceted nature is commonly referred to as the wave-particle duality of light, and as a result, light can be viewed as either a wave or as a particle in a moment of time[20]. When light is addressed by its wave-like properties, it is generally described according to its wavelength[20]. The wavelength (λ) measures the distance between two crests of an oscillating wave, and the number of wavelengths that pass through a point within a given time is known as the frequency (ν). The wavelength and frequency are inversely related, and the constant of proportionality is equal to the speed of light (c) in a vacuum, 3 x 10^8 m/s:

$$c = \lambda\nu$$

The range of the possible frequencies of electromagnetic radiation are given in the electromagnetic spectrum, shown in ***Figure 1.2***.

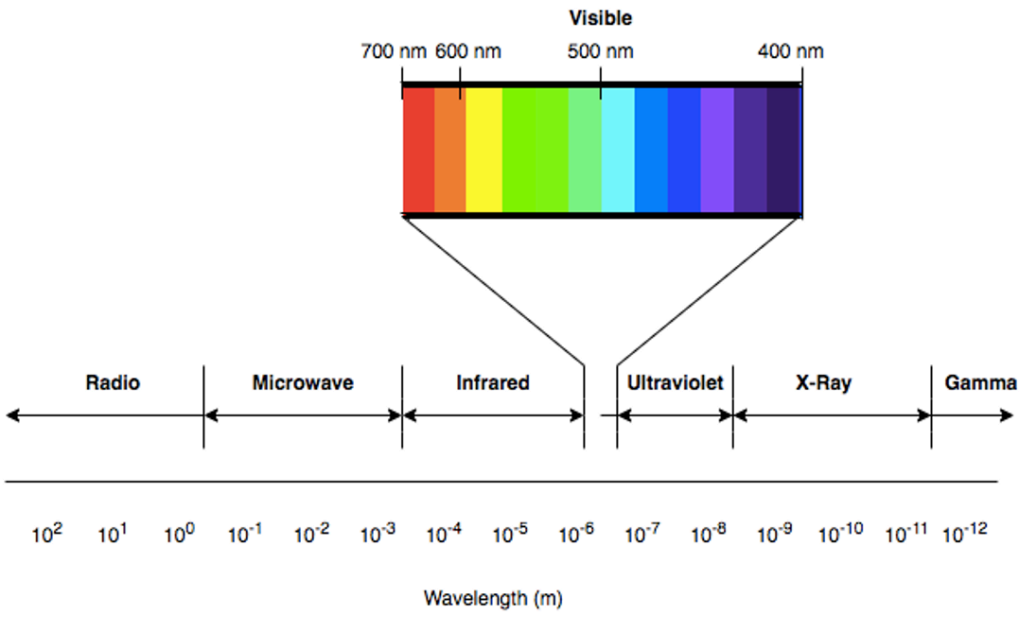

Figure 1.2: The Electromagnetic Spectrum.

The spectrum is given in order of increasing frequency, or conversely, decreasing wavelength. Radio waves have the lowest frequency and longest wavelength, and gamma rays have the highest frequency and shortest wavelength. When light is considered according to its particle-like properties, it can be seen that the frequency of EMR is directly related to its energy, and therefore, the spectrum is given in order of increasing energy as well. According to the particle perspective, light consists of photons, and each photon carries energy proportional to its frequency, as can be seen in the equation below:

$$E = h\nu$$

where E is the energy of a photon, h is Planck's constant (6.626×10^{-34} J·s), and ν is the frequency of the photon. Because both of the above equations include frequency, the following equation can be arranged:

$$E = \frac{hc}{\lambda}$$

Because the electromagnetic spectrum has varying energies, different regions can be used to elicit different information about chemical species through spectroscopy[20]. Within the field of spectroscopy, it is common for spectroscopists to present these spectral regions according to their wave numbers, which has units of inverse centimeters (cm^{-1}), rather than their wavelengths or frequencies due to historical reasons[20]. Equations showing the relationships between wavelength and wave numbers, as well as frequency and wave numbers, are given below:

$$\tilde{\nu} = 1/\lambda \qquad \nu = \tilde{\nu}c$$

Spectral regions in this work will be presented using wave numbers as is common for research presented using Raman spectroscopy.

1.2.2 TRANSITIONS

Spectroscopy utilizes Electromagnetic Radiation (EMR) to investigate an atom or molecule's different energy states[19]. Atoms and molecules have quantized energy states, and this energy must be matched by the energy of the light that interacts with the atom or molecule for a transition between the energy states to occur[20]. These transitions allow chemists to access information about bond lengths, vibrational frequencies, energy levels and much more[19].

A molecule has four types of molecular motion-- translational, vibrational, rotational, and electronic motion-- that can all engage in transitions caused by introduction of EMR to the molecule[19]. Translational motion is the lowest in energy and occurs when the molecule moves from one point in space to another[19]. Bond length and angles do not change in this type of motion. Rotational motion is higher in energy and involves an axis of rotation by which the atoms outside of the axis revolve. Rotational motion can be induced by microwave radiation, though the molecule must have a permanent dipole moment in order to absorb the energy from the microwave frequency in this way[19]. Vibrational motion, even higher in energy, involves the stretching, like a spring, and bending of chemical bonds[20]. Stretching motions can be symmetric, where the movement on both sides of the molecule are in-phase with one another, or antisymmetric, where the motion is out-of-phase[19]. Bending motions can also be in-phase and out-of-phase, causing further descriptions of bending, such as rocking, scissoring, wagging, and twisting[19, 20]. EMR from the Infrared (IR) region induces these vibrational movements, and IR and Raman Spectroscopy allow for investigations into these movements[20]. Finally, electronic motions involve the movement of electrons within the molecule, especially through the excitement to higher

energy levels. These types of motions are the highest in energy, and as such require light from the Visible and Ultra-Violet regions of the electromagnetic spectrum for these transitions to occur[20]. These transitions can be investigated using UV-Vis Spectroscopy, although transitions in the visible light region can be seen without instrumentation when chemical species undergo a color change.

1.2.3 VIBRATIONAL SPECTROSCOPY

Of the four types of motion, vibrational motion is the focus of this thesis. Vibrational motion can be described by classical and quantum mechanical models. In the classical model, two masses are connected by a coiled spring[19].The spring compresses when the two masses are pushed towards each other, and it extends when the two masses are pulled apart. The force required to change the length of the spring between the two masses is described by Hooke's Law:

$$F = -kx$$

where F is the force, k is the force constant, and x is the displacement of the spring. The negative sign in the equation illustrates that a force applied will cause a displacement in the opposite direction[19]. When a force is applied and the spacing of the masses reaches its equilibrium point, the direction of displacement changes. In other words, compression will lead to expansion and expansion will lead to compression. When no dissipative forces are present, this cycle continues, and it is described as oscillation. The potential energy of this oscillation can be described by the following equation:

$$E_{potential} = \frac{1}{2}kx^2$$

In the Harmonic Oscillator model, the spring is considered to represent the bond length between two masses, and it is described by a simple potential function, with the above equation substituting potential energy for harmonic potential, V[19].

$$V(x) = \frac{1}{2}kx^2$$

The harmonic potential represents the energy of the spring as it is infinitely compressed and infinitely expanded. This equation is represented graphically by a parabola, and at small deviations from the equilibrium bond length between two masses, where the potential energy is equal to zero, the harmonic potential is a good approximation for the potential energy of a bond, as can be seen in ***Figure 1.3***[19].

In the quantum mechanical Harmonic Oscillator model, the vibration around a bond length's equilibrium distance is described by using a set of wave functions[19]. These wave functions describe corresponding allowed vibrational energies, and they can be found by substituting for the Hamiltonian operator with the following expression:

$$\hat{\mathrm{H}} = \frac{-\hbar^2}{2\mu}\frac{d^2}{dx^2} + \frac{1}{2}kx^2$$

The energy levels derived from applying eigenfunctions to the Hamiltonian[19]. An eigenfunction of an operator, such as the Hamiltonian, is a function that returns its original value times a constant after being acted upon by an operator. As a result of this derivation, the energy levels of the harmonic oscillator model are described by the equation below and are quantized and equally spaced.

$$E_n = \left(n + \tfrac{1}{2}\right)hv_0 \quad where\ n = 0, 1, 2, \ldots, n$$

This equation suggests that the lowest energy state is not one in which the molecule is at rest, as the energy is not equal to zero. This value is known as the zero point energy[19].

Finally, the frequency of oscillation is given by the equation below, though it requires the values of both the reduced mass, μ, and the spring rigidity, k, to be known.

$$V_0 = \frac{1}{2\pi}\sqrt{\frac{k}{\mu}}$$

As stated above, the harmonic oscillator model has limits in its approximations and works best at distances close to the equilibrium bond length, as can be seen in ***Figure 1.3***. A better approximation to the vibration of molecules would be the anharmonic approximation, which is shown in red in the figure. As the distance becomes shorter than the equilibrium bond length, the potential energy rises steeply due to the repulsion between the two atoms' electron clouds. When the bond length increases, it eventually reaches an asymptote due to the electron clouds being too far apart for a chemical bond to form between the two atoms.

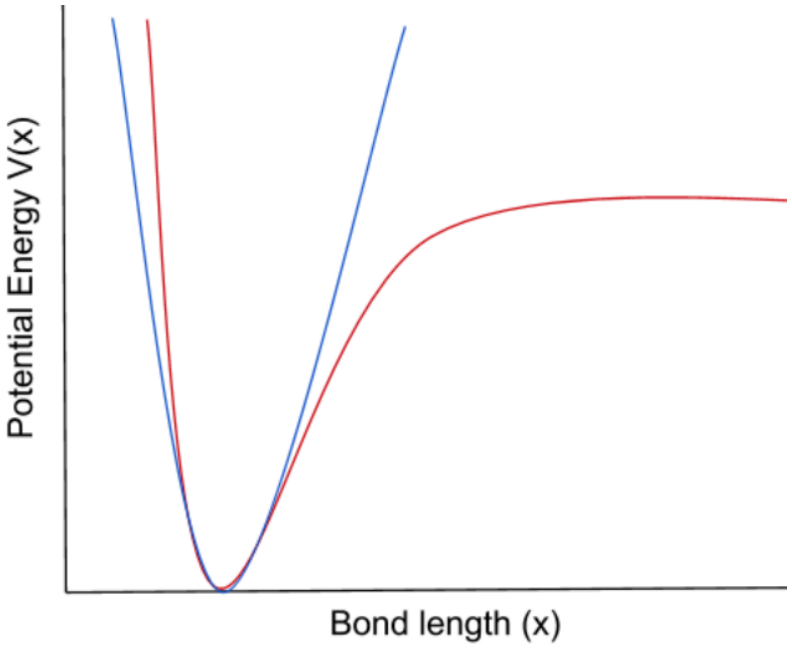

Figure 1.3: Potential energy as a function of bond length. The red curve represents an anharmonic approximation for bond length, while the blue curve represents the harmonic oscillator model.

The anharmonic approximation can account for these changes because it is described by the Morse potential, rather than the harmonic potential. Additionally, the model has its energy levels described by a more complex equation that accounts for the unequal spacing between energy levels[19]. As the energy levels increase, the spacing between them decreases[19]. This difference in spacing between the energy levels corresponds to the fact that multiple frequencies can be found experimentally. Only one frequency would be present if the harmonic model were more accurate[19].

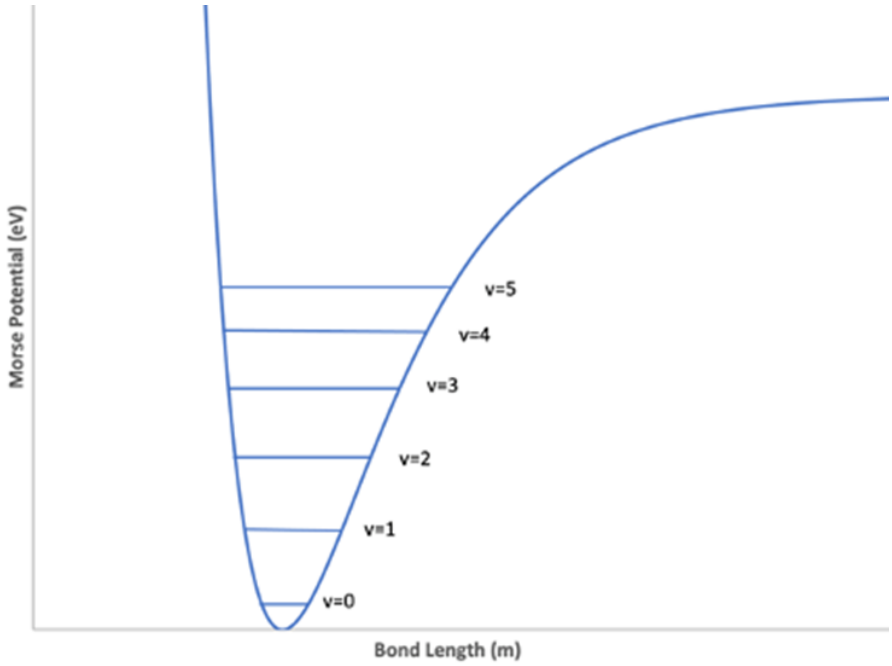

Figure 1.4: Morse Potential with energy levels shown.

1.2.4 SELECTION RULES

Selection rules govern the transitions that can occur between different energy states of a system. Each spectroscopic method has its own selection rules, and for vibrational spectroscopy, transitions that are allowed satisfy $\Delta n = \pm 1$, based on the derivation of the quantum mechanical harmonic oscillator model[19]. At room temperature, typically only the ground state has an appreciable population of electrons, so often the transition $n=0 \rightarrow n=1$

is the only one observed[19]. However, transitions can begin from an excited state, and when these occur, they are known as hotbands[19]. Finally, high sensitivity of modern instruments allows the observation of overtone transitions as well, which occur when an electron starts in the n=0 state and is promoted to an energy level higher than n=1. These are much weaker absorptions than the n=0 → n=1 transition, but they are allowed to occur because the anharmonic potential does not rigorously obey the $\Delta n = \pm 1$ rule[19].

Within the electromagnetic spectrum range that will be used in this thesis, rotational spectroscopy is also observed. The transitions in rotational IR spectroscopy are governed by $\Delta J = \pm 1$, and rotational Raman spectra obey $\Delta J = 0; \pm 2$, where J is analogous to the angular momentum quantum number, l[19]. As a result of both rotational and vibrational transitions being present in IR and Raman spectroscopy, the peaks observed can be divided into three branches: P, Q, and R. The P branch is at lower frequency and is associated with transitions of $\Delta J = -1$ for IR and $\Delta J = -2$ for Raman. The R branch occurs at higher frequency for transitions of $\Delta J = +1$ and $\Delta J = +2$ for IR and Raman, respectively. The Q branch is where $\Delta J = 0$, and it lies in-between the P and R branches[19].

1.2.5 RAMAN SPECTROSCOPY

Raman Spectroscopy has become incredibly useful for identifying organic, inorganic, and biological samples. Extremely beneficial is the fact that spectra can generally be measured for solids, liquids and gases[21]. Once rather expensive, Raman spectrometers are now able to be used in a variety of settings and applications, including as a means of gun powder residue detection with low-cost, handheld spectrometers[21]. Additionally, research-grade Raman spectrometers in the laboratory are becoming

increasingly adept at studying chemical systems, as Raman databases now have spectra for more than 15,000 compounds[21].

Raman Spectroscopy is a form of vibrational spectroscopy that is complementary to the information gained from IR spectroscopy, though the method in which this information is gathered differs[22]. Rather than directly observing the absorption of radiation, like is the case in Infrared and other forms of spectroscopy, Raman Spectroscopy observes the radiation's scattering[22].

Raman Spectroscopy originated when Sir C. V. Raman discovered the Raman Effect alongside K.S. Krishnan in 1928[23]. Using a spectroscope, or spectrometer that uses the human eye as a detector, Raman and Krishnan noticed that when filtered sunlight or a strong mercury lamp was shown on benzene, a wavelength different than that of the incident light was returned back to them[21,23]. This change in wavelength was a result of what is now known as the Raman Effect, where a photon is scattered by a molecule[19]. The never-before-seen scattered spectral profile is now known as a Raman spectrum[21]. Through further investigation that utilized excitation sources of different wavelengths, Raman found that a molecule always exhibited the same difference in frequency between the excitation light and the light given off by the molecule after scattering. Additionally, by using different molecules for his research, Raman found that this difference in frequency was unique for each molecule he investigated[21]. For his profound work in discovering this new type of light scattering, Sir C. V. Raman was awarded the Nobel Prize in Physics in 1930[21].

Raman Scattering involves the collision of a photon with the vibrational modes of a molecule, and this collision can result in an amount of energy and momentum being transferred between the molecule's vibrational energy and the colliding photon[19]. In Raman

spectroscopy, this typically involves a laser, emitting higher energy radiation than the complementary IR technique, that excites an electron to a higher electronic state[22]. This higher energy state is temporary, and it is often described as a "virtual" state. The decay from this virtual state back to the vibrational energy level is what leads to the emission of the scattered radiation[22]. There are three possible ways that this scattering transition can occur; Rayleigh, Stokes, and Anti-Stokes scattering can all occur in Raman Spectroscopy and are shown in ***Figure 1.5***.

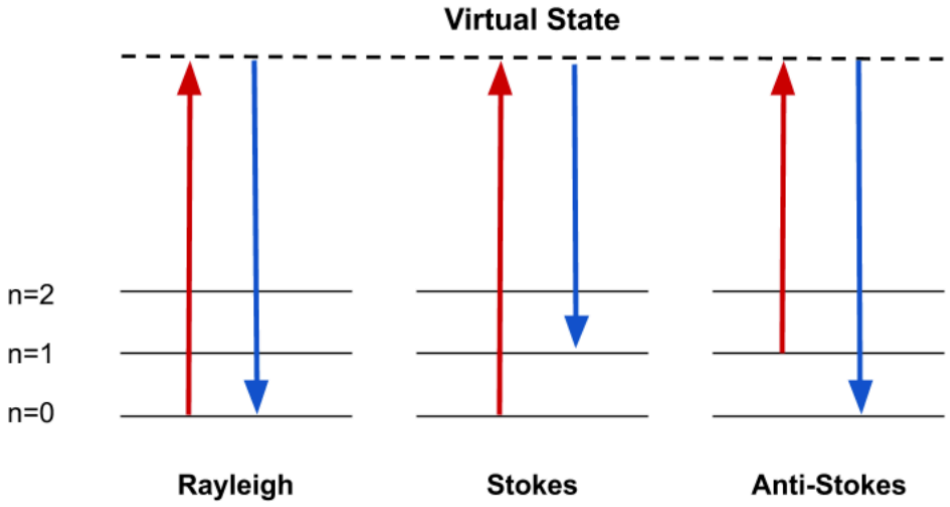

Figure 1.5: The three scattering possibilities, Rayleigh, Stokes and Anti-Stokes are shown. The red arrow indicates an electron being promoted to the virtual state, and the blue arrow indicates this electron relaxing back down to a vibrational energy state.

Rayleigh Scattering is the most common of the three. In this phenomenon, the laser light interacts with the chemical system, which is then promoted to a virtual state. The energy level of the electron when it relaxes and returns from the virtual state is equal to the initial energy level of the electron. Because the energy of excitation and relaxation are the same, the difference in frequency between the incident laser light and scattered light is zero. This is known as an elastic process[21]. The other two possibilities, Stokes and Anti-

Stokes Raman Scattering, are inelastic processes, where the energy of the scattered light is not equal to the energy of the incident laser light[21]. In Stokes scattering, the electron is initially in its ground state. It is excited to a virtual state by the laser light, and then it relaxes to an energy level that is above its initial ground state. The electron does not completely relax to the ground state because it has gained energy from the laser light[19]. In Anti-Stokes scattering, the electron is already in an excited energy level above its ground state when it is promoted by the incident light. The electron then relaxes from this virtual state all the way to its ground state, causing the sample being studied to lose energy[19]. Stokes and Anti-Stokes scattering occur at about $1/10^6$ that of Rayleigh Scattering. Of the two inelastic scattering possibilities, the Anti-Stokes scattering is much less common, as it requires a sample to already be in an excited state before interacting with laser light[19].

In order for a molecule to undergo this Raman scattering, or in other words, be Raman active, it must be able to have a change in polarizability[22]. The polarizability of a molecule, denoted by α, dictates the difficulty of changing or distorting the electron cloud by applying an external electric field[21]. In general, larger molecules and molecules with a greater number of electrons have a greater polarizability. This asymmetric change in polarizability is the primary selection rule for Raman transitions. Additionally, the frequency of the laser's light should not be the same as the transition being studied. For this reason, EMR sources in the visible range are typically used[19]. The benefit of the visible range being used is that interferences that typically reside in the infrared region can be eliminated[19].

Raman Spectrometry utilizes a Raman spectrometer, which is made up of the fundamental components of a radiant source, typically a laser, a wavelength discriminator,

filters, and a detector, all of which are described with the block diagram given in ***Figure 1.6***.

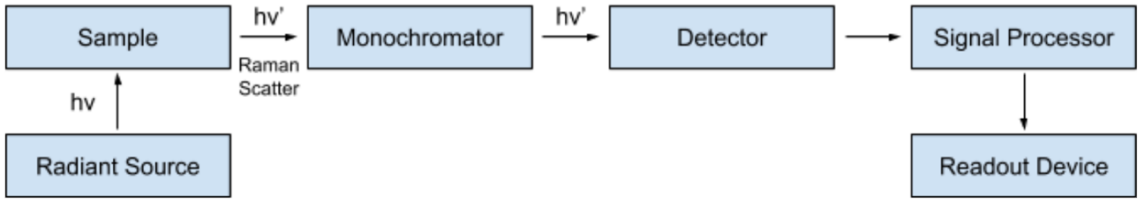

Figure 1.6: A block diagram of a typical Raman Spectrometer is shown.

The radiant source is typically a laser because it is monochromatic, meaning only one wavelength of light is emitted, and because it has a high intensity, which is needed for the relatively weak Raman scattering to be generated[21]. This laser is pointed through filters and onto a lens to focus the light onto the sample, and the Raman, or scattered light will return back through this lens[21]. The Rayleigh scattered light is reduced as the Raman light passes through mirrors and filters to the detector[21]. The detector then processes the signals and develops a spectrum.

A Raman spectrum shows the intensity of scattered light on the y-axis versus its Raman Shift on the x-axis. The intensity has an arbitrary value and does not have any units. These values are typically normalized, so that the intensity of transitions can be relatively compared to other transitions for the system. The intensity is also notable for illustrating that Rayleigh Scattering has a much greater intensity than Stokes scattering, which is greater than Anti-Stokes. IR intensities are generally greater than those in a Raman spectrum[21]. The Raman Shift is measured in wave numbers and is equal to the difference between the frequency of the incident and scattered radiation, as is described for the Stokes and Anti-Stokes Raman Scattering above[21]. Raman spectra are typically recorded from 10

to 4000 cm^{-1}, though the laser line and lack of organic molecules' vibrational modes often disregards the region from 10 to 400 wave numbers[24].

1.3 THEORETICAL CHEMISTRY

Computer models for quantum chemical analysis have been in use for decades. With advances in computer hardware and theoretical models, these calculations are increasingly accurate and efficient. As a result, computational methods are able to obtain sufficiently reliable results in the absence of experimental procedures[25]. Chemists are able to investigate the properties of molecules that are difficult to examine experimentally and even study molecules not yet known to exist. Consequently, the field of theoretical chemistry is vast, and with the readily available software packages being present in many laboratories already, chemists are unlocking the structure and behavior of an unimaginable number of systems.

1.3.1 POTENTIAL ENERGY SURFACES

Potential energy surfaces, or reaction coordinate diagrams, are studied throughout one's education in chemistry. One of the most recognizable, and earliest to be used, is the depiction of a chemical reaction progressing from reactants to products with the energy of each reaction coordinate being shown. An example of this diagram is shown below in ***Figure 1.7***.

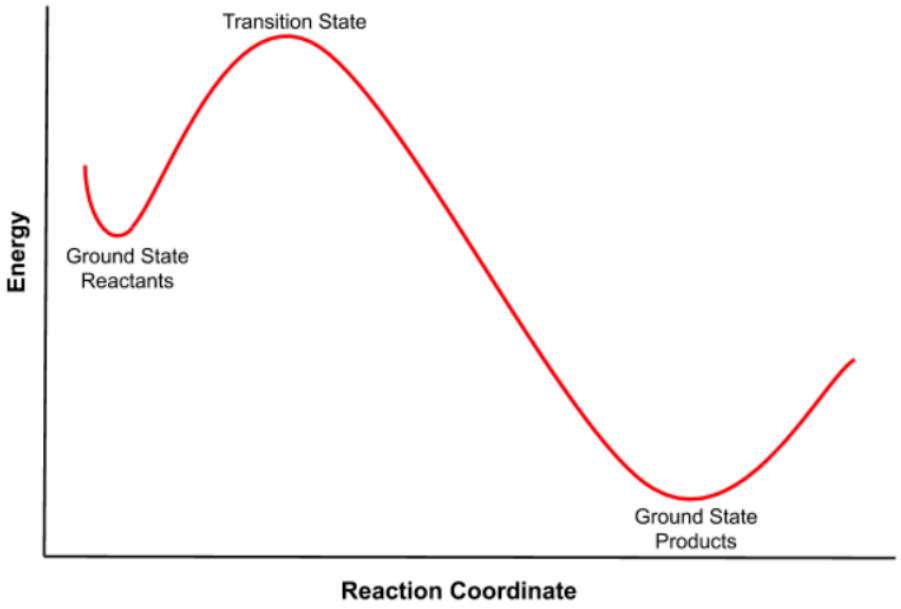

Figure 1.7: Potential energy surface of a chemical reaction

As depicted in the labels of ***Figure 1.7***, the energy minima indicate the equilibrium structures of the reactants and the products, and the location of the energy maximum defines the transition state. These three points, reactant, product, and transition state, are all stationary points, meaning both the equilibrium and transition states can be determined from calculations by searching for an energy minimum and an energy maximum, respectively[19].

Quantum chemistry software has been developed in order for the Schrödinger Equation to be solved at these points. These theoretical methods require approximations to be made, however. The severity of these approximations determines the accuracy of the results obtained, how widely applicable the model is to chemical systems, and the cost, or computational time, required to complete a calculation. If the approximation is less accurate, the method can be widely applied and is less expensive. For this reason, methods

are chosen based on the balance between the accuracy of the method and the cost of running the calculations[19].

1.3.2 THE SCHRODINGER EQUATION

In 1926, Erwin Schrödinger published a paper including a differential equation that showed how a quantum system evolved over time and explained the wave properties of electrons in atoms[26,27]**.** This Schrödinger equation describes the wave properties of an electron in terms of its position, mass, total energy, and potential energy. The equation is based on the electron's wave function, which describes the electron wave in space, or the atomic orbital in which the electron resides[22]. The simplest notation of the Schrödinger Equation is included below:

$$\widehat{H}\psi = E\psi$$

In this equation, H represents the Hamiltonian operator, E is the energy of the electron and ψ is the wave function of the electron[19]. The Hamiltonian operator, often referred to as just the Hamiltonian, includes the total kinetic energy and potential energy of the electron's system. The wave function is unique to the given electron in a particular orbital[22].

The Schrödinger Equation, however, can only be solved analytically for systems that contain one electron. Multi-electron systems, like those presented in this thesis, must therefore calculate approximate values for the wave-functions and observables[19]. These approximations are determined by the method and basis set used.

1.3.3 THE HARTREE-FOCK METHOD

Because the Schrödinger Equation only provides an analytical solution for the one-electron case, in order to produce a practical quantum mechanical theory, three approximations to Schrödinger Equation must be made to solve multi-electron systems. The first approximation is known as the Born-Oppenheimer approximation. This estimation assumes that nuclei are stationary from the perspective of the electron, due to the nuclei moving excessively slower than the electrons that orbit them[19]. As a result, the nuclear kinetic energy is equal to zero and the nuclear-nuclear Coulombic energy term is equal to a constant. Therefore, the position of the nuclei, but not the velocities, affect the electronic wave function[19]. The resulting equation is known as the Electronic Schrödinger Equation and is written:

$$\widehat{H}^{el}\psi^{el} = E^{el}\psi^{el}$$

This approximation, however, is not enough for the general case (many-electron systems) to be solvable. The second approximation that must be made is the Hartree-Fock approximation. The wave function is assumed to be an antisymmetrized product of one-electron wave functions called spin orbitals[28]. In other words, the electrons move independently of one another. Each electron is still affected by a mean field of the other electrons within the system[19]. To demonstrate antisymmetric nature of the wave function upon the interchange of electron coordinates, the wave function is written as a Slater determinant of the form:

$$\psi = \frac{1}{\sqrt{n!}}\begin{vmatrix} \chi_1(1) & \chi_2(1) \dots & \chi_n(1) \\ \chi_1(2) & \chi_2(2) \dots & \chi_n(2) \\ \dots & \dots & \dots \\ \chi_1(n) & \chi_2(n) \dots & \chi_n(n) \end{vmatrix}$$

Where Ψ is the wave function, n is the number of electrons, and χ is the spin orbital. The different rows in the determinant represent individual electrons, so the interchange of two electrons' coordinates will result in an interchange of two rows within the determinant. This procedure is equivalent to multiplying the determinant by -1, confirming the antisymmetric nature of exchanging two electrons' positions[19]. In addition to illustrating the antisymmetry of the wave function, the use of the determinant illustrates that electrons are paired. No two rows are the same within the Slater determinant, which would not be the case if there were a third electron in the orbital. Therefore, as a result of the Hartree-Fock approximation, it is understood that at most two electrons reside in an orbital, which is further illustrated by the fact that only two spin functions exist, α and β, within a spin orbital[19]. These two functions allow for the electrons in the same orbital to have magnetic spins that are opposite in direction, satisfying the Pauli Exclusion principle that no two electrons can have the same set of quantum numbers[22].

The Hartree-Fock equations, a set of differential equations that involve each individual electron environment, arise out of the stipulations that result from the Hartree-Fock approximation. These equations are capable of being solved numerically, though with difficulty, and the generation of the lowest energy set of molecular orbitals by these equations is known as the self-consistent-field (SCF) procedure[19]. A third approximation is used to transform these equations into a set of algebraic equations in order to decrease the difficulty of solving the Schrödinger equation. The Linear Combination of Atomic Orbitals (LCAO) approximation makes the assumption that one-electron wave functions for the hydrogen atom will closely resemble the one-electron solutions for the many-electron molecule being investigated[19]. This process results in the wave function of the

molecular orbitals, Ψ_i, being expressed as a summation of a basis set of atomic orbitals, or basis functions, ϕ:

$$\psi_i = \sum_{\mu}^{basis\ functions} c_{\mu i}\, \phi_\mu$$

Despite the advantage of having a numeric estimate to the Schrödinger equation for many-electron systems, the Hartree-Fock Method contains limitations to its accuracy. The total energies calculated using finite basis sets are too positive[19]. Because the group of electrons are considered as a rigid cloud that influences the individual electrons, there is not as much opportunity for electrons to correlate, or adjust, their motion for the motion of the other electrons. As a result, there is a greater extent of electrons getting in the way of one another than would be the case if the electrons' instantaneous interactions were not replaced by a "mean field" of influence[19]. This increased interaction between electrons causes the predicted electron repulsion energy to be too large, and therefore causes the predicted total energy to be too large as well[19]. This difference between the energy presented by the limited Hartree-Fock Method and the exact Schrödinger energy is known as the correlation energy[19]. Additionally, systematic error is present within the Hartree-Fock Method that results in equilibrium bond distances being shorter than experimental lengths and calculated vibrational frequencies being larger than the experimental frequencies[19].

1.3.4 DENSITY FUNCTIONAL THEORY

Because of the limitations in the Hartree-Fock model, various other methods have been developed to improve its accuracy, though these adjustments can bring rise to greater

computational costs. One of these approaches to advancing the accuracy of the Hartree-Fock Model is through the use of Density Functional Theory (DFT). DFT has been used extensively in physical, quantum, and computational chemistry[27]. This approach to improving the Hartree-Fock model is based on an electron gas of uniform density, the idealized many-electron problem, having an available, exact solution to the Schrödinger equation[19]. DFT utilizes functionals, which take a function as an input and output a number, or in other words, are functions of functions[27]. In 1964, Pierre Hohenberg and Walter Kohn showed that the total electronic energy and other observable properties are a functional of the electron density, n(r)[29]. This functional could be expressed as the Kohn-Sham equation[19]:

$$E^{DFT} = E_T + E_V + E_J + E_{XC}$$

Which adapted the analogous Hartree-Fock partition function of the total electronic energy of an atom, molecule, or ion:

$$E^{HF} = E_T + E_V + E_J + E_K$$

In this equation, E_T is the total kinetic energy of the electrons, E_V is the electron-nuclear potential energy, E_J is the Coulombic energy of the electrons, and E_K is the exchange energy of the electrons[19]. In the DFT partition function, the Hartree-Fock exchange energy is substituted for the E_{XC} term, which is the exchange/correlation energy[19]. This one determinant describes the electron density, and as a result, it is key to the success or failure of DFT[30]. The exchange energy results from the Pauli exclusion principle, as no two electrons occupy the same space, but exchanging of their positions allows for added stability[30]. The correlation energy accounts for the remaining many-body effects of the electrons[30]. Essentially, these exchange and correlation contributions are incorporated as

external data, generated by a self-consistent-field (SCF) formalism, for solving the Schrödinger equation. Because these exchange and correlation terms are derived from idealized problems, though, density functional models, unlike the Møller-Plesset models discussed later, are not limited to an exact solution of the Schrödinger equation[19].

Overall, DFT is greatly successful in part because simple approximations, like those made for the exchange-correlation terms, perform remarkably well for many systems, especially for structure prediction[30]. These approximations allow for inexpensive computational costs with more reliable results than Hartree-Fock Method and its descendants. However, DFT has the fault of being neither size consistent nor variational, so there is no way to systematically improve the functional to achieve an arbitrary level of accuracy[19]. Additionally, DFT has challenges describing van der Waals interactions, which proves an especially difficult problem as DFT methods are applied to areas of biological importance, where many noncovalent interactions occur simultaneously[30,31].

1.3.5 METHODS AND BASIS SETS:

As described earlier, the methods and basis sets that are chosen in computational chemistry must weigh the cost of running calculations with the accuracy that they return. Because the Mississippi Center for Supercomputing Research (MCSR) is made available to students at the University of Mississippi, calculations that would otherwise be much too expensive to consider running on typical lab computers were able to be used.

Varying computational methods were utilized to elicit optimized structures of the diacetyl/water clusters and generate theoretical Raman spectra, with the goal of comparing and understanding experimental results with theory. Initial calculations utilized the most methods, as each method was evaluated in its effectiveness in finding and optimizing

lowest energy structures before moving onto calculations with more computationally demanding cluster optimizations. The six methods chosen to optimize and investigate the 1/1 diacetyl/water complexes were: B3LYP, B3LYP-D3, M06-2X, M06-2X-D3, MP2, and ω-B97XD. Additionally, single-point energy calculations were run on B3LYP and MP2 optimizations using the restricted CCSD(T) method. Each method was run with the aug-cc-pVTZ basis set and tight convergence criteria. These methods and basis set will be described below.

B3LYP and B3LYP-D3

The B3LYP method, which stands for Becke, 3-parameter, Lee-Yang-Parr, was originally developed to study vibrational absorption and circular dichroism[32]. This method is a hybrid functional, as it combines exact energy exchanges from the Hartree-Fock method with the exchange-correlation energy of DFT[19]. B3LYP is one of the most popular methods used, though it has been shown to be inadequate in dealing with dispersion-dominated non-covalent interactions[33]. While this note seems counterintuitive to its use in optimizing and predicting spectra for clusters like those presented in this work, it has been shown to have good agreement with experimental Raman spectra[34]. The correction factor for B3LYP generated spectra using aug-cc-pVTZ basis set in comparison to experimental vibrational spectra is 0.968[35].

B3LYP-D3 utilizes the same hybrid functional, though it also includes a non-local dispersion correction that helps to account for typically poorly-described van der Waals forces[36]. The DFT-D3 method was chosen to make this correction, as it has been shown to perform better with Becke-type exchange[37].

M06-2X and M06-2X-D3

The M06-2X functional, which is of the Minnesota '06 suite of functionals, is a parameterized version of DFT like B3LYP. This functional was developed with the goal of providing better results for weakly correlated systems, and it utilizes databases of barrier heights, noncovalent interactions, and more to accomplish this task[38,39]. It is for this reason that this method was chosen out of the Minnesota functionals, as M06-2X has a better performance than its counterparts M06 and M06-L when dealing with main-group chemistry and noncovalent interactions[39]. Like with B3LYP, the addition of the DFT-D3 method to the M06-2X method accounts for additional dispersion corrections. The correction factor for M06-2X generated spectra is 0.956[35].

MP2:

The Hartree-Fock wave function and ground state energy are approximate solutions to the Schrödinger equation, as stated earlier in reference to the many-electron systems. However, these values can be used to determine the exact Hamiltonian[19]. Møller-Plesset Models utilize the assumption that the Hartree-Fock wave function and energy are very similar to the exact wave function and ground-state energy[19]. This assumption allows for an estimation of the correlation energy of molecules. The single-reference second-order Møller-Plesset perturbation theory (MP2) is among the most widely used correlated wave function methods in electronic structure theory[40]. The MP2 Model is size consistent, meaning the calculated energy increases proportionally to the molecular size, and not variational, which is less important, but means the model does not produce an energy value that represents a bound to the exact energy. The model produces unique results and is well

defined, but because of the lack of variational quality, the calculated energy may be lower than the exact value[19].

The MP2 model is used in this research because it provides very accurate electronic energies for small molecules when large basis sets are used[27]. Diacetyl and water clusters are relatively small molecules, amounting to 25 total atoms in a 1/5 Diacetyl/Water cluster, and the basis set aug-cc-pVTZ is extensive. Larger molecules are too computationally expensive for this method to prove useful[27]. The scaling factor for the MP2 method and the aug-cc-pVTZ basis set is 0.953[35].

ω-B97XD

The *ω*-B97XD functional is based in a Becke functional, B97, which is a DFT method. In addition, this functional contains a parameter that controls the partitioning of the interelectronic distance, *ω*, a parameter corresponding to an adjustable fraction of short-range exact exchange, X, and a dispersion correction, D[41, 42]. This dispersion correction makes *ω*-B97XD the superior choice to *ω*-B97X when dealing with systems where non-covalent interactions are expected to be significant[42]. The correction factor for *ω*-B97XD generated spectra using aug-cc-pVTZ basis set in comparison to experimental vibrational spectra is 0.957[35].

rCCSD(T) single point energy

CCSD(T), coupled-cluster with single and double perturbative triple excitation, is considered the gold standard method amongst computational chemists, as it provides an accuracy comparable to experiment within chemical accuracy[45,46]. The coupled cluster (CC) method attempts to introduce interactions among electrons within clusters and the coupling among these clusters of electrons into calculations of the wave function[47]. The

partially spin-restricted rCCSD(T) puts restrictions on the amplitudes of the wave function, allowing for shorter computational time. In this work, the rCCSD(T) method was used to determine energies of structures, meaning it did not optimize the structures listed, but rather used the output geometries of other methods to determine the energy of that structure.

aug-cc-pVTZ

Correlation consistent basis sets are widely used for both ab initio and DFT calculations and are especially useful for calculating properties such as atomization energies and geometries of molecules[43]. They are designed using ab initio methods and are based in the systematic accounting of correlation energy[43]. This correlation consistent (cc) basis set has been augmented (aug) with an extra diffuse function in each orbital angular momentum. This augmentation is helpful for the description of intermolecular interactions. It should be noted that when using molpro calculations, such as for the single-point rCCSD(T) energy calculations, this basis set is denoted as avtz. Finally, this is a triple-zeta basis set, meaning it is more accurate and computationally expensive than aug-cc-pVDZ, like is used in the work presented by Dargent, et. al[5].

CHAPTER 2: EXPERIMENTAL STUDY OF DIACETYL/WATER COMPLEXES

2.1 LIQUID-PHASE RAMAN SPECTRA

Liquid diacetyl is yellow in color and emits its notorious buttery smell in its vapor. Work done by Profeta, et. al determined the IR active vibrational modes of diacetyl in its solid, liquid, and gas states[48]. The work also presented the Raman vibrational modes of liquid and gas states[48]. In this study, the Raman active modes of liquid- and gas-phase diacetyl will be confirmed and compared to theoretical findings. The first experimental findings involved the second harmonic (532 nm) output from a YAG:Nd laser and 1800-g/cm^{-1} grating was used to gather a Raman spectrum of liquid diacetyl. The resulting experimental data from the Raman spectrometer is shown in the figure below.

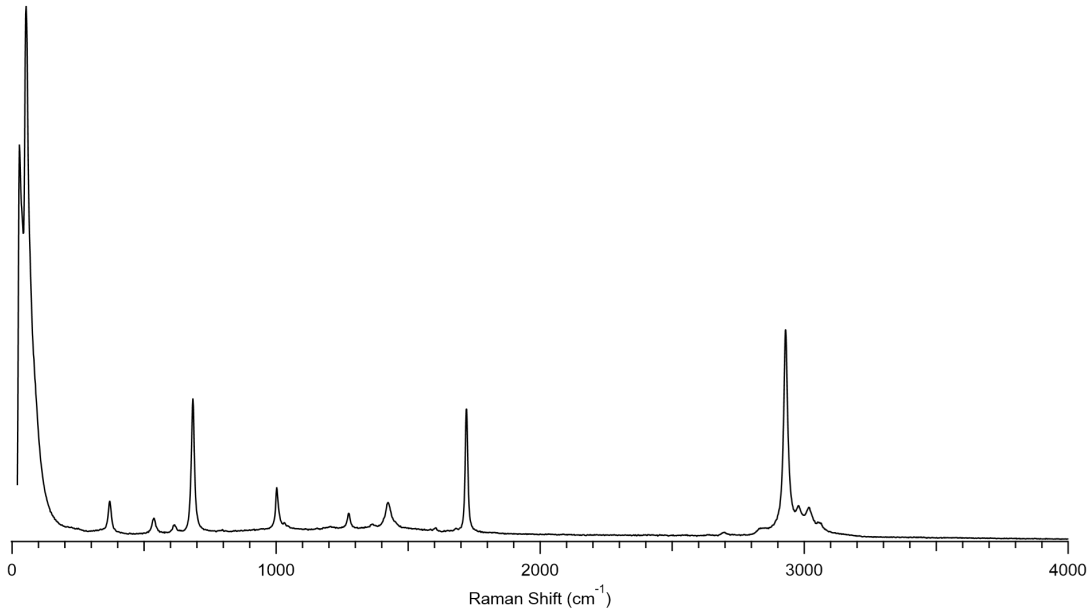

Figure 2.1: The experimental Raman spectrum of liquid diacetyl is shown.

In the spectrum presented above, the peak with the maximum intensity, present at 53.24 cm^{-1}, is a result of the laser line, and it does not represent the vibrational motion of the system being studied. Peaks outside of the diagnostic range correspond to vibrational modes that are not the focus of this work, so they are not included in the discussion of experimental or vibrational spectra in this study. Within the diagnostic range of the spectrum of liquid diacetyl, carbonyl stretching occurs at 1721.33 cm^{-1}. This agrees with the finding of Profeta, et. al that this vibrational mode occurs at 1720 cm^{-1}. The C-H stretching modes are present at 2929.83 cm^{-1}, and the C-H scissoring modes occur at 2978.03 cm^{-1}. A final C-H stretching motion can be seen in the final peak that appears at 3018.18 cm^{-1}.

While the liquid diacetyl data is informative for the work presented in this thesis, greater interest is expressed in the interactions of diacetyl and water molecules in their gaseous form. The gas phase is more representative of the interest in the role of diacetyl in the atmosphere and e-cigarettes. As such, Raman spectra of diacetyl and diacetyl/water mixtures was obtained using Gas-Phase Raman techniques that are explained below.

2.2 GAS-PHASE RAMAN SPECTRA

Initial attempts at gathering a Raman spectrum of the headspace of diacetyl had very poor resolution. The spectrum that was gathered was centered around the intense peak of the carbonyl stretching mode that is known to occur around 1720 cm^{-1}. The second harmonic (532 nm) output from a YAG:Nd laser and 1800-g/cm^{-1} grating were used to gather this spectrum. From a quick pass over the range 1400 cm^{-1} to 2000 cm^{-1}, only the

peak corresponding to the carbonyl stretching mode could be identified. The figure below shows this result.

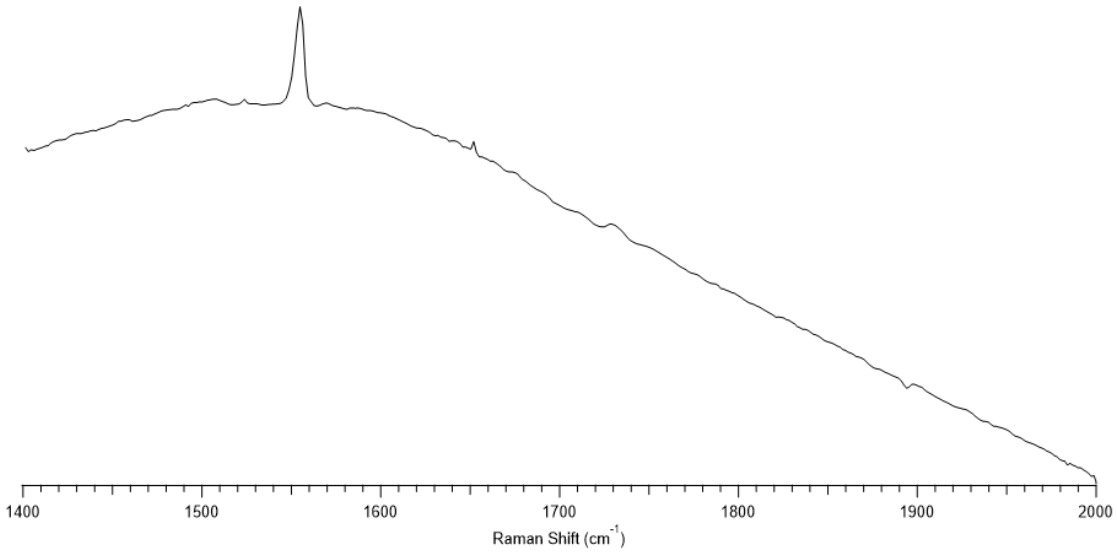

Figure 2.2: The experimental headspace Raman spectrum of diacetyl is shown for the range 1400 cm^{-1} – 2000 cm^{-1}.

When this spectrum is compared to sharpness and resolution of the liquid diacetyl experimental spectrum shown in ***Figure 2.1***, it is evident that the headspace technique used was not sufficient for investigating the Raman active vibrational modes of diacetyl.

Moving forwards, a vacuum cell constructed by Ashley Williams within the Hammer Group could be used. This cell allows for the gathering of experimental spectra of diacetyl and diacetyl/water mixtures in the gas-phase. The apparatus allows for direct attachment to the microscope of the Raman Spectrometer, and therefore simple data collection. With more time dedicated to this research, this experimental data would be very useful for qualifying the theoretical calculations that had to be the focus of this work with the inability to collect quality gas-phase data.

CHAPTER 3: THEORETICAL STUDY OF DIACETYL/WATER COMPLEXES

3.1 OPTIMIZATION OF DIACETYL

An initial structure of diacetyl was built using the *GaussView 6* program. This input geometry was then optimized using B3LYP and M06-2X methods with the aug-cc-pVTZ basis set. This optimization was completed by first starting at less computationally expensive basis sets, such as 6-31G, and moving up with more expansive basis sets, such as 6-311+G(*d, p*), 6-311++G(*2df, 2pd*), and aug-cc-pVDZ. As the calculations moved up these basis sets, the checkpoint files were copied over to new folders, so that the more expansive basis set would begin with the optimization that the lower level of theory had just completed. This process has been reciprocated for optimizations of the water clusters that follow, and each optimization has ended with the basis set of aug-cc-pVTZ and a tight convergence. Both the B3LYP and M06-2X methods converged to the structure shown below.

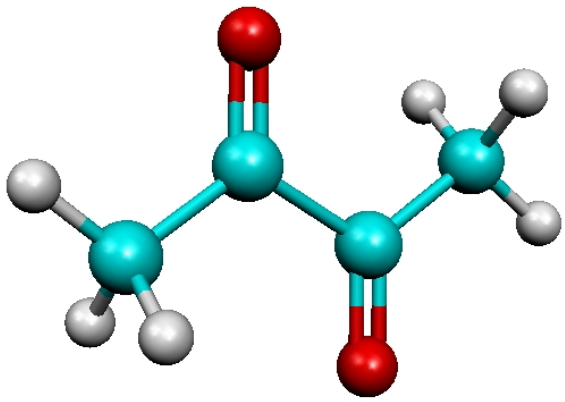

Figure 3.1: The B3LYP optimized geometry of Diacetyl is shown.

The cartesian coordinates from the output geometry that was obtained with the B3LYP method were used to do an additional optimization using the MP2 method. This optimization allowed for theoretical spectra to be obtained for both the B3LYP and MP2 methods, which is useful to compare the DFT method with the ab initio method. Frequency calculations were conducted using *Gaussian 09* Software for the already optimized diacetyl structures. These output files were then generated into Raman spectra using a LabView program constructed within the Hammer Group. The two spectra generated using the MP2 and B3LYP optimized geometries are compared to the experimental spectrum obtained of liquid diacetyl in ***Figure 3.2*** below.

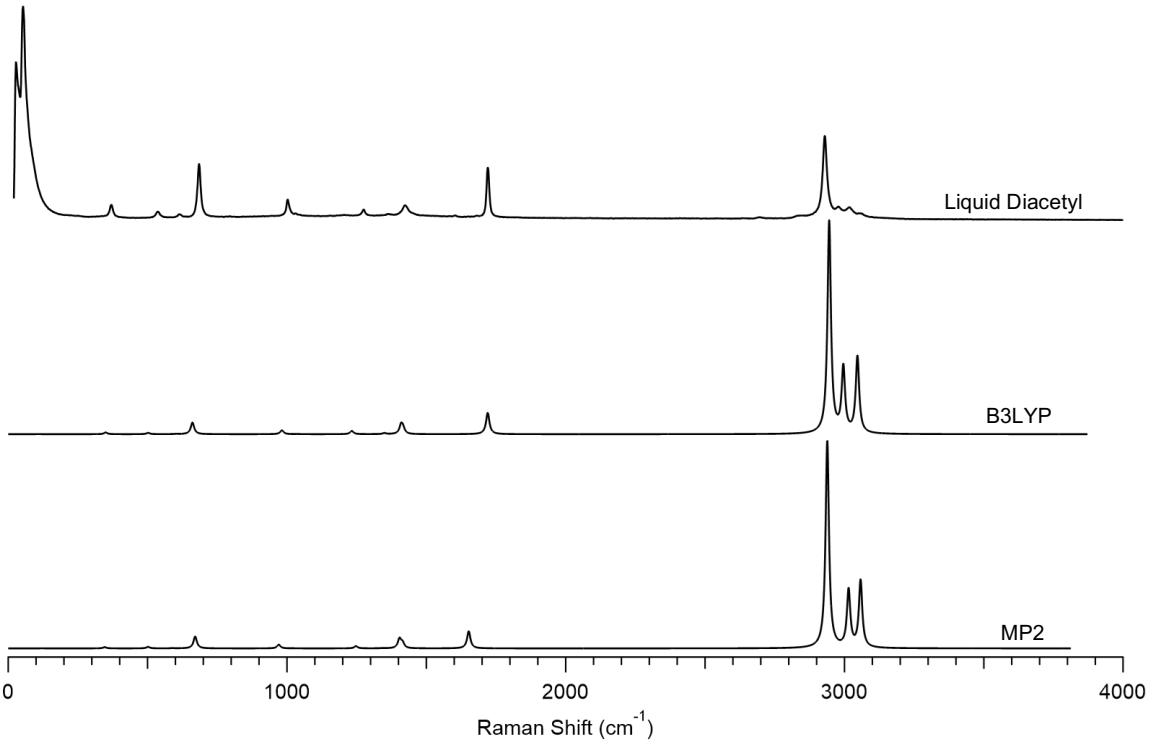

Figure 3.2: The experimental Raman spectrum (top) of liquid diacetyl is compared to the simulated spectra provided by the B3LYP (middle) and MP2 (bottom) methods.

Ignoring the laser line of the experimental spectrum, the most intense vibrational peaks are present at around 1720 cm^{-1} and 3000 cm^{-1}. The effect made by the increasing number of water molecules in the diacetyl clusters on these peaks will be the focus of the

spectroscopic study in this thesis. Additionally, when water molecules are present, it is expected that peaks at higher energy will appear as a result of the vibrational motions of the water molecule, allowing for investigation of the effect diacetyl has on the water molecules that interact with it.

The theoretical Raman active vibrational modes involving the carbonyl groups and methyl groups of the diacetyl molecule were determined by using *GaussView 6* software to open the output files of frequency calculations. This software enabled the Raman active modes to be animated in order to determine the type of motion that the molecule has and the frequency at which it occurs. The theoretical and experimental frequencies of these vibrational modes are compared in the table below. Only the vibrational modes in the diagnostic region are considered, as these frequencies will shift more as a result of the interactions with water than the frequencies that correspond with the low-energy internal motion of the diacetyl molecule. The descriptions of the vibrational modes included were designated as in work done by Durig, et. al[49].

Vibrational Assignment	Vibrational Mode Description	Experimental Freq. (cm^{-1})	B3LYP Freq.(cm^{-1})	MP2 Freq. (cm^{-1})
ν_{23}	Symmetric C=O stretch	1721.33	1720.22	1652.11
ν_{25}	Symmetric C-H Stretch	2929.83	2945.21	2938.31
ν_{26}	Symmetric C-H Stretch	2929.83	2945.25	------
ν_{27}	Antisymmetric C-H Stretch	2978.03	2995.69	3014.87
ν_{28}	Antisymmetric C-H Stretch	2978.03	2995.95	------
ν_{29}	Antisymmetric C-H Stretch	3018.18	3046.57	3057.79
ν_{30}	Antisymmetric C-H Stretch	3018.18	3047.20	------

Table 3.1: The vibrational modes of diacetyl as determined by experimental data and the MP2 and B3LYP theoretical models are given.

Of the two theories used in the calculations, it appears that the B3LYP method is a significantly better predictor of the carbonyl stretching frequency than the MP2 method. The B3LYP method differs from experimental results by 1.11 cm^{-1}, whereas the MP2

prediction is 69.22 cm^{-1} lower in energy than the experimental carbonyl stretching frequency. Additionally, the B3LYP method predicts the antisymmetric C-H stretching motions to be closer to the experimental frequencies than the MP2 method does. Therefore, although the MP2 method is considered to be the better computational method, the B3LYP method appears to be a better model for predicting the experimental Raman spectrum of diacetyl. Because of the differing strengths in computational and experimental agreement, the MP2 and B3LYP methods will be used to describe the optimized geometries and frequencies of water clusters throughout this thesis.

3.2 1/1 DIACETYL/WATER COMPLEXES

Starting structures for the 1/1 Diacetyl/Water clusters were constructed by placing a water molecule in locations that allowed for possible hydrogen bonding and electrostatic interactions with the already optimized structure of diacetyl, shown in ***Figure 3.1***. A total of eleven input geometries were constructed according to this method of "chemical intuition" by using *GaussView 6* software. These input geometries were then optimized using B3LYP and M06-2X methods, finishing with the aug-cc-pVTZ basis set at tight convergence, just as the diacetyl molecule alone was optimized. Three unique structures resulted from this optimization, and the cartesian coordinates from the three output geometries were then used as inputs for the optimization of the structures with B3LYP-D3, M06-2X-D3, MP2, and ω-B97XD methods. The three unique geometries of the 1/1 Diacetyl/Water clusters are presented in ***Figure 3.3***.

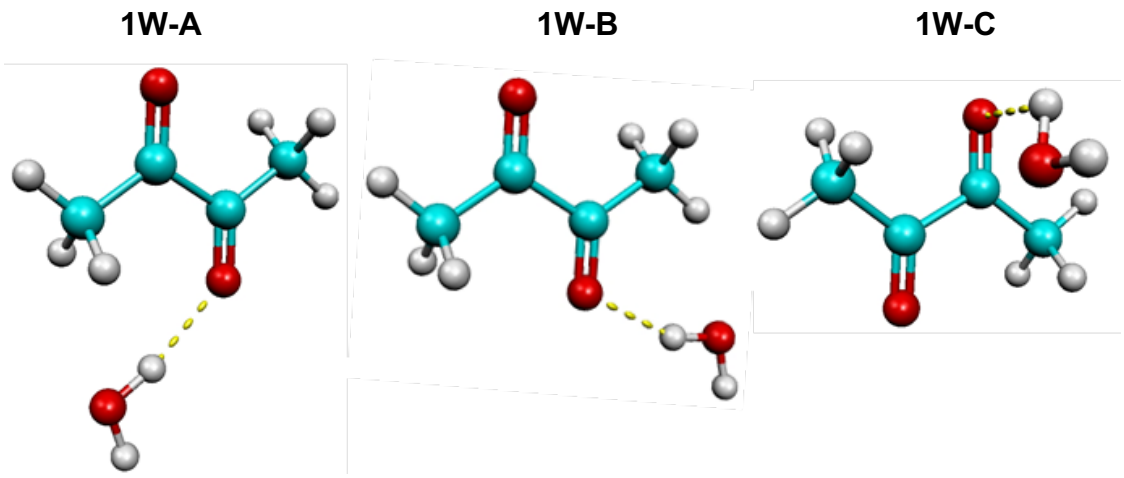

Figure 3.3: Lowest energy structures for 1/1 Diacetyl/Water clusters are shown in order of increasing relative energy. Images were constructed from MP2 output geometries.

Structure 1W-A involves the water molecule hydrogen bonding to the oxygen of a carbonyl group and engaging in electrostatic interactions with two of the three hydrogen atoms present on the methyl group on the opposite side of the molecule. Structure 1W-B similarly involves a water molecule hydrogen bonded to a carbonyl of diacetyl. In this structure, the oxygen of the water molecule is involved in an electrostatic interaction with one hydrogen atom on the methyl group adjacent to the carbonyl to which it is hydrogen bonded. Finally, structure 1W-C also has a water molecule hydrogen bonding with a carbonyl group, though the hydrogen bond is out of the plane of the carbon backbone, and therefore the water molecule does not engage in electrostatic interactions with the hydrogen atoms on either methyl group.

These three structures coincide with the structures found in previous work done by Dargent, et. al[5]. In this study, the structures that Dargent and colleagues identified as S_1, S_2, and S_3 are the same as the structures identified as 1W-B, 1W-A, and 1W-C, respectively. The difference in order between the structures is a result of the first two structures in both works being essentially isoenergetic, as is explained below.

The relative energies of 1W-A, 1W-B, and 1W-C were pulled from the output files of each of the six aforementioned methods. Additionally, a single-point energy calculation using the restricted CCSD(T) method with avtz basis set was utilized to determine the energetics of the optimized structures presented by the B3LYP and MP2 methods. The B3LYP method was chosen because of its past success in explaining experimental spectra within research done by the Hammer Group and its success in predicting the experimental spectrum of diacetyl alone. The MP2 method was chosen for the single-point energy calculation because it is an ab initio method, and it does not include the assumptions that the DFT methods like B3LYP do. These energies are presented in terms of relative kilocalories per mole in ***Table 3.2*** below:

Method	1W-A	1W-B	1W-C
B3LYP	0.00	-0.18	---------
B3LYP-D3	0.00	0.08	---------
M06-2X	0.00	0.22	0.62
M06-2X-D3	0.00	0.22	0.60
MP2	0.00	0.03	0.71
ω-B97XD	0.00	0.10	---------
B3LYPgeom-rCCSD(T)*	0.00	0.02	---------
MP2geom-rCCSD(T)*	0.00	0.05	0.85

Table 3.2: The relative energies of the three lowest energy structures for 1/1 Diacetyl/Water clusters are shown in kcal/mol. *Denotes a single-point energy computation.

As can be seen from the table above, the DFT methods B3LYP, B3LYP-D3, and *ω*-B97XD could not detect the third structure, 1W-C. Additionally, the two single-point energy computations illustrate that the structures designated 1W-A and 1W-B are essentially isoenergetic, despite the larger energy differences presented by other methods illustrated in ***Table 3.2***. Because these results of the computational investigation of the 1/1 Diacetyl/Water clusters coincided with previous work, these structures were then used to build the 1/2 Diacetyl/Water Clusters.

Just as it was decided that the B3LYP and MP2 methods would be used for the single-point energy calculations, the results of these two methods were used to generate simulated spectra and the corresponding vibrational modes for the three structures. The simulated spectra of the B3LYP optimized 1W-A and 1W-B are shown in ***Figure 3.4***.

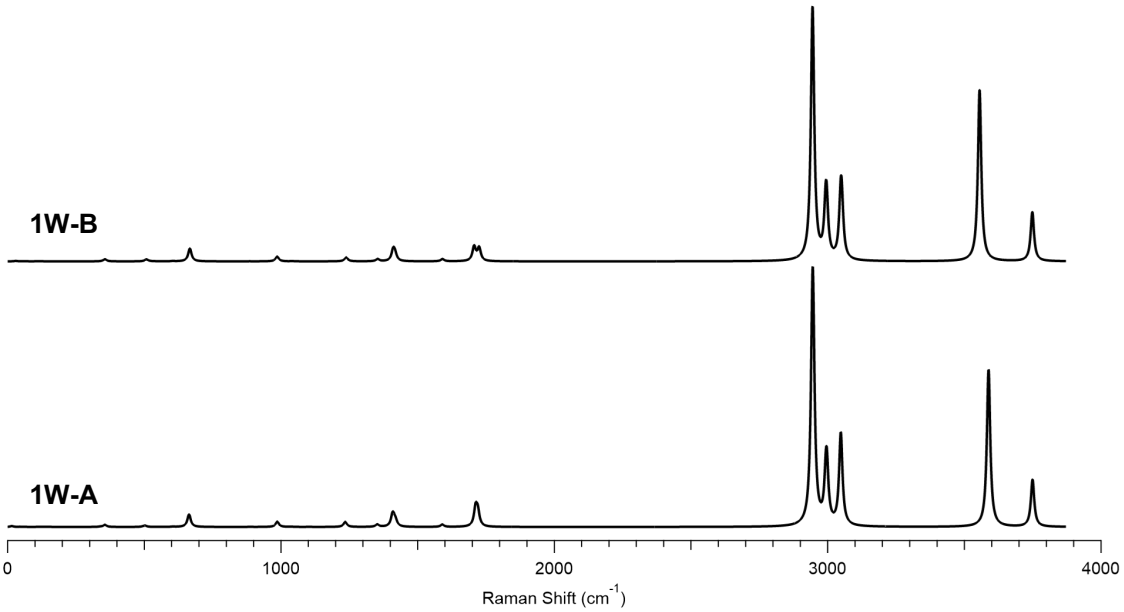

Figure 3.4: The simulated Raman spectra for the B3LYP optimized structures 1W-A and 1W-B are shown.

A zoomed in view of the region 1200 cm^{-1} to 2000 cm^{-1} is shown in the figure below to illustrate the effect on the carbonyl stretching motion.

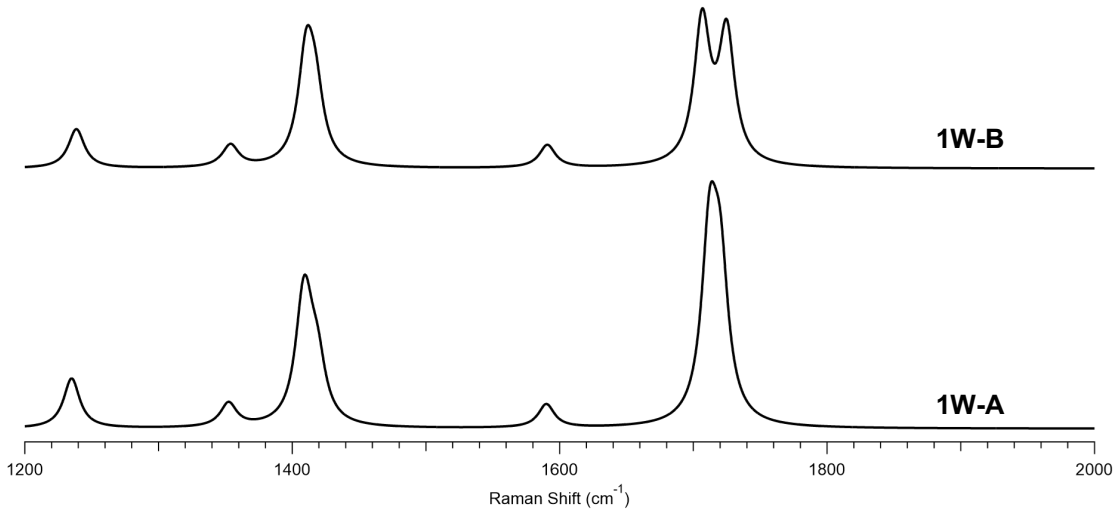

Figure 3.5: The simulated Raman spectra for the B3LYP optimized structures 1W-A and 1W-B are shown from 1200 to 2000 cm^{-1}.

While the two structures are essentially isoenergetic according to the single-point energy calculations, there are two readily apparent differences in the spectra for 1W-A and 1W-B. These differences are related to the lengths of the hydrogen bond present and the distance of the electrostatic interactions at play between the methyl groups and water molecules. These distances are shown in ***Figure 3.5***.

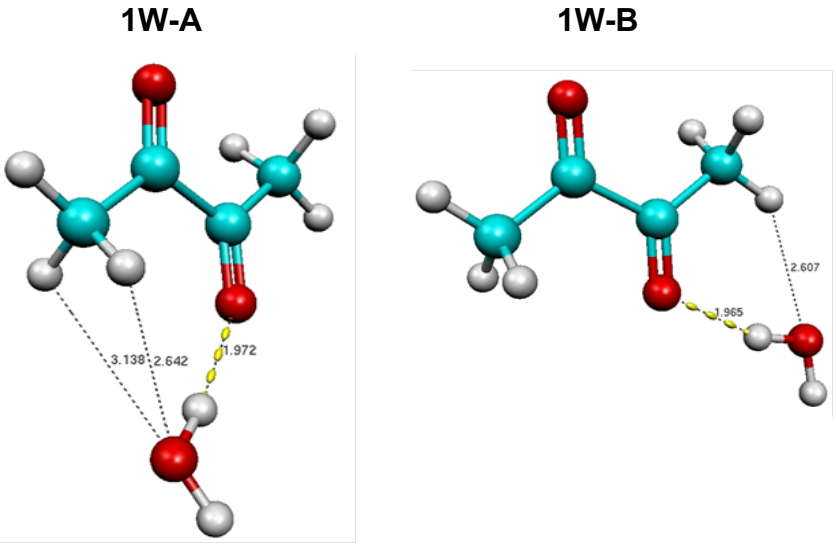

Figure 3.6: The distances (in Angstroms) of the interactions between the water and diacetyl molecules in the B3LYP optimized 1/1 Diacetyl/Water structures are shown.

The carbonyl stretching frequency at 1724.90 cm^{-1} for 1W-B appears to be split compared to its corresponding peak for 1W-A at 1720.17 cm^{-1}. Additionally, the symmetric stretching of the water molecule for the 1W-B structure is red shifted to 3555.75 cm^{-1}, which is 2.74 cm^{-1} lower in energy than the symmetric stretch frequency for 1W-A. This lower energy peak could be the result of the oxygen atom of the water molecule having a shorter electrostatic interaction distance for 1W-B than in 1W-A. Additionally, the shorter hydrogen bond length for 1W-B could be causing the Raman frequency of the stretching vibrations to be lower for the water molecule. These vibrational modes, as well as additional motions within the two structures are described in ***Table 3.3***.

Vibrational Assignment	Vibrational Mode Description	1W-A Freq.(cm^{-1})	1W-B Freq. (cm^{-1})
ν_{30}	Symmetric C=O Stretch	1712.21	1706.56
ν_{31}	Asymmetric C=O Stretch	1720.17	1724.90
ν_{32}	CH_3 umbrella	2944.28	2944.10
ν_{33}	CH_3 umbrella	2946.31	2945.28
ν_{34}	Asymmetric C-H Scissoring	2993.54	2992.86
ν_{35}	Asymmetric C-H Scissoring	2996.74	2995.92
ν_{36}	Asymmetric C-H Stretching	3047.45	3047.92
ν_{37}	Asymmetric C-H Stretching	3049.02	3051.96
ν_{38}	Symmetric HOH Stretching	3558.49	3555.75
ν_{39}	Asymmetric HOH Stretching	3749.47	3748.69

Table 3.3: The vibrational modes of 1W-A and 1W-B as determined by the B3LYP method are given.

As with the B3LYP optimized structures, the MP2 optimized 1W-A and 1W-B structures are very similar in their spectra and vibrational modes. The MP2 method, though, shows a larger difference in the symmetric stretching motions of water between the 1W-A and 1W-B structures, with 1W-B being 28.36 cm^{-1} lower in energy than the corresponding vibrational mode of 1W-A. This red shift can be seen in the spectra shown in ***Figure 3.6***.

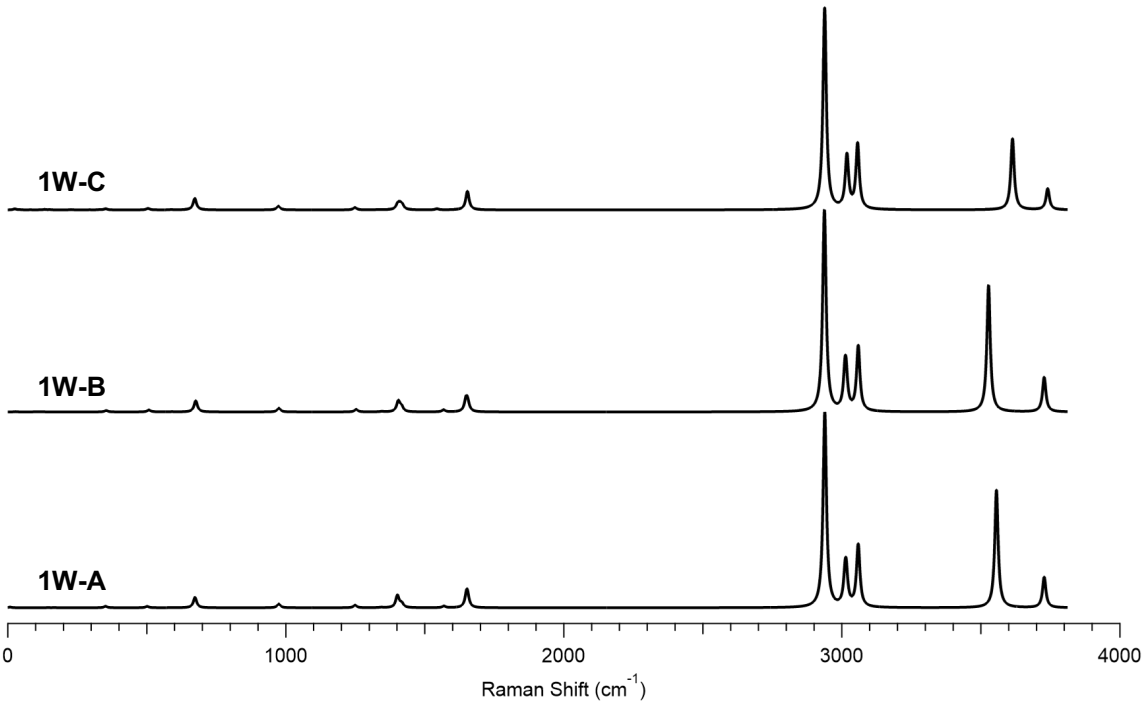

Figure 3.7: Simulated Raman spectra for MP2 optimized structures 1W-A, 1W-B, and 1W-C are shown.

This larger difference in the water molecule's symmetric stretching mode for the MP2 optimized 1W-A and 1W-B structures is a result of the electrostatic interaction of 1W-B being 0.283 Å shorter than the electrostatic interactions of 1W-A. For the B3LYP method, this difference in is only 0.035 Å.

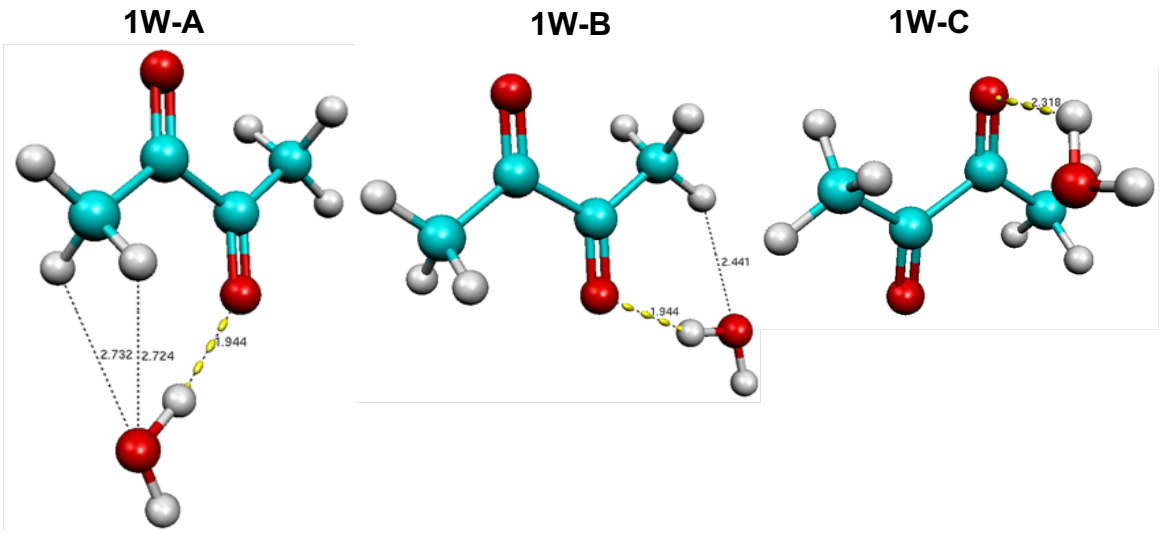

Figure 3.8: The distances (in Angstroms) of the interactions between the water and diacetyl molecules in the MP2 optimized 1/1 Diacetyl/Water structures are shown.

Unlike the B3LYP method, the MP2 method predicted a third structure, 1W-C. This structure has similar frequencies for the vibrational modes listed in ***Table 3.4***, with the largest difference arising for the symmetric and asymmetric stretching modes of water. The symmetric stretching mode occurs at 3613.59 cm^{-1}, and the asymmetric stretching mode occurs at 3740.21 cm^{-1}. Both of these vibrational modes are higher in energy, or blue shifted, for 1W-C compared to 1W-A or 1W-B. This increase in energy for the water molecule's stretching frequencies is reasonable, as the water molecule in 1W-C is not stabilized by favorable electrostatic interactions with the hydrogen molecules of a methyl group like is the case in structures 1W-A and 1W-B. This lack of interaction between the methyl group and water molecule is likely the reason that the scissoring motions of the

methyl group are higher in energy for 1W-C as well. Additionally, as can be seen in ***Figure 3.6***, the hydrogen bond length of 1W-C is 0.374 Å longer than the hydrogen bonds present in 1W-A and 1W-B. This weaker stabilization of the water molecule contributes to the stretching modes of the water molecule being higher in energy for 1W-C than for 1W-A or 1W-B.

A zoomed in version of the spectra in the figure below provides a better visualization of the effects that these hydrogen bond and electrostatic interactions have on the carbonyl stretching motions within the structures. Between the three structures, the carbonyl stretch frequencies in 1W-C are the highest energy at 1653.06 and 1655.08 cm^{-1} for the symmetric and asymmetric motions, respectively. This increase in energy is likely a result of the longer hydrogen bond that is present in this structure.

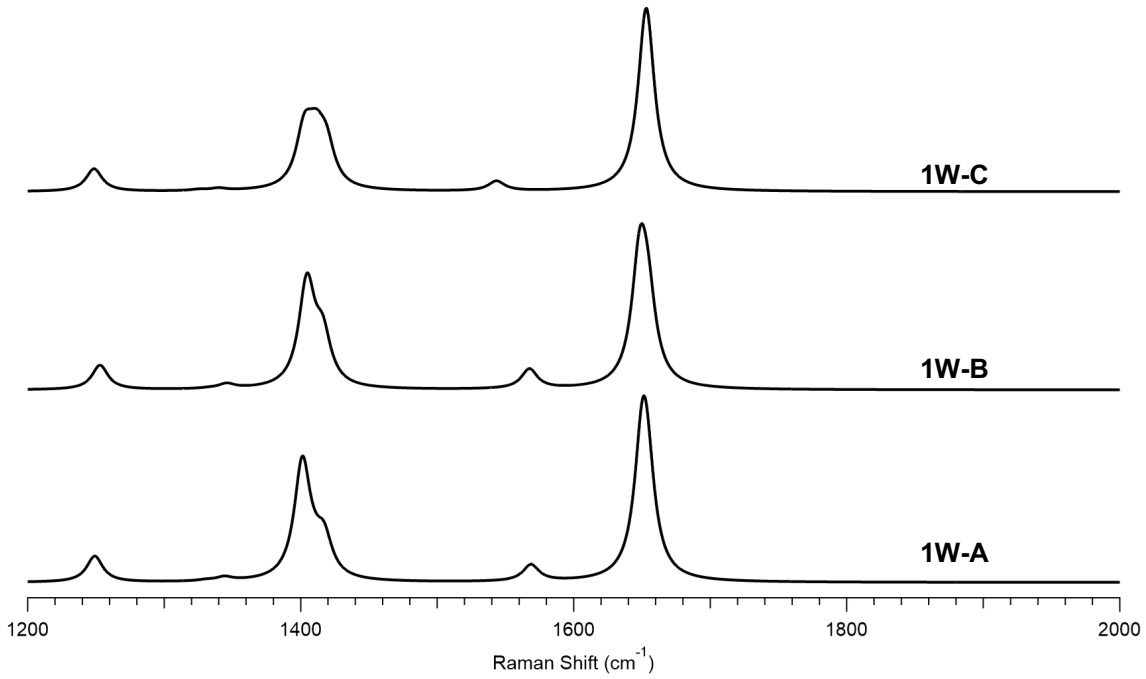

Figure 3.9: Simulated Raman spectra for MP2 optimized structures 1W-A, 1W-B, and 1W-C are shown from 1200 to 2000 cm^{-1}.

These vibrational modes, as well as others that were pulled from the output files of the three 1/1 Clusters using *Gaussview 6* Software are shown in ***Table 3.4***.

Vibrational Assignment	Vibrational Mode Description	1W-A Freq.(cm^{-1})	1W-B Freq. (cm^{-1})	1W-C Freq. (cm^{-1})
ν_{30}	Symmetric C=O Stretch	1650.42	1648.47	1653.06
ν_{31}	Asymmetric C=O Stretch	1653.84	1654.35	1655.08
ν_{32}	CH_3 umbrella	2937.88	2936.10	2937.95
ν_{33}	CH_3 umbrella	2939.07	2938.27	2938.12
ν_{34}	Asymmetric C-H Scissoring	3011.46	3011.07	3017.38
ν_{35}	Asymmetric C-H Scissoring	3015.18	3014.75	3018.77
ν_{36}	Asymmetric C-H Stretching	3058.02	3058.51	3056.49
ν_{37}	Asymmetric C-H Stretching	3059.79	3059.66	3057.05
ν_{38}	Symmetric HOH Stretching	3555.88	3527.52	3613.59
ν_{39}	Asymmetric HOH Stretching	3727.65	3727.62	3740.21

Table 3.4: The vibrational modes of 1W-A, 1W-B, and 1W-C as determined by the MP2 method are given.

Between the two methods, it appears that that MP2 frequency calculations show a more exaggerated difference in the vibrational modes of the 1/1 Diacetyl/Water structures. However, the predicted carbonyl stretching frequencies for the MP2 method are more than 50 cm^{-1} less than those predicted by the B3LYP method. Whether this finding is a result of the MP2 method underpredicting the energy of the structure or the difficulty that the B3LYP method can have with dispersion-dominated non-covalent interactions is unknown without comparison to experiment[19,33]. When comparing these two theoretical methods with the experimental spectrum of liquid diacetyl, the B3LYP method was a much better predictor of the carbonyl stretching frequency. Therefore, it is more likely that the large difference in the predicted frequencies results from the MP2 method underpredicting the frequency, like is the case for the carbonyl stretch of diacetyl alone.

3.3 1/2 DIACETYL/WATER COMPLEXES

Like with the construction of the one water clusters, *Gaussview 6* software was used to construct the clusters with two water molecules from the optimized one water structures

using “chemical intuition.” Work done by Dargent, et. al. on 1/2 Diacetyl/Water complexes was used as a guide, and eighteen input geometries were constructed[44]. Three of these were built using the output files within the supplementary information provided in Dargent and colleagues’ study[44]. The input files built using the *Gaussview 6* program were first optimized using B3LYP until the aug-cc-pVTZ basis set and tight convergence was achieved. These output geometries were then inputted into optimizations with the MP2 method and aug-cc-pVTZ basis set, again with tight convergence. The three structures pulled from supplementary information were both inputted and optimized using the MP2 and B3LYP methods separately.

From these input geometries, the two methods optimized the 1/2 Diacetyl/Water clusters into twelve unique structures. Two additional enantiomeric structures were found for the structures identified as 2W-A and 2W-B, but because these enantiomers were energetically equivalent, and they were excluded from the work presented by Dargent et. al, only one enantiomer is included in the images and tables presented below[44]. The enantiomer that is shown was chosen to be the orientation that aligned with the orientation of the other 1/2 Diacetyl/Water structures that were found so that comparison between the clusters could be more readily visible.

Both the MP2 method and B3LYP method found two structures that the other method did not. This left eight shared structures that both the methods could optimize. These eight shared structures are presented as their MP2 optimized geometries alongside the two structures that MP2 alone could find. The shared geometries were shown in this manner because this research was done in comparison to the work presented by Dargent et. al, and the structures they presented were constructed using the MP2 method[44]. These

output geometries can be seen in ***Figure 3.8***. Additionally, as was done in the paper by Dargent et. al, the structures are labeled in order of increasing energy according to the MP2 computed relative energy values. The structures labeled 2W-A, 2W-B, 2W-C, 2W-D, and 2W-E are further confirmed to increase in energy alphabetically by the single-point rCCSD(T) energy calculations done on their MP2 optimized geometries. It should be noted that due to ordering the structures by the MP2 computed energies, the naming of the structures presented in the figures below do not coincide with increasing energy according to the B3LYP method or their single-point energy calculations.

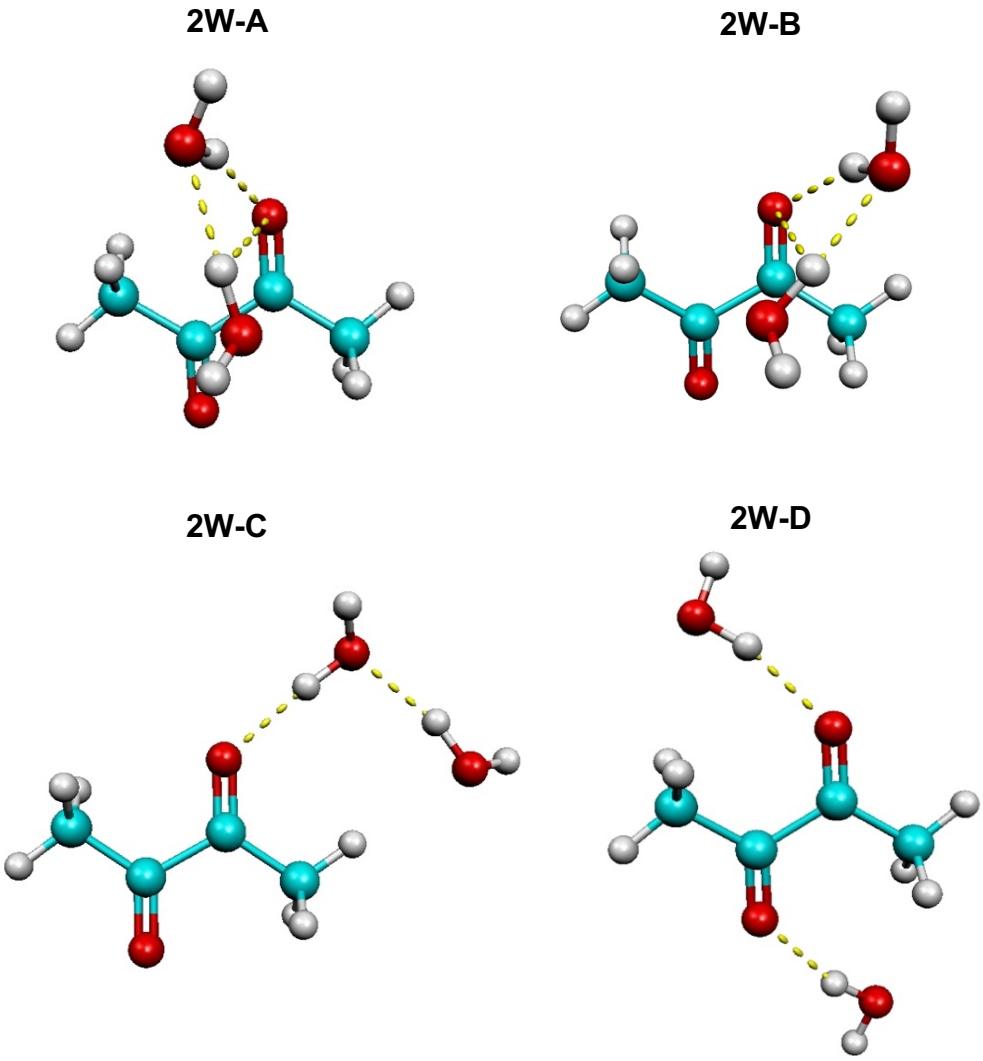

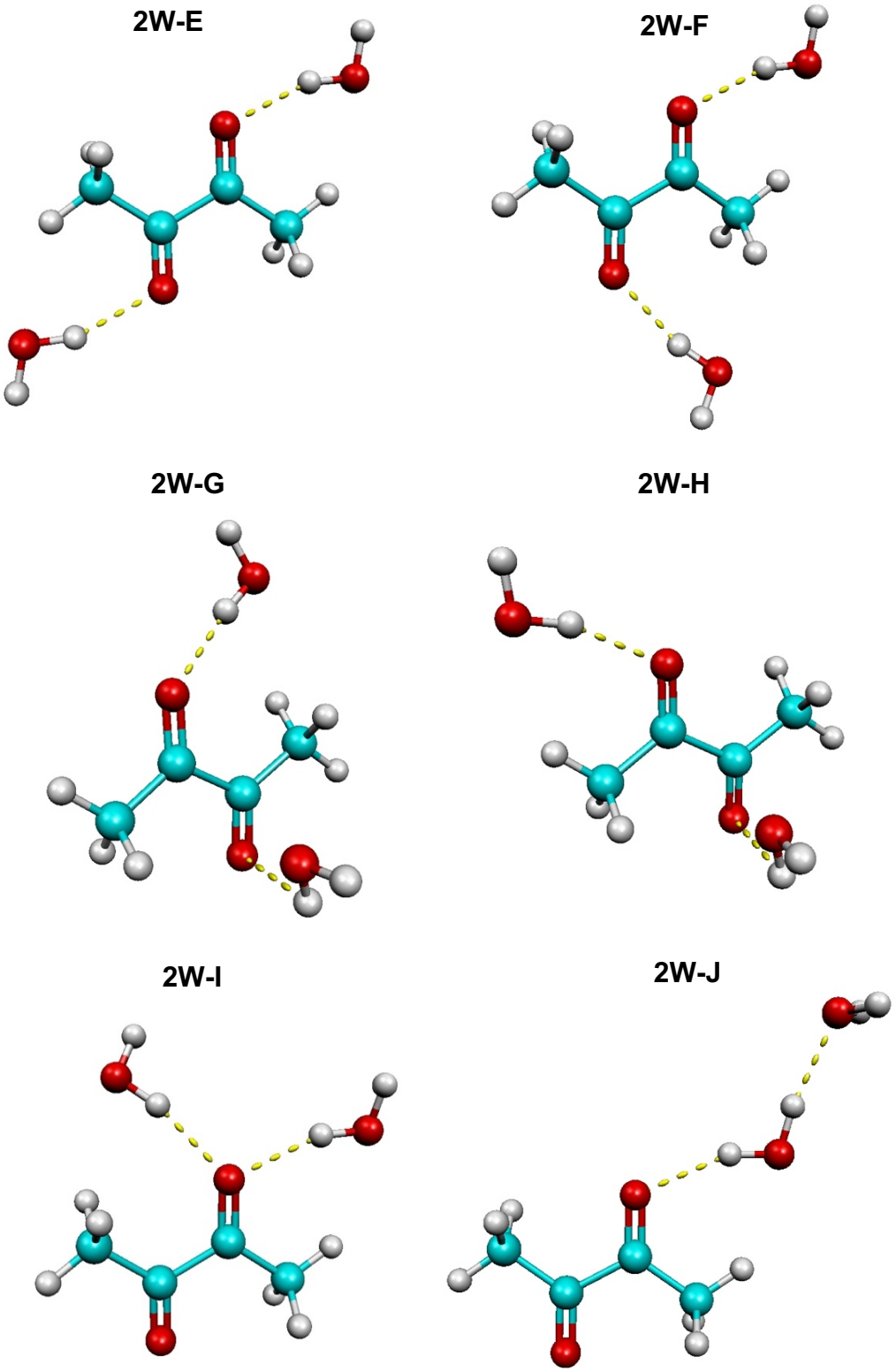

Figure 3.10: Lowest energy structures using the MP2 method for 1/2 Diacetyl/Water clusters are shown in order of increasing relative energy.

The structures designated as 2W-G and 2W-H in ***Figure 3.8*** could not be optimized using the B3LYP method. These two structures include a water molecule that is hydrogen bonded to a carbonyl oxygen perpendicular to the carbon backbone. This hydrogen bonding in the z-axis of the molecule is similar to the hydrogen bonding present in the 1W-C structure that the B3LYP method could not find. It appears that the B3LYP method has difficulty with structures that involve hydrogen bonded water molecules like those in 1W-C, 2W-G, and 2W-H. Dealing with dispersion-dominated non-covalent interactions is a known difficulty of the B3LYP method, and this appears to be proven by the failure of the B3LYP method to find these three structures[33].

However, the MP2 method appears to have difficulty in predicting the 1/2 Diacetyl/Water structures as well. The B3LYP method found two structures that could not be optimized using the MP2 method. These additional structures are labeled as 2W-K and 2W-L in ***Figure 3.7***. The MP2 method optimized these structures further to be equivalent to 2W-A and 2W-B.

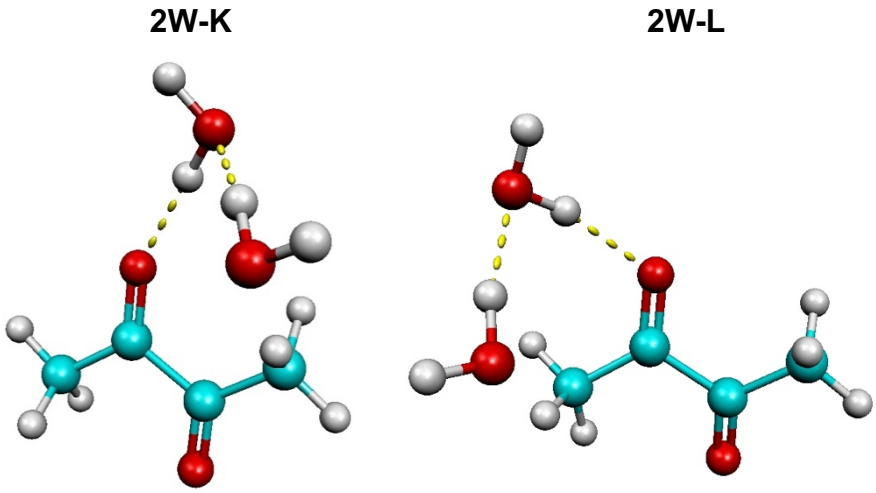

Figure 3.11: 1/2 Diacetyl/Water clusters that could only be optimized using the B3LYP method are shown in order of increasing relative energy.

While the structure 2W-K appears to be similar to 2W-A and 2W-L appears to be similar to 2W-B, the relative energies and bond lengths were of a significant enough

difference for these two structures not found by the MP2 method to be considered unique. These differences in relative energies between 2W-A and 2W-K and between 2W-B and 2W-L are shown in the table below. Also included are the relative energies of the remaining unique 1/2 Diacetyl/Water structures presented in ***Figure 3.8*** and ***Figure 3.9***.

Structure	MP2	B3LYP
2W-A	0.00	0.00
2W-B	0.11	-0.29
2W-C	2.32	0.19
2W-D	4.05	2.41
2W-E	4.22	2.25
2W-F	4.47	2.65
2W-G	4.53	--------
2W-H	4.63	--------
2W-I	4.88	3.14
2W-J	5.57	2.99
2W-K	---------	0.03
2W-L	---------	0.05

Table 3.5: The relative energies of the structures for 1/2 Diacetyl/Water clusters are given in kcal/mol for both methods used: B3LYP and MP2.

Because the ordering of the Diacetyl/Water clusters' relative energies differs between the MP2 method and B3LYP method, single-point energy rCCSD(T) calculations with a triple zeta basis set were done on the five lowest energy structures presented by the MP2 method, as well as the B3LYP optimized 2W-K and 2W-L structures. These B3LYP structures were included in the single-point energy calculations because the relative energies of 2W-K and 2W-L are lower than that of 2W-D and 2W-E as determined by the B3LYP output files. The five structures not mentioned above were not included in this calculation because performing the single-point energy computations for all of the unique structures would require a large amount of time and computational cost. Further, as is explained in the discussion of the clusters involving three water molecules, only these lowest energy structures were used to construct the clusters of greater size, so the information forewent by excluding the other structures does not adversely affect the

calculations of complexes to follow. The results of the single-point energy calculations on the B3LYP and MP2 optimized 2W-A, 2W-B, 2W-C, 2W-D, 2W-E, 2W-K, and 2W-L structures are shown as relative energies in kilocalories per mole the table below.

Structure	MP2geom-rCCSD(T)	B3LYPgeom-rCCSD(T)
2W-A	0.00	0.00
2W-B	0.14	-0.30
2W-C	2.14	1.17
2W-D	3.88	3.07
2W-E	4.07	3.19
2W-K	---------	1.04
2W-L	---------	1.08

Table 3.6: The relative single-point energies of the five lowest energy 1/2 Diacetyl/Water clusters are given in kcal/mol for both B3LYP and MP2 optimized geometries.

Immediately noticeable are the large discrepancies between the values computed for the B3LYP method and the MP2 method. The most important of these differences is that the lowest energy structure for the two methods is not in agreement. The single-point calculation for the MP2 geometries predicts 2W-A to be the lowest in energy, whereas the calculation for the B3LYP geometries predicts 2W-B to be the lowest energy structure. These two structures differ in the dihedral angles in which the water molecules are coordinated, as can be seen in the B3LYP and MP2 optimized geometries shown in ***Figure 3.12*** and ***Figure 3.13***, respectively.

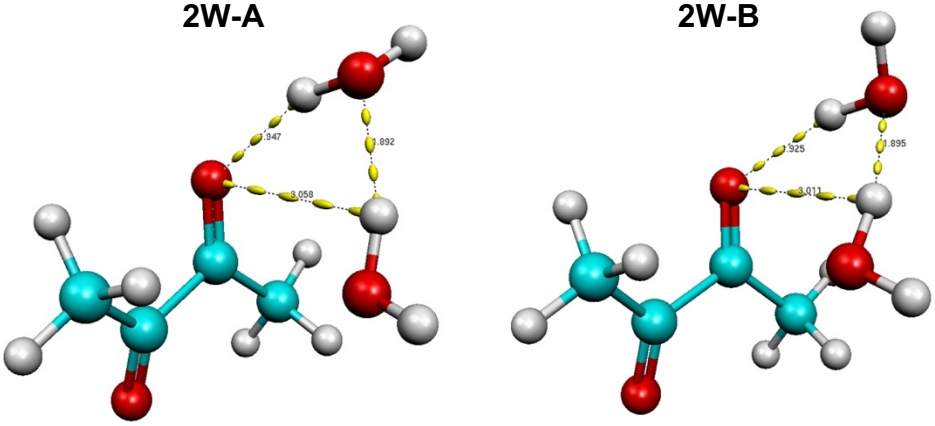

Figure 3.12: The hydrogen bond distances (in Angstroms) of the B3LYP optimized 2W-A and 2W-B structures are shown.

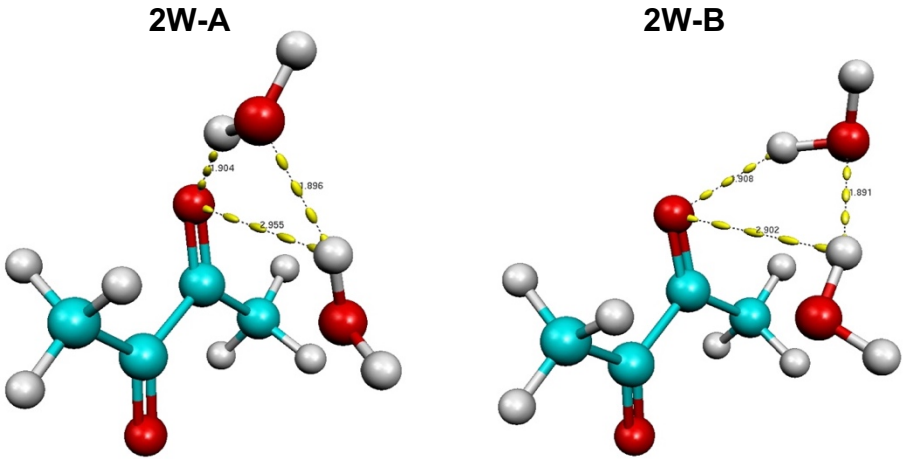

Figure 3.13: The hydrogen bond distances (in Angstroms) of the MP2 optimized 2W-A and 2W-B structures are shown.

In the B3LYP geometries, the 2W-B structure appears to have the carbonyl oxygen involved in shorter hydrogen bonds. One of these bonds is 0.022 Å shorter and the other is 0.047 Å shorter than the corresponding hydrogen bonds in 2W-A. While these differences are not extensive, this shortening of the distance between the water molecules and the diacetyl molecule could account for why the single-point energy calculation of the B3LYP geometry predicts structure 2W-B to be 0.30 kcal/mol lower in energy than 2W-A. The single-point energy calculations for the MP2 structures, however, show 2W-A being the lower energy structure. Like the B3LYP geometries, the hydrogen bonding distances in 2W-B are shorter than those in 2W-A. Therefore, the MP2 method must be accounting for another stabilizing, or destabilizing factor, in calculating 2W-A to be lower in energy that the B3LYP method does not. Since the single-point energy calculations alone could not determine the true lowest energy structure, it was decided that additional methods would be used, like in the case of the 1/1 Diacetyl/Water Complexes.

The output geometry of the MP2 method with aug-cc-pVTZ basis set and tight convergence was inserted into input files for calculations run with M06-2X, M06-2X-D3,

B3LYP-D3, and ω-B97XD methods. Each of the geometries was first optimized from the cartesian coordinates using the aug-cc-pVDZ basis set, and further optimization to reach a triple zeta basis set with tight convergence were done using the check point files of the previous calculation. The relative energies of the 2W-A and 2W-B structure are given for all methods used in ***Table 3.7***.

Method	2W-A	2W-B
B3LYP	0.00	-0.29
B3LYP-D3	0.00	0.07
M06-2X	0.00	0.34
M06-2X-D3	0.00	0.34
MP2	0.00	0.11
ω-B97XD	0.00	0.15

Table 3.7: The relative energies of the two lowest energy structures for 1/2 Diacetyl/Water clusters are shown in kcal/mol.for the six computational methods used.

Despite the different values presented by the B3LYP method and its single-point energy differences, the order as proposed by the MP2 method and its single-point energy calculations was used to name the structures presented in this work. This naming method allows for the order to remain consistent throughout this thesis and to coincide with the work done by Dargent, et. al. This ordering is also supported by the additional four methods that place 2W-A as the lower energy structure compared to 2W-B. It should be noted that the increase of more than 1 kcal/mol in energy for 2W-K and 2W-L according to the single-point energy calculations of the B3LYP structures illustrates that these structures are not energetically equivalent to 2W-A and 2W-B, though the MP2 method calculated 2W-K and 2W-L to be. These structures are named at the completion of the MP2 optimized structures, despite their energies being lower than those of 2W-C, 2W-D, and 2W-E because all of the MP2 optimized structures are named in comparison to one another.

After confirming the naming of the clusters in order of increasing relative energies, the structures could be investigated for patterns. The lowest energy structures, 2W-A and 2W-B, contain a cyclical arrangement of the water molecules that allows for three hydrogen bonds to be present in the cluster, compared to only two hydrogen bonding interactions in the rest of the structures. The four lowest energy structures mirror the results found by Dargent, et. al[44]. However, Dargent et. al found that the structures labeled here as 2W-E, 2W-F, 2W-G, and 2W-H increase energetically in the order: 2W-G, 2W-E, 2W-H, 2W-F. The differences between these structures can be associated with the electrostatic interactions present between the water molecules and methyl groups, as each of these four structures has the same number of hydrogen bonds. The energy differences computed between this work and the study done by Dargent, et. al could be attributed to the use of a triple zeta basis set with tight convergence in this work, whereas previous work used a double zeta basis set with tight convergence.

The structure that Dargent et. al designated as the "π_like_π_like_trans" could not be found using the B3LYP or MP2 methods[44]. Attempts to optimize the structure at the aug-cc-pVDZ level by using the coordinates given in the supplemental information of the paper were successful. However, once this output geometry was taken up to the aug-cc-pVTZ basis set and tight convergence, the geometry optimized to the structure that is labeled in this work as 2W-E. Additionally, the research done in this thesis found the structure designated as 2W-J, which is not included in the work presented by Dargent, et. al[44]. The 2W-J structure involves the oxygen atom of the first water molecule hydrogen bonded to a carbonyl group, with the second water molecule hydrogen bonded in the plane of the carbon backbone. This structure, unlike the other geometries, has the second water

molecule away from the methyl group, so there are not favorable electrostatic interactions. This lack of electrostatic interactions explains the higher relative energy for the structure.

As was done with the 1W-A, 1W-B, and 1W-C structures, simulated spectra were created to see the effect that the interactions between the water and diacetyl molecules had on the carbonyl stretching vibrational modes and the motions of the water molecules. The spectra of the geometries optimized by the B3LYP method are shown first in ***Figure 3.14***.

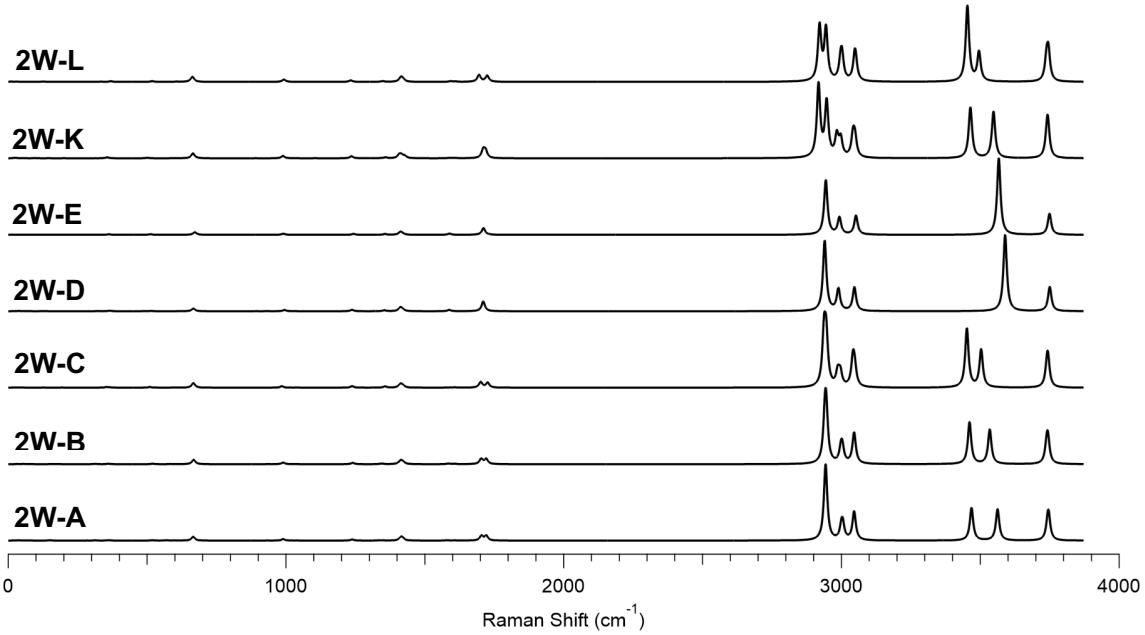

Figure 3.14: Simulated Raman spectra for the B3LYP optimized structures 2W-A, 2W-B, 2W-C, 2W-D, 2W-E, 2W-K, and 2W-L are shown.

The most evident changes that result from the frequency calculations of the different 1/2 Diacetyl/Water Clusters in this figure can be seen with the vibrational modes of the methyl groups and the water molecules. First, splitting can be seen in the C-H stretching motion present at around 2950 cm^{-1} in 2W-K and 2W-L. For 2W-K, the frequencies are located at 2917.58 cm^{-1} and 2946.70 cm^{-1}, and for 2W-L, the peaks are present at 2921.32 cm^{-1} and 2944.34 cm^{-1}. This splitting pattern likely results from the fact that both of these structures have a water molecule engaged in electrostatic interactions with one face of the methyl group, causing the motions to have a greater difference in

energy than the other structures where the water molecule is centered over the methyl group. Splitting is also seen in five of the structures for the stretching motion of water centered around 3500 cm^{-1}. The largest splitting between these motions is present in 2W-A, where the difference between 3468.41 cm^{-1} and 3562.19 cm^{-1} is equal to 93.78 cm^{-1}. Only a single peak is shown for the structures 2W-D and 2W-E for this vibrational mode because the two clusters are completely symmetrical, whereas the other structures have two unequal motions from the lack of symmetry present. In order to have a better visualization of the carbonyl stretching motions, the spectra are presented only in the range of 1200 to 2000 cm^{-1} in the figure below.

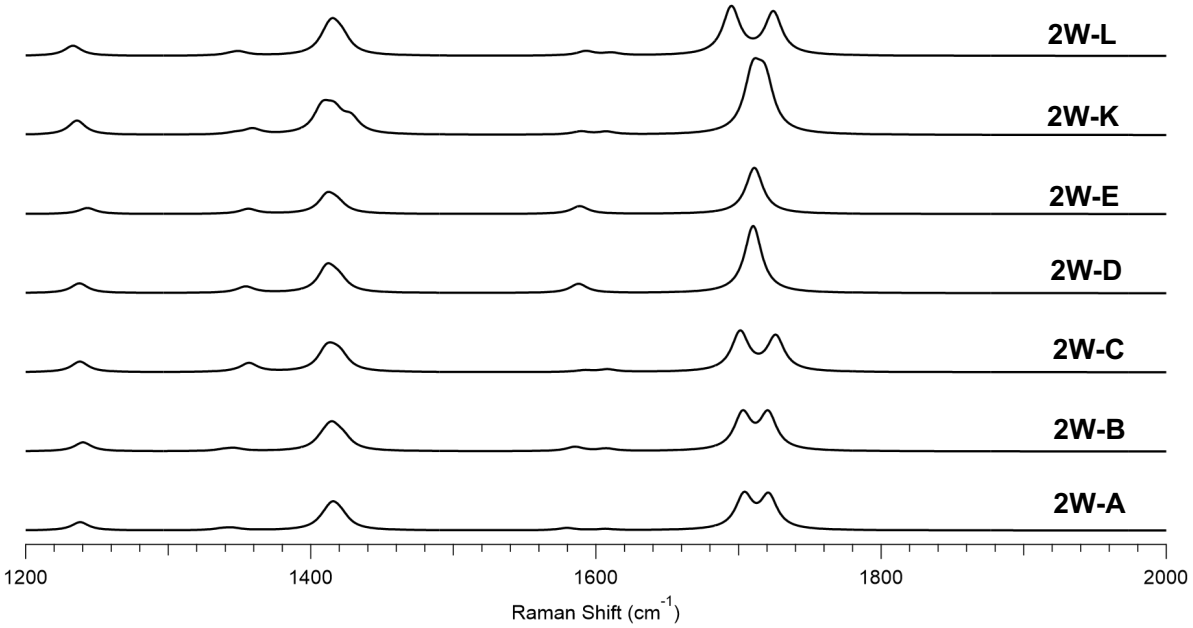

Figure 3.15: Lowest energy structures using the MP2 method for 1/2 Diacetyl/Water clusters are shown in order of increasing relative energy.

The location of the carbonyl stretching frequencies are very similar amongst the seven B3LYP structure presented in ***Figure 3.15***. Like with the methyl and water vibrational motions, the carbonyl stretching frequencies differ most notably in the splitting of the peaks. The largest splitting difference for this vibrational mode is shown in 2W-L with peaks at 1694.96 cm^{-1} and 1724.45 cm^{-1}. The 2W-D and 2W-E structures once again

do not show visible splitting as a result of their symmetry. The simulated frequencies for the vibrational modes of the seven structures presented in Figure 3.14 and Figure 3.15 are shown in ***Table 3.8*** below.

Vibrational Assignment	Vibrational Mode Description	2W-A Freq. (cm^{-1})	2W-B Freq. (cm^{-1})	2W-C Freq. (cm^{-1})	2W-D Freq. (cm^{-1})	2W-E Freq. (cm^{-1})	2W-K Freq. (cm^{-1})	2W-L Freq. (cm^{-1})
ν_{37}	Symmetric C=O stretching; HOH wagging	1703.91	1702.90	1701.15	1708.57	1709.54	1709.95	1694.96
ν_{38}	Asymmetric C=O stretching. HOH wagging	1721.18	1720.75	1726.10	1710.31	1711.09	1718.62	1724.45
ν_{39}	CH_3 umbrella	2942.24	2940.74	2937.43	2939.57	2943.71	2917.58	2921.32
ν_{40}	CH_3 umbrella	2943.46	2945.43	2945.32	2939.73	2943.72	2946.70	2944.34
ν_{41}	Asymmetric C-H Stretching	3000.02	2998.23	2986.70	2988.71	2992.39	2983.34	2996.96
ν_{42}	Asymmetric C-H Stretching	3004.66	3003.12	2996.02	2989.15	2992.73	2997.44	3002.00
ν_{43}	Asymmetric C-H Stretching	3045.67	3045.55	3041.53	3046.70	3052.33	3041.93	3048.10
ν_{44}	Asymmetric C-H Stretching	3046.29	3046.36	3047.87	3047.10	3052.84	3049.00	3051.25
ν_{45}	Symmetric O-H Stretching	3468.41	3461.24	3451.70	3587.94	3562.73	3464.40	3453.52
ν_{46}	Symmetric O-H Stretching	3562.19	3534.05	3503.09	3589.62	3566.64	3547.61	3495.30
ν_{47}	Asymmetric O-H Stretching	3742.69	3739.08	3740.31	3749.69	3748.70	3740.42	3738.59
ν_{48}	Asymmetric O-H Stretching	3746.10	3743.49	3743.63	3750.14	3749.23	3743.39	3745.14

Table 3.8: The vibrational modes of 2W-A, 2W-B, 2W-C, 2W-D, 2W-E, 2W-K, and 2W-L as determined by the B3LYP method are given.

Theoretical spectra were also constructed for the lowest energy structures that were optimized using the MP2 method. Because the MP2 method could not find the 2W-K and 2W-L structures to be different from 2W-A and 2W-B, only the spectra of 2W-A, 2W-B, 2W-C, 2W-D, and 2W-E are included in ***Figure 3.16*** and ***Figure 3.17***. The entire range of frequencies calculated are included in ***Figure 3.16***, while ***Figure 3.17*** focuses on the range showing the carbonyl stretching frequencies.

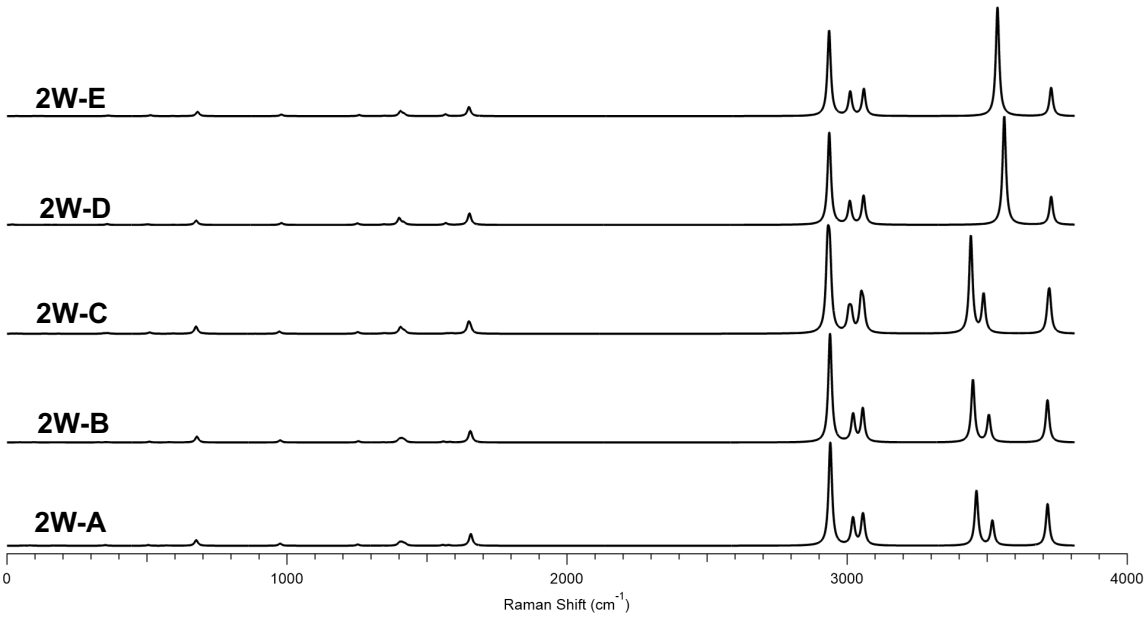

Figure 3.16: Lowest energy structures using the MP2 method for 1/2 Diacetyl/Water clusters are shown in order of increasing energy.

The same trend of splitting of the stretching motions of water that was seen in the B3LYP method's simulated spectra is seen for the MP2 method. The 2W-D and 2W-E structures do not show splitting as a result of their symmetry, and the mode is shown at higher energy than the peaks of the same vibrational motion for 2W-A, 2W-B, and 2W-C. The 2W-D and 2W-E structures do not have water molecules coordinated together, but the water molecules in 2W-A, 2W-B, and 2W-C all have coordinate water molecules that likely leads to this vibrational motion being red shifted to lower energy in their spectra.

The splitting seen in the carbonyl stretching motions of the B3LYP optimized structures was not seen in the geometries that were optimized using the MP2 method. The MP2 method also continues to predict these motions to be at much lower frequencies than the B3LYP method, with the carbonyl stretching peaks shown in ***Figure 3.17*** being more than 50 cm^{-1} lower in energy than those present in ***Figure 3.15***.

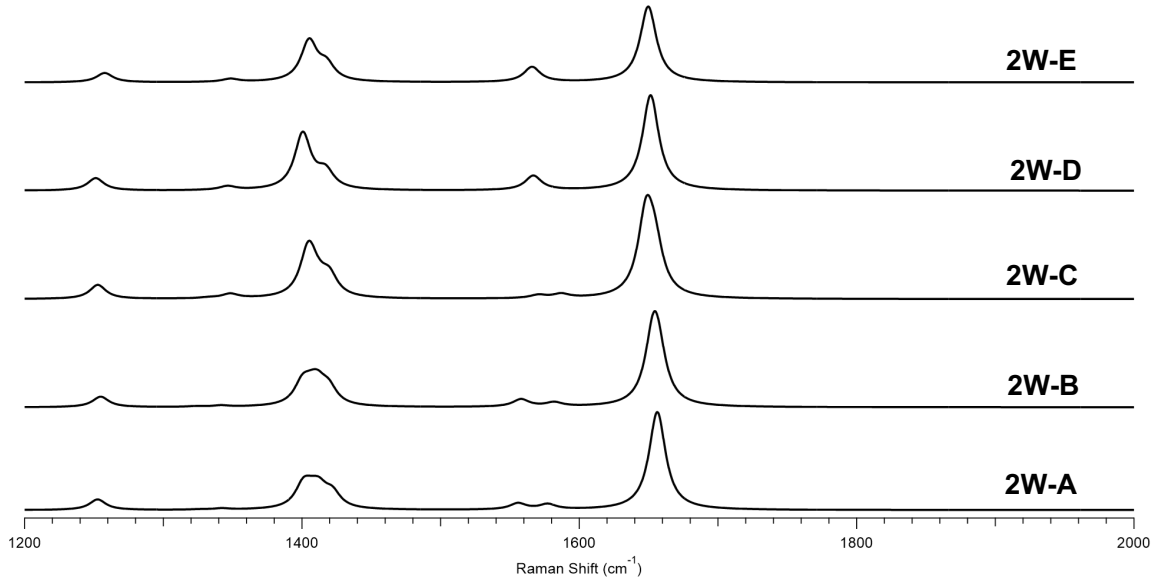

Figure 3.17: Lowest energy structures using the MP2 method for 1/2 Diacetyl/Water clusters are shown in order of increasing

The exact values of the frequencies associated with the vibrational modes predicted for the five lowest energy structures optimized by the MP2 method are shown in Table 3.9 below.

Vibrational Assignment	Vibrational Mode Description	2W-A Freq. (cm^{-1})	2W-B Freq. (cm^{-1})	2W-C Freq. (cm^{-1})	2W-D Freq. (cm^{-1})	2W-E Freq. (cm^{-1})
ν_{37}	Symmetric C=O stretching; HOH wagging	1655.97	1653.53	1648.25	1651.42	1649.72
ν_{38}	Asymmetric C=O stretching; HOH wagging	1657.49	1657.14	1654.60	1651.59	1650.09
ν_{39}	CH_3 umbrella	2938.93	2937.99	2930.33	2936.18	2935.62
ν_{40}	CH_3 umbrella	2940.94	2939.99	2938.26	2936.31	2935.82
ν_{41}	Asymmetric C-H Stretching	3019.53	3019.51	3006.12	3009.35	3010.76
ν_{42}	Asymmetric C-H Stretching	3022.23	3022.55	3014.81	3009.61	3010.98
ν_{43}	Asymmetric C-H Stretching	3055.06	3055.83	3049.92	3058.61	3059.63
ν_{44}	Asymmetric C-H Stretching	3058.61	3056.39	3058.42	3058.95	3059.98
ν_{45}	Symmetric O-H Stretching	3461.77	3449.16	3441.75	3559.37	3533.35
ν_{46}	Symmetric O-H Stretching	3518.62	3506.02	3487.25	3561.06	3536.84
ν_{47}	Asymmetric O-H Stretching	3715.42	3714.44	3717.85	3727.92	3727.66
ν_{48}	Asymmetric O-H Stretching	3715.91	3716.50	3723.18	3728.48	3728.34

Table 3.9: The vibrational modes of 2W-A, 2W-B, 2W-C, 2W-D, and 2W-E as determined by the MP2 method are given.

As with the 1/1 Diacetyl/Water complexes, the 1/2 Diacetyl/Water complexes show that the MP2 method predicts the carbonyl stretching motion to be much lower in energy than the B3LYP method, and the B3LYP method does not accurately optimize and predict the lowest energy structure. The understanding behind these findings would be best understood through comparison to experiment.

3.4 1/3 DIACETYL/WATER COMPLEXES

Unlike using all of the 1/1 Diacetyl/Water clusters to make the 1/2 Diacetyl/Water cluster input geometries, the construction of the 1/3 Diacetyl/Water clusters using all of the structures found for the 1/2 Diacetyl/Water clusters would be extremely computationally expensive. For example, if each of the twelve structures was used to create three input geometries for the clusters with three water molecules, then thirty-six input geometries would have to be optimized. Instead, only the five lowest energy structures determined for the 1/2 Diacetyl/Water clusters were used to build 1/3 Diacetyl/Water clusters using Gaussview 6 software. Once again, water molecules were added using chemical intuition, which resulted in input geometries including the new water molecule at sites where it could have favorable hydrogen bonding or electrostatic interactions with the optimized 1/2 Diacetyl/Water structure.

Eighteen input geometries were constructed, and these input files were optimized initially using the B3LYP method. For two structures, the optimization at the lowest level of theory included the dispersion corrected B3LYP-D3 method when the B3LYP method failed to optimize the structure. However, the subsequent optimizations leading up to a tight convergence with the aug-cc-pVTZ basis set were all done using only the B3LYP

method and the geometries found in the checkpoint files. This process resulted in twelve unique structures. The B3LYP output geometries were then included in the input files that were optimized using the MP2 method. These were optimized at lower basis sets before the checkpoint geometries were used to reach a triple zeta basis set with tight convergence. The twelve unique geometries are presented in order of increasing relative energy according to the MP2 method in the figure below. As was the case with the two water clusters, the B3LYP method and MP2 method differ in their energetic findings of the clusters, but in order to maintain consistency and assist in the comparison of energetics, the structures are listed according to the MP2 method.

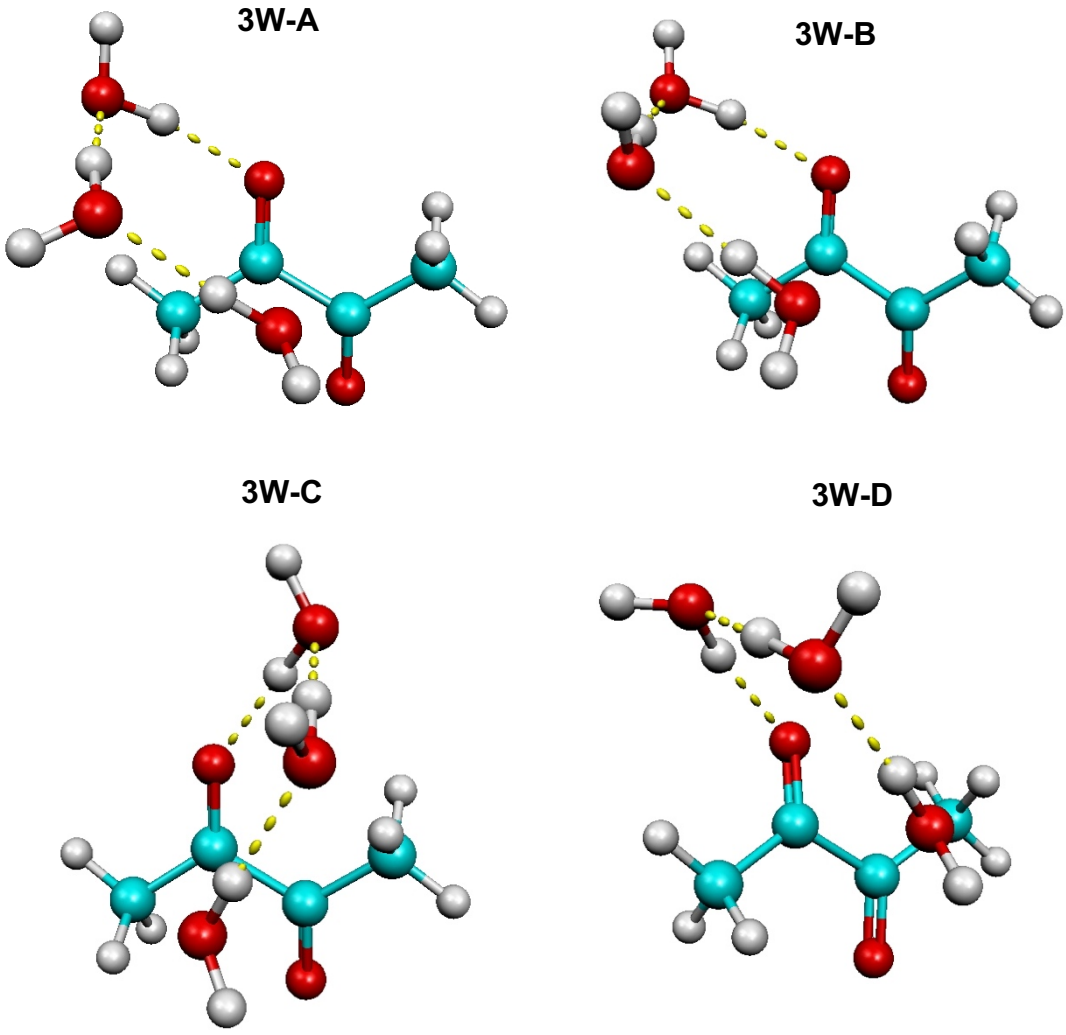

3W-E

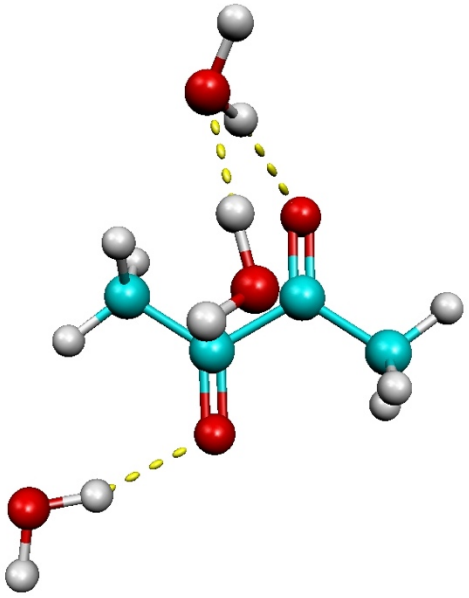

3W-F

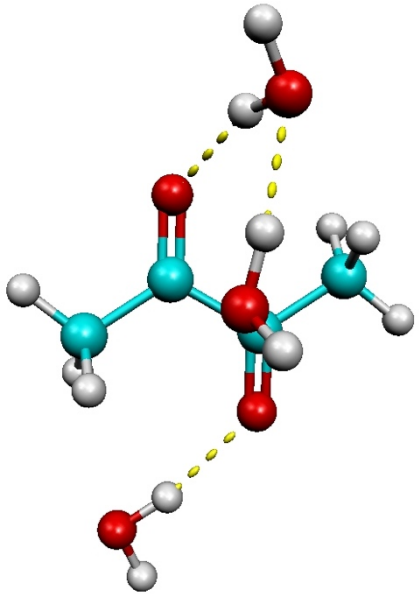

3W-G

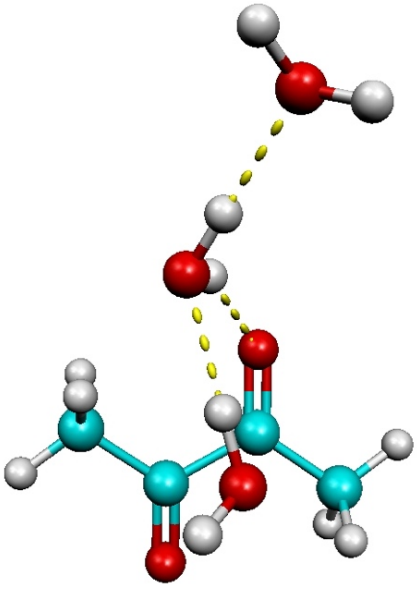

3W-H

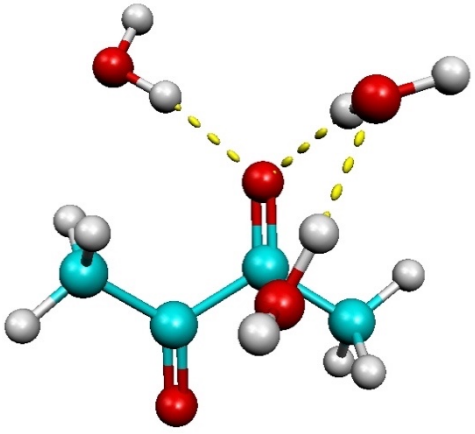

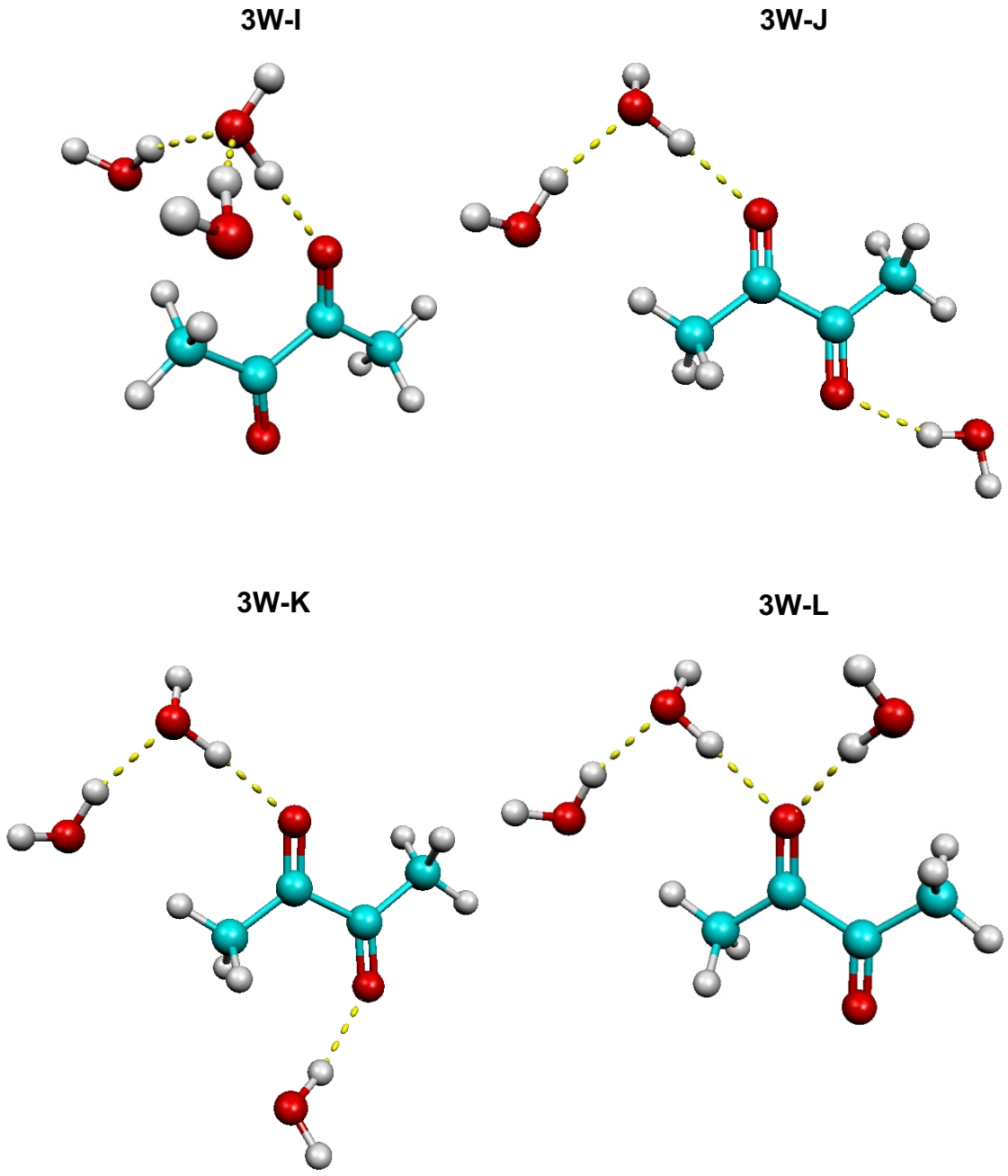

Figure 3.18: Lowest energy structures using the MP2 method for 1/3 Diacetyl/Water clusters are shown in order of increasing relative energy

The four lowest energy structures, 3W-A, 3W-B, 3W-C, and 3W-D, all involve three water molecules that are coordinated in an arc, beginning with a water molecule

hydrogen bonded to a carbonyl oxygen. The four structures have the largest differences in the rotations of the water molecules involved in the hydrogen bonds. The structures 3W-A, 3W-B, and 3W-D all have this arc of water molecules starting on the lateral side of the carbonyl, and the hydrogen bond network finishes its progression in the medial direction. The 3W-C structure, however, has the hydrogen bond network arcing in the opposite direction, initiating on the medial side and finishing in the lateral direction. The 3W-E and 3W-F structures, the next two lowest in energy, have two water molecules coordinated to a carbonyl and the third water molecule coordinated with the other carbonyl oxygen. The pair of water molecules come out of the plan of the carbon backbone while the singular water molecule is in the plane of the backbone. This singular water molecule engages in favorable electrostatic interactions with the adjacent methyl group through the hydrogen atom in the plane of the carbon backbone for 3W-E and through the two hydrogen atoms going into and out of the plane in 3W-F. In 3W-G and 3W-I, a water molecule is hydrogen bonded to one of the carbonyl oxygens and is also coordinated to the other two water molecules. For 3W-G, these water molecules come out of the plane of the backbone, and for 3W-I, these water molecules are located medial to the carbonyl oxygen. The structure in-between these two, 3W-H, is like the structures presented in 3W-E and 3W-F, except the singular water molecule is coordinate to the same carbonyl as the pair of water molecules. The final three structures, 3W-J, 3W-K, and 3W-L, all include hydrogen bonding within the plane of the carbon backbone. For each of the structures, two of the water molecules are coordinated together and the third is hydrogen bonding alone. In 3W-J and 3W-K, this third water molecule is hydrogen bonding to a different carbonyl than the paired water molecules. For 3W-L, the singular water molecule is hydrogen bonded to the

same carbonyl as the paired water molecules. The relative energies, which account for the order and naming of the structures, that result from these structural differences are shown in the table below.

Structure	MP2	B3LYP
3W-A	0.00	0.00
3W-B	0.07	0.19
3W-C	0.16	0.75
3W-D	0.29	0.20
3W-E	3.84	4.70
3W-F	3.91	4.88
3W-G	4.28	4.47
3W-H	5.36	5.90
3W-I	5.61	4.44
3W-J	6.58	4.72
3W-K	6.99	5.29
3W-L	7.26	5.79

Table 3.10: The relative energies of the 1/3 Diacetyl/Water clusters are given in kcal/mol for both B3LYP and MP2 optimized geometries.

Although both the B3LYP and MP2 methods determined that 3W-A was the lowest energy structure and that 3W-B was the second lowest in energy, there is discrepancy in the ordering of the following structures. Especially pertinent was the determination of the true ordering of structures 3W-A, 3W-B, 3W-C, and 3W-D, as these structures were all within 1 relative kcal/mol. In order to clarify these relative energy values, the additional methods of B3LYP-D3, M06-2X, M06-2X-D3, and ω-B97XD were used alongside the single-point energy calculations on the B3LYP and MP2 optimized geometries.

Method	3W-A	3W-B	3W-C	3W-D
B3LYP	0.00	0.19	0.75	0.20
B3LYP-D3	0.00	0.05	0.06	0.25
M06-2X	0.00	0.02	-0.11	0.27
M06-2X-D3	0.00	0.02	-0.13	0.27
MP2	0.00	0.07	0.16	0.29
ω-B97XD	0.00	0.04	0.00	0.14
*B3LYPgeom-rCCSD(D)	0.00	-0.11	-0.06	0.17
*MP2geom-rCCSD(D)	0.00	0.05	-0.11	0.35

Table 3.11: The relative energies of the 1/3 Diacetyl/Water clusters are given in kcal/mol for both B3LYP and MP2 optimized geometries. *Denotes a single-point energy computation.

Instead of the triple zeta basis set that was used for the 1/1 and 1/2 Diacetyl/Water complexes, only a double zeta basis set was used for the single-point energy calculations of the B3LYP and MP2 optimized geometries due to time and computational cost constraints. All of the methods except B3LYP place 3W-D as being the highest in energy relative to 3W-A, 3W-B, and 3W-C. However, there are discrepancies as to how 3W-A, 3W-B, and 3W-C should be ordered. As the entirety of this thesis follows the example set by Dargent et. al. and the precedent of using the MP2 method to order the structures has been set, the original order according to the MP2 method was maintained. It can be seen that the structure denoted as 3W-C is calculated to be lower in energy than 3W-A by four of the eight methods used and equivalent to 3W-A by one of the methods, though. Additionally, the single-point energy calculation of the B3LYP optimized structure determined that 3W-B was the lowest in energy. 3W-A and 3W-B differ in the dihedral angles of the hydrogen bonds between the water molecules, so the difference in energies that was determined by the different methods could result from the experimental information that B3LYP uses to qualify its calculations as a DFT method. 3W-C has the water molecules arranged on the opposite side of the carbonyl than the structures presented in 3W-A and 3W-B. The methods that calculate 3W-C to be the lowest in energy are not solely DFT nor ab initio methods, so the reasoning behind this change in energetic ranking cannot be explained as simply as the 3W-B structure has been. In order to explain the possible reasoning for the differing rankings between 3W-A and 3W-C, images were constructed so that the hydrogen bond lengths and angles could be examined in the two structures. The figure below shows these values for the MP2 structure.

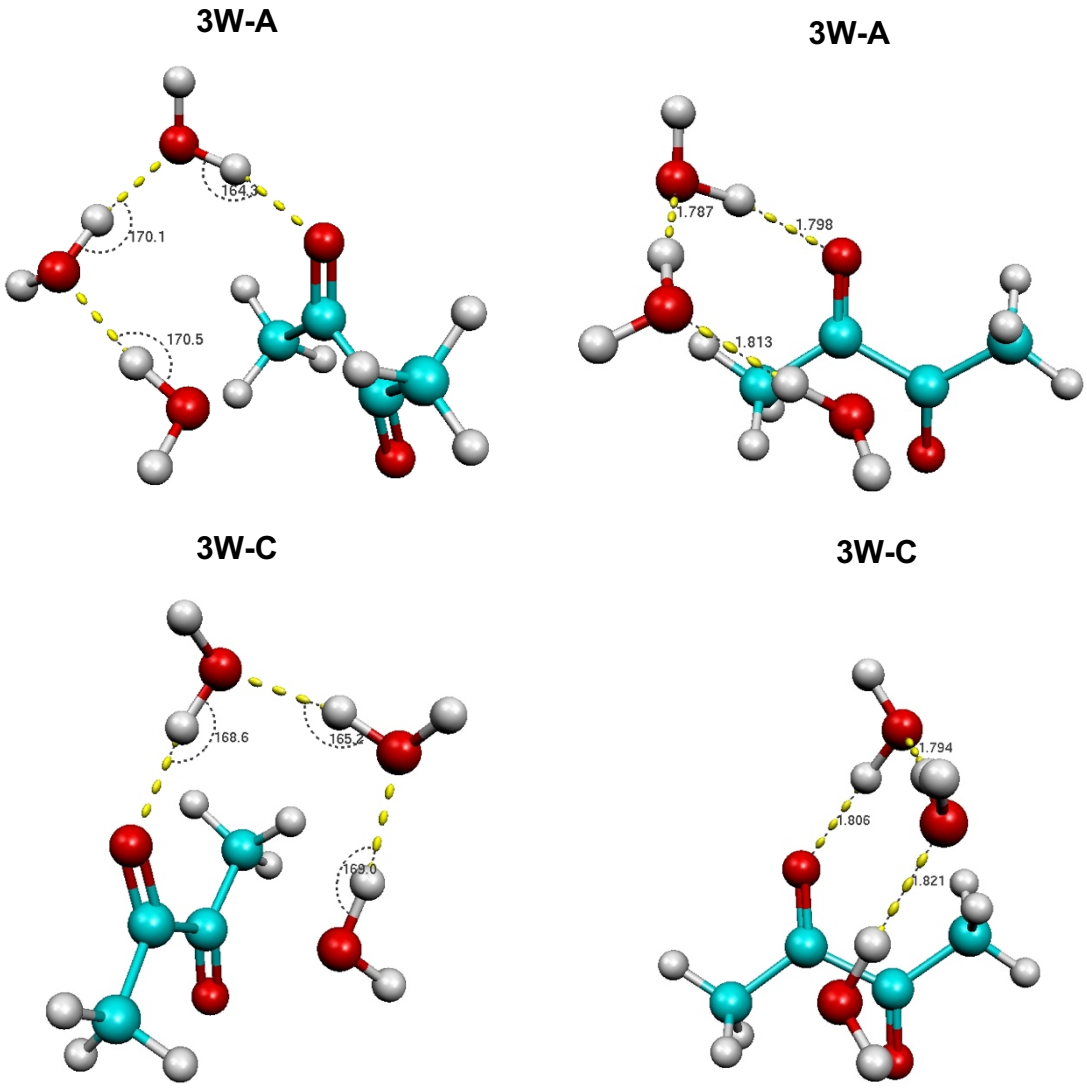

Figure 3.19: The bond angles and bond lengths of the hydrogen bond network in the MP2 optimized structures 3W-A and 3W-C are shown.

When looking at the hydrogen bond angles, the 3W-A structure appears to be more optimal, as the bonds are closer to the desired 180° than in 3W-C[50]. Additionally, the hydrogen bond lengths in 3W-A are shorter on average, which tends to indicate stronger hydrogen bonds[50]. The M06-2X method, and its dispersion corrected M06-2X-D3 method, were designed for better estimation of weakly correlated and noncovalent systems, so its ranking of 3W-C as lower than 3W-A is likely due to data inputted by the DFT method or

other parameters that are not included in the MP2 method[38,39]. This explanation of 3W-C being more accurate to experimental data could also be applied to the reasoning of both the single-point energy calculations placing 3W-C as the lowest energy structure. The rCCSD(T), or in this case the rCCSD(D), calculations provide an accuracy comparable to experiment[45,46]. Therefore, the true order of these structures could likely be elicited from experimental data that could not be retrieved in the time provided for this thesis. As such, the order of 3W-A below 3W-B and 3W-C is maintained because the computational information available and precedent of using the MP2 method to order structures dictate this ordering.

These energetics of the four lowest energy structures are explored further using the frequency calculations of the B3LYP and MP2 optimized geometries. The B3LYP theoretical spectra is shown first, with the frequencies of the vibrational modes detailed in the table that follows.

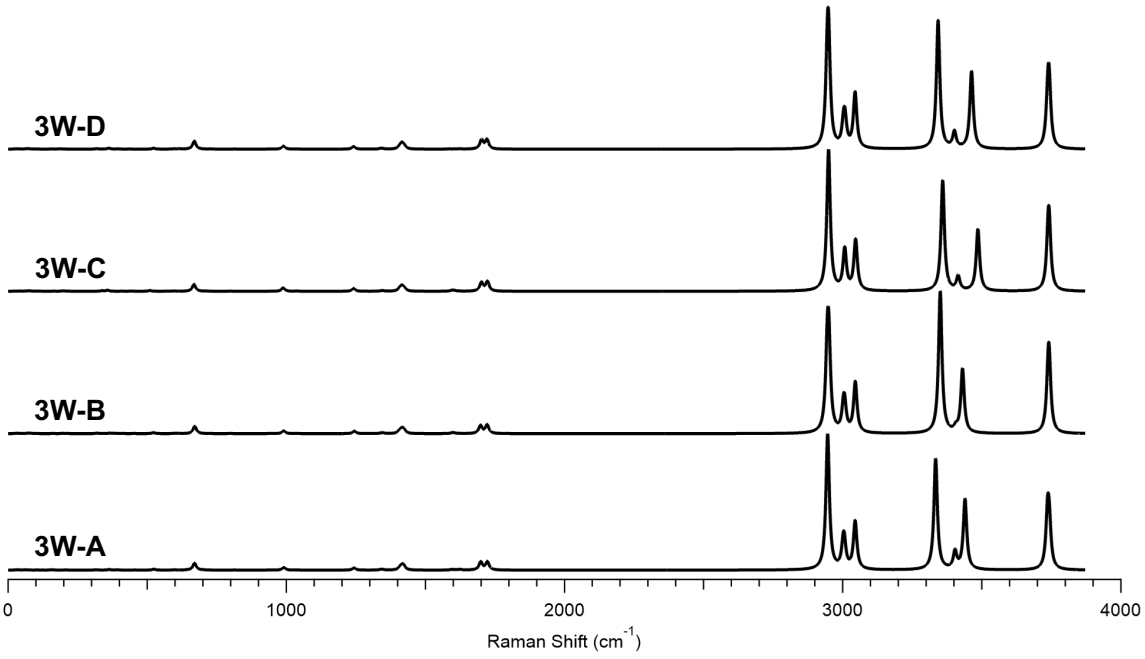

Figure 3.20: The simulated Raman spectra are shown for the B3LYP optimized 3W-A, 3W-B, 3W-C, and 3W-D structures.

The vibrational modes of the methyl groups and water molecules are very similar for the structures presented in the figure. The most notable difference is the absence of a small peak around 3400 cm^{-1} in 3W-B. It appears that this peak, located at 3406.31 cm^{-1} is being overshadowed by the peak at 3430.74 cm^{-1}. These different stretching motions of the water molecules are not as separated in 3W-B as in the other structures. This lesser separation could be due to the different dihedral angles of the hydrogen bond network that are present in 3W-B. This vibrational mode is of additional importance because the 3W-C and 3W-D structures have frequencies that are 46.30 and 23.48 cm^{-1} higher in energy than the lowest energy structure. This higher energy stretching motion of the water molecules could indicate that the hydrogen bonding network is weaker in these two structures compared to 3W-A and 3W-B[51]. The weaker hydrogen bond network would help to explain the energetic ranking of these four structures by the B3LYP method.

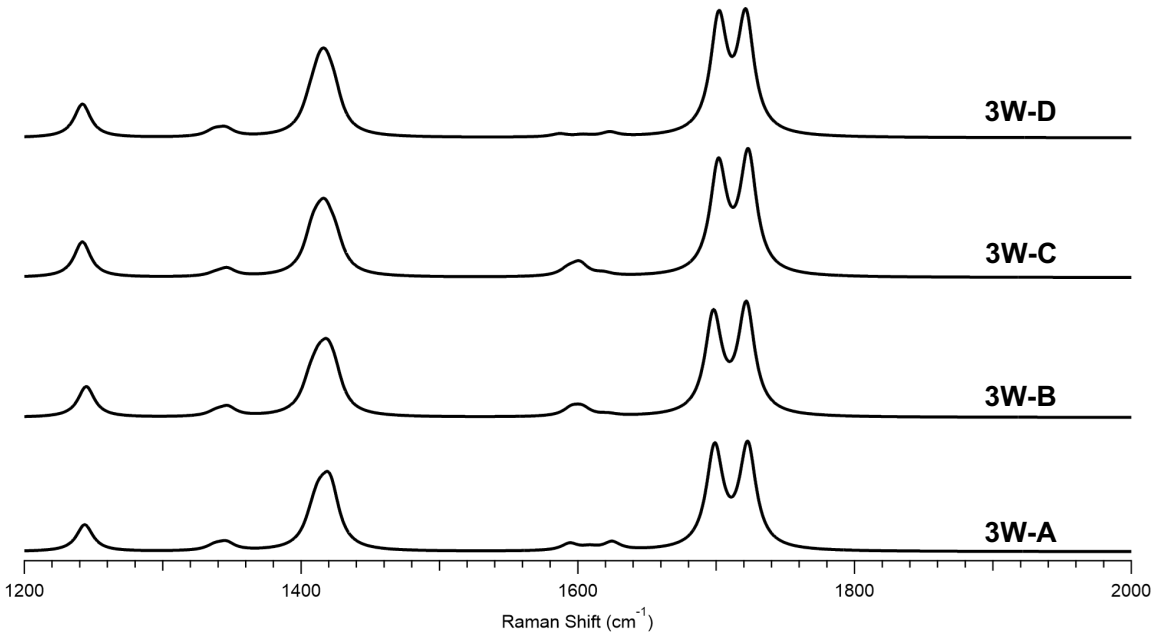

Figure 3.21: The simulated Raman spectra are shown for the B3LYP optimized 3W-A, 3W-B, 3W-C, and 3W-D structures for the range 1200 to 2000 cm^{-1}.

The carbonyl vibrational modes are shown in the figure above. As can be seen by this figure and the vibrational mode assignments in the table below, the carbonyl stretching frequencies are all very similar for the four structures. The largest difference in these vibrational modes is between 3W-B and 3W-D, and these frequencies only differ by 3.84 cm^{-1}. The four structures all coordinate the water molecules in a chain that spans one side of the carbonyl, and they all include the same number of hydrogen bonds, so similar frequency values are reasonable.

Vibrational Assignment	Vibrational Mode Description	3W-A Freq. (cm^{-1})	3W-B Freq. (cm^{-1})	3W-C Freq. (cm^{-1})	3W-D Freq. (cm^{-1})
ν_{44}	Symmetric C=O stretching; HOH wagging	1698.91	1697.99	1701.57	1701.83
ν_{45}	Asymmetric C=O stretch; HOH wagging	1722.82	1721.84	1723.19	1721.40
ν_{46}	Symmetric CH_3 umbrella	2945.35	2944.75	2948.90	2945.03
ν_{47}	Asymmetric CH_3 umbrella	2946.27	2950.41	2949.28	2949.67
ν_{48}	Asymmetric C-H Stretching	3001.56	3002.65	3006.29	3003.11
ν_{49}	Asymmetric C-H Stretching	3005.69	3006.93	3007.86	3008.39
ν_{50}	Asymmetric C-H Stretching	3044.17	3045.12	3045.82	3044.00
ν_{51}	Asymmetric C-H Stretching	3045.71	3046.22	3047.58	3045.51
ν_{52}	Symmetric O-H Stretching	3334.09	3350.65	3359.47	3342.94
ν_{53}	Asymmetric O-H Stretching	3403.75	3406.31	3415.01	3401.61
ν_{54}	Asymmetric O-H Stretching	3439.65	3430.74	3485.95	3463.13
ν_{55}	Asymmetric O-H Stretching	3735.96	3738.59	3738.52	3736.58
ν_{56}	Asymmetric O-H Stretching	3737.17	3739.38	3739.46	3740.04
ν_{57}	Asymmetric O-H Stretching	3742.86	3742.85	3742.93	3743.30

Table 3.12: The vibrational modes of 3W-A, 3W-B, 3W-C, and 3W-D as determined by the B3LYP method are given.

The MP2 optimized structures were also investigated using theoretical Raman spectra. Both the 3W-C and 3W-D show shouldering of the O-H stretching motions that does not appear in the spectra of 3W-A and 3W-B. This shouldering appears to be a result of the larger spread in the asymmetric stretching modes of the water molecules in these two structures compared to 3W-A and 3W-B.

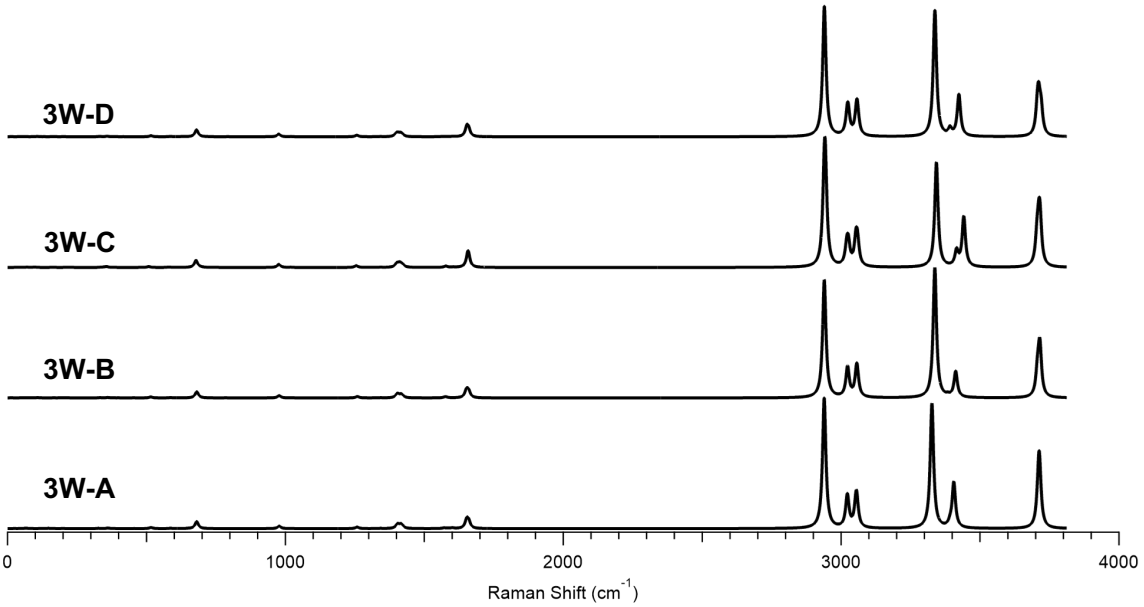

Figure 3.22: The simulated Raman spectra are shown for the MP2 optimized 3W-A, 3W-B, 3W-C, and 3W-D structures.

When the carbonyl stretching motions are investigated for the structures, there is not an obvious trend as the structures become higher in energy. 3W-B has the lowest energy carbonyl stretching mode, and 3W-D has the highest energy stretching frequency, though the difference between the motions is only 4.93 cm^{-1}. The difference between these structures can be associated with the dihedral angles of the coordinated water molecules, so the carbonyl group in 3W-B must be more stabilized due to the angle differences in the 3W-B structure. The symmetric and asymmetric carbonyl stretching frequencies have the smallest spread for the 3W-C structure, which is sensible due to its structural differences from the other three lowest energy geometries. The coordinated water molecules are more medial to the molecule, so the different carbonyl groups are more equally stabilized by the water molecules than in 3W-A, 3W-B, and 3W-D. The range of the symmetric and asymmetric stretches are visualized by the broadening of the peaks in the spectra shown below.

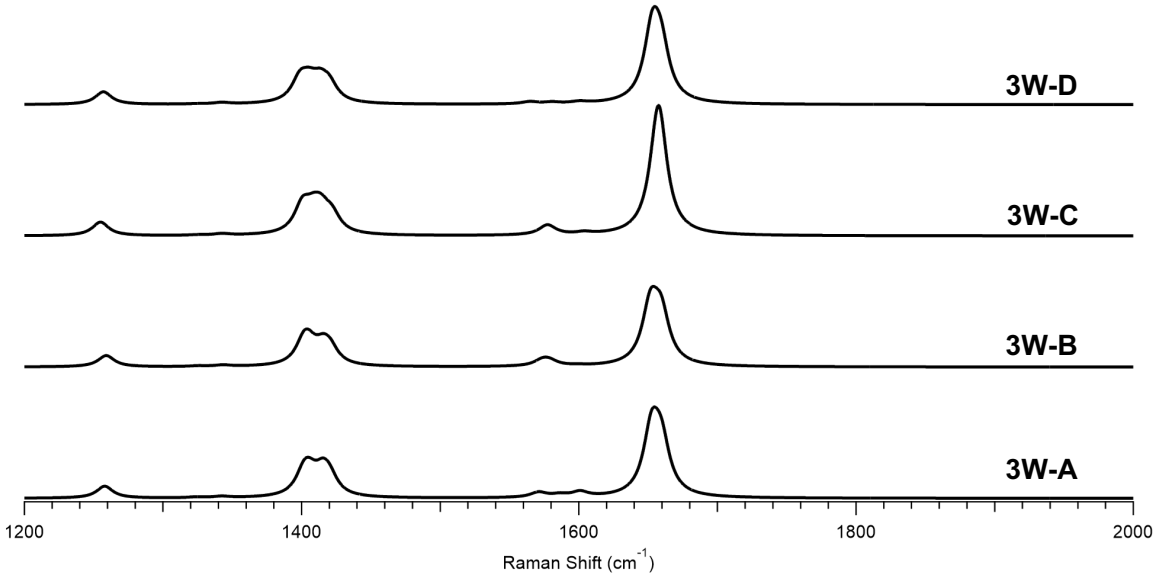

Figure 3.23: The simulated Raman spectra are shown for the MP2 optimized 3W-A, 3W-B, 3W-C, and 3W-D structures for the range 1200 to 1800 cm^{-1}.

All of the motions for the carbonyl groups, methyl groups, and water molecules are described in the table below, and their frequencies are listed according to the vibrational modes.

Vibrational Assignment	Vibrational Mode Description	3W-A Freq. (cm^{-1})	3W-B Freq. (cm^{-1})	3W-C Freq. (cm^{-1})	3W-D Freq. (cm^{-1})
ν_{44}	Symmetric C=O stretching; HOH wagging	1652.57	1651.68	1656.61	1653.02
ν_{45}	Asymmetric C=O stretch; HOH wagging	1659.60	1659.42	1657.83	1659.40
ν_{46}	Symmetric CH_3 umbrella	2939.18	2939.40	2939.60	2939.66
ν_{47}	Asymmetric CH_3 umbrella	2939.32	2939.72	2943.29	2939.91
ν_{48}	Asymmetric C-H Stretching	3021.33	3022.37	3020.36	3022.16
ν_{49}	Asymmetric C-H Stretching	3023.12	3023.73	3026.03	3025.25
ν_{50}	Asymmetric C-H Stretching	3053.54	3055.98	3053.48	3056.17
ν_{51}	Asymmetric C-H Stretching	3056.39	3057.85	3059.10	3058.91
ν_{52}	Symmetric O-H Stretching	3326.79	3337.23	3342.94	3337.42
ν_{53}	Asymmetric O-H Stretching	3391.65	3384.20	3415.60	3391.96
ν_{54}	Asymmetric O-H Stretching	3405.56	3412.28	3441.45	3423.90
ν_{55}	Asymmetric O-H Stretching	3710.20	3706.95	3705.30	3706.94
ν_{56}	Asymmetric O-H Stretching	3713.14	3714.32	3711.43	3711.30
ν_{57}	Asymmetric O-H Stretching	3713.96	3715.43	3715.65	3719.68

Table 3.13: The vibrational modes of 3W-A, 3W-B, 3W-C, and 3W-D as determined by the MP2 method are given.

3.5 1/4 DIACETYL/WATER COMPLEXES

Unlike the construction of the clusters with two and three water molecules, the construction of the four water clusters used more than just the lowest energy structures of the previous clusters to make the input geometries. The four lowest energy structures from the 1/3 Diacetyl/Water complexes (3W-A, 3W-B, 3W-C, 3W-D) as well as three additional structures (3W-G, 3W-I, and 3W-L) were used to construct the 1/4 Diacetyl/Water complexes. A water molecule was added to the already optimized geometries in locations that allowed for additional hydrogen bonding or electrostatic interactions. The inclusion of 3W-G, 3W-I, and 3W-L was centered around these hydrogen bonding and electrostatic opportunities; the three structures were chosen because they represent the different orientations of three water molecules in the 1/3 Diacetyl/Water complexes.

A total of thirty-two input geometries were constructed using these methods. Twenty-nine of these input geometries were initially optimized using the B3LYP method, and after an optimization at the aug-cc-pVTZ basis set and tight convergence level, these geometries were optimized using the MP2 method. Three of these structures that were optimized by the MP2 method were significantly different than the geometry that resulted from the B3LYP optimizations. As a result, the MP2 optimized geometries were used as input files for an additional B3LYP optimization. Through these methods, a total of twenty-three unique geometries were obtained, with the MP2 optimized structures shown below.

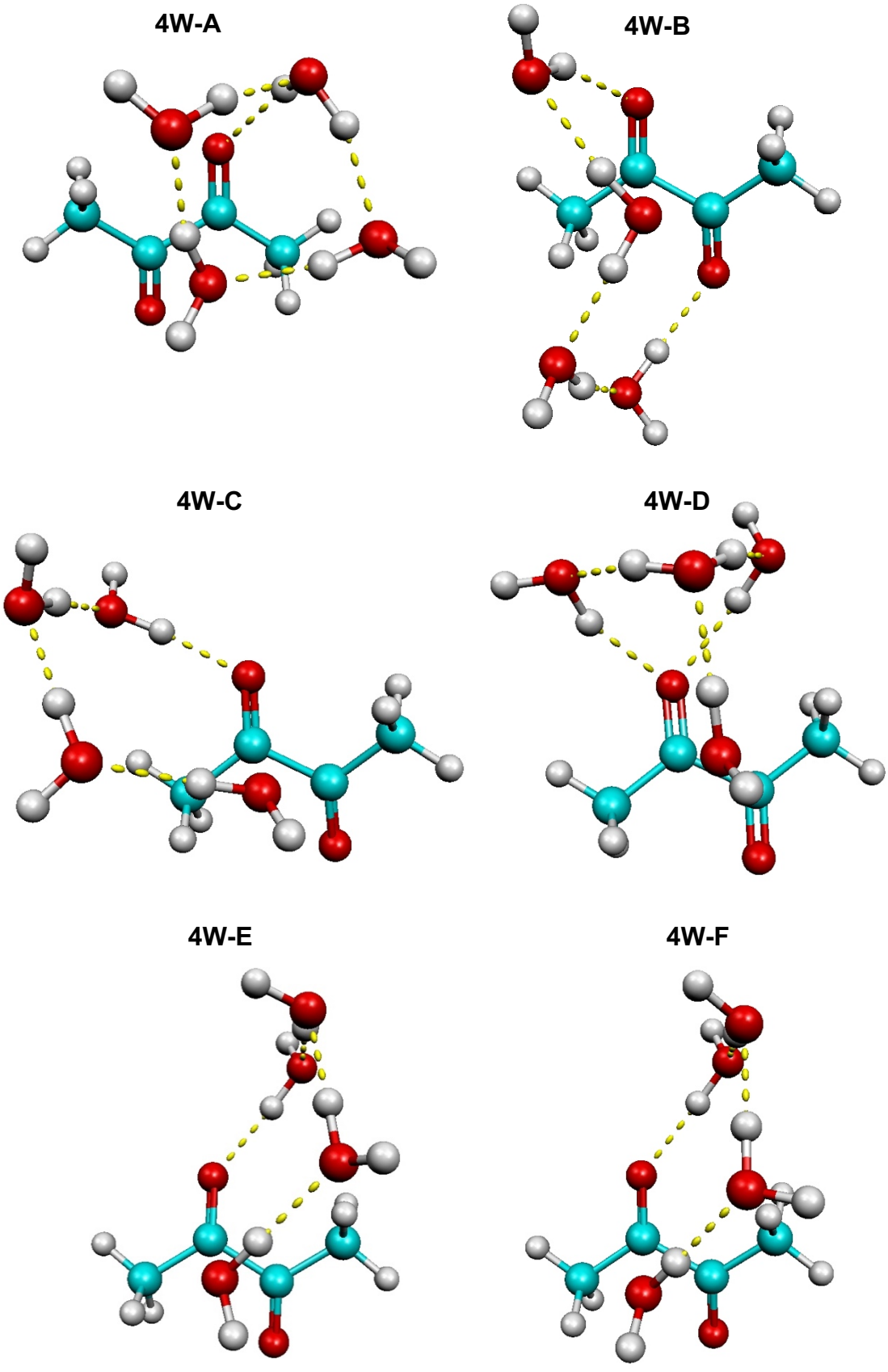
4W-A
4W-B
4W-C
4W-D
4W-E
4W-F

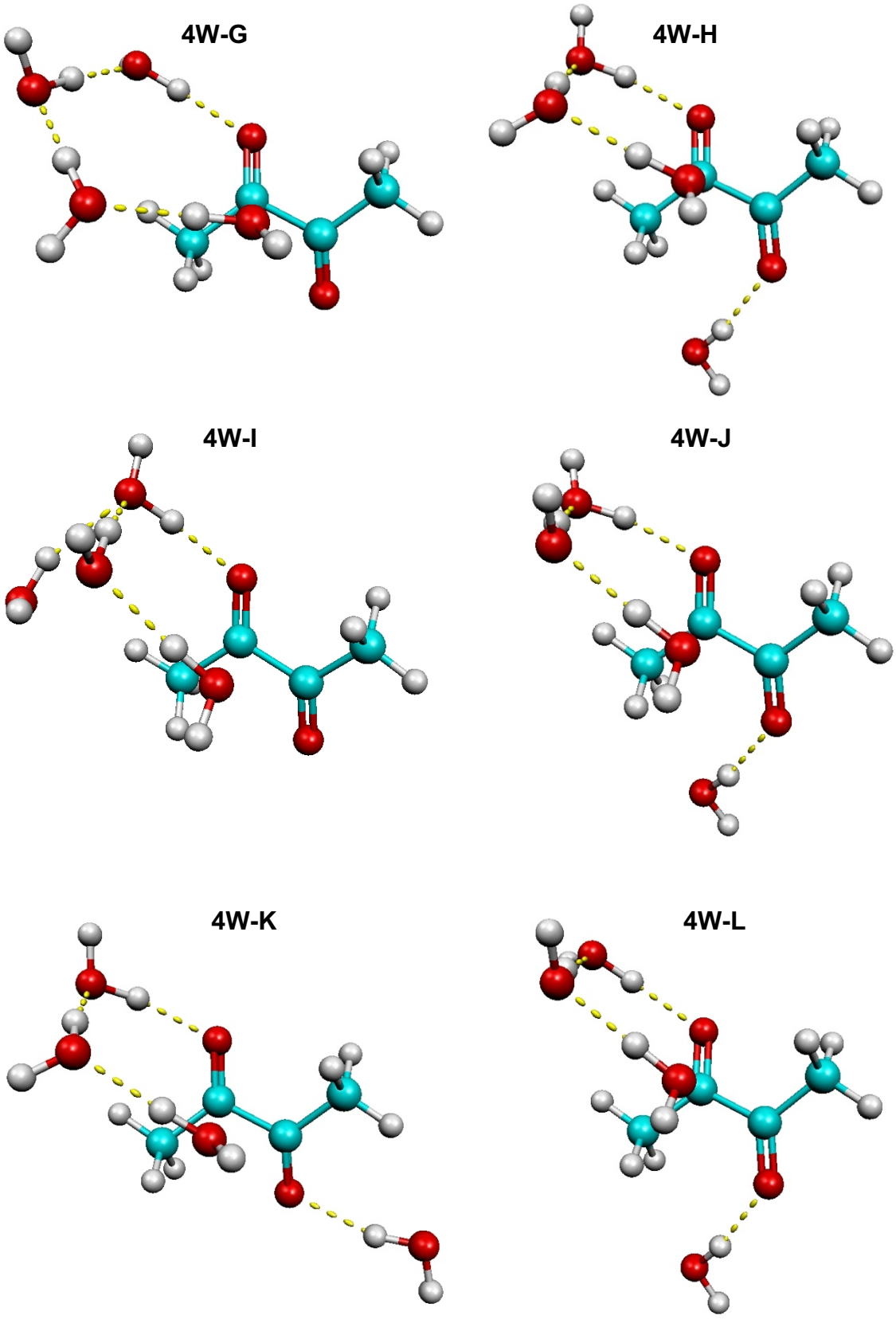
4W-G
4W-H
4W-I
4W-J
4W-K
4W-L

4W-M

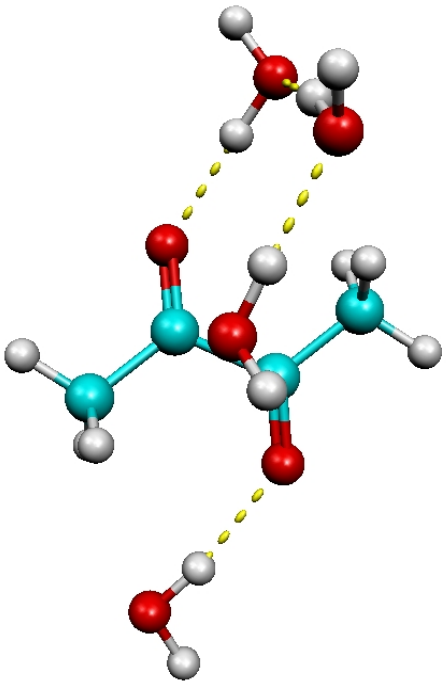

4W-N

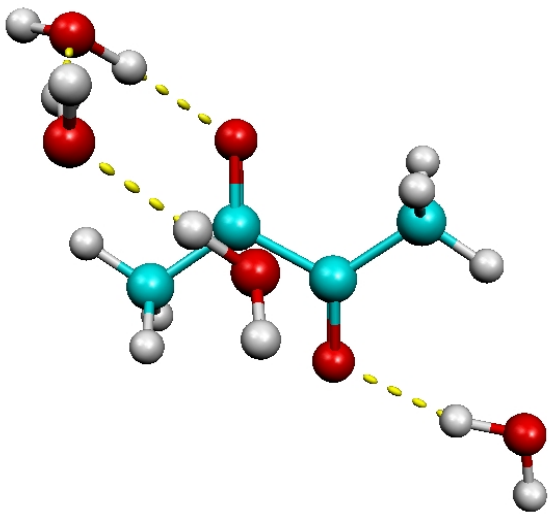

4W-O

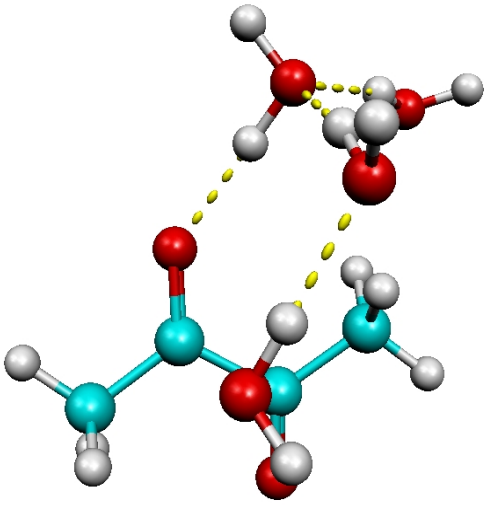

4W-P

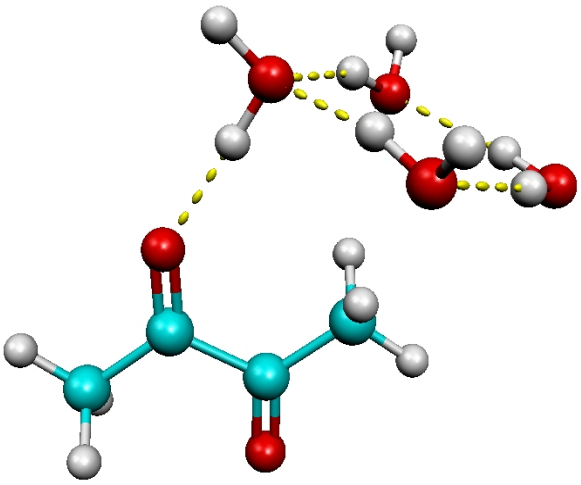

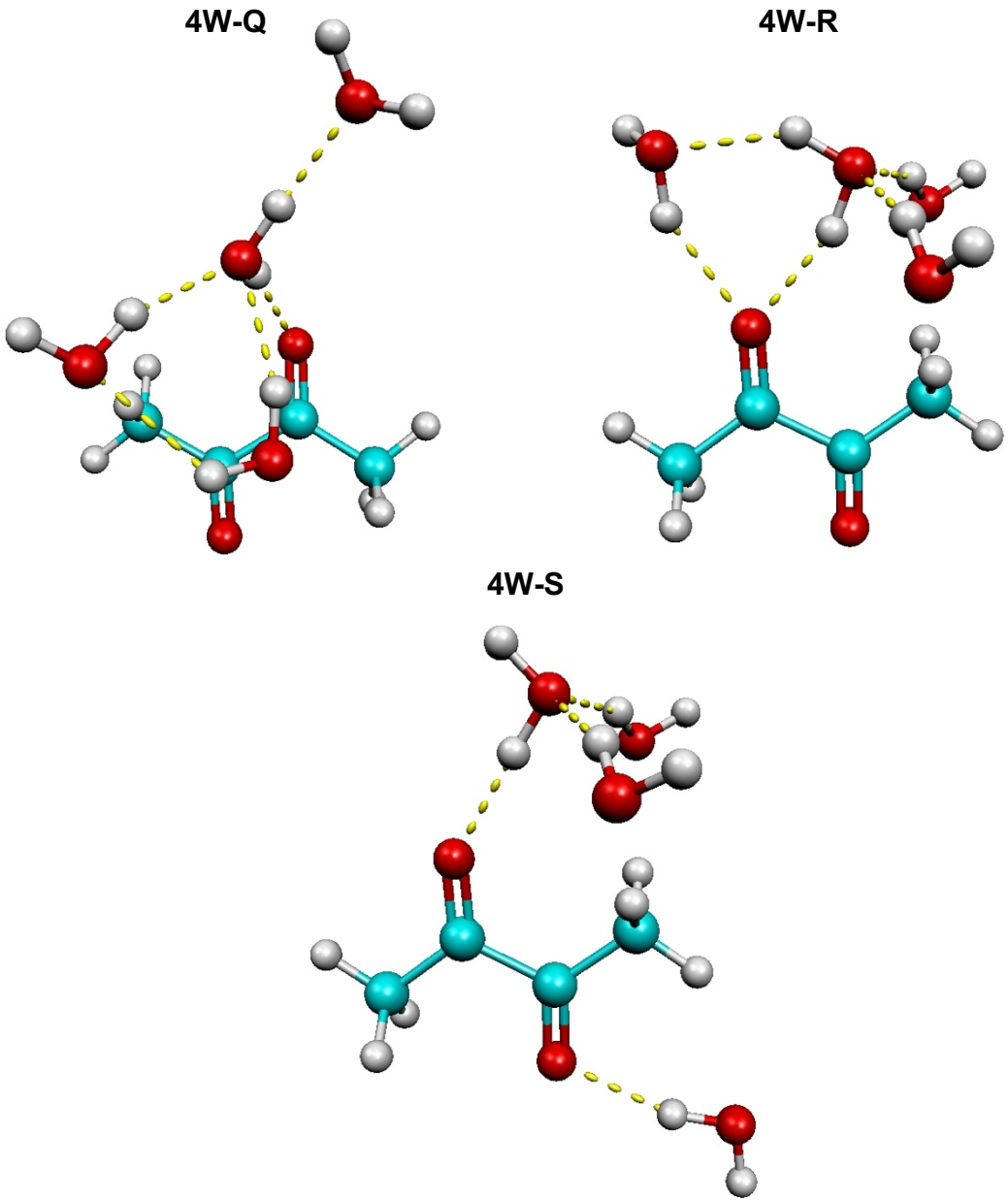

Figure 3.24: Lowest energy structures using the MP2 method for 1/4 Diacetyl/Water clusters are shown in order of increasing relative energy.

The first six structures that are presented above include all four water molecules in a hydrogen bond network. In general, the number of water molecules involved in the hydrogen bond network decreases as the energy of the structure increases. This is sensible because hydrogen bonding is a stabilizing force, and more of these interactions would lower the energy of the overall structure.

As described previously, three of the B3LYP optimized geometries became significantly different when they were optimized by the MP2 method. Because of this, the three MP2 optimized structures, shown as 4W-A, 4W-B, and 4W-D above, were used as input geometries so that B3LYP could determine the energetics of these structures as well. The initial B3LYP structures that MP2 could not optimize are shown in the figure below, and they are labeled in order of increasing energy at the end of the MP2 ordering, as this method could not detect these structures. Additionally, one of the output geometries produced by the B3LYP method could not be optimized to the tight convergence criteria, so this structure is also included in the figure below.

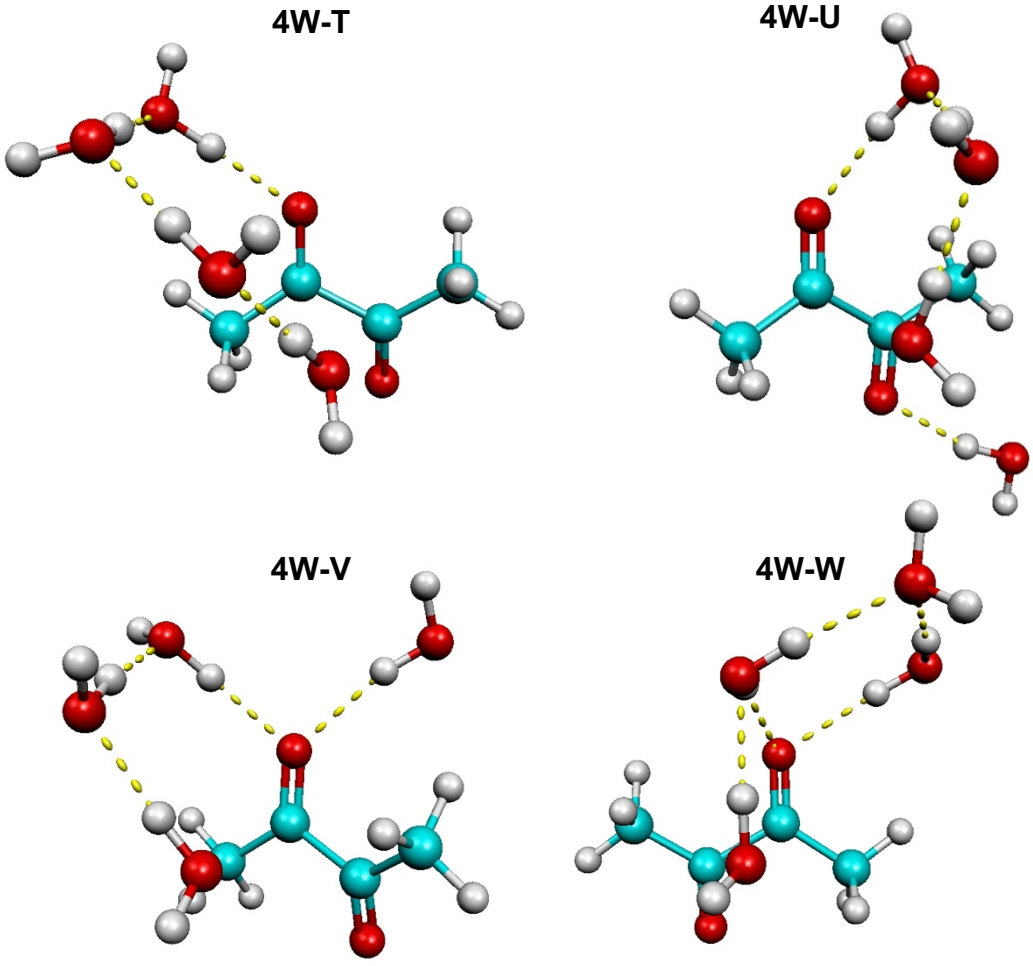

Figure 3.25: Lowest energy structures that could only be found using the B3LYP method for 1/4 Diacetyl/Water clusters are shown in order of increasing relative energy.

The 4W-T structure that could not be optimized by the MP2 method in the time available for this thesis appears to be very similar to the structures labeled as 4W-C and 4W-G with changes in the dihedral angles created by the hydrogen bonding of the water molecules. The angles of these hydrogen bonds appear sharper in 4W-T than in 4W-C and 4W-G. A figure comparing these structures and their bond lengths and angles is shown below.

The structure shown here as 4W-U was optimized by the MP2 method to become 4W-B. The structures 4W-V and 4W-W became 4W-D and 4W-A, respectively. It is unclear why 4W-U became the 4W-B structure the MP2 method optimized the structure further to, especially when similar arrangements exist in the MP2 optimized structures, like in 4W-M. However, it is likely that the MP2 method calculated the arrangement shown in 4W-U as being too destabilizing, and for this reason, it optimized the structure further to 4W-B. The reason for why 4W-V optimized to 4W-D is not clear either, though it should be noted that the increase in hydrogen bonds likely means the structure was more stable. Finally, 4W-W also resulted in an increase in hydrogen bonding between water molecules when the MP2 method optimized this structure. The resultant structure was therefore more energetically favorable, as can be seen by the relative energies listed for all twenty-three unique 1/4 Diacetyl/Water Complexes shown in ***Table 3.14***. These three structures that the MP2 method optimized 4W-U, 4W-V, and 4W-W down to were then used as new input geometries for the B3LYP method to optimize. The input geometries that resembled the MP2 structures 4W-A, 4W-B, and 4W-D were optimized by the B3LYP method to structures that resembled the input. This is shown by the relative energies listed under the B3LYP method for these three structures.

Structure	MP2	B3LYP
4W-A	0.00	0.00
4W-B	1.92	3.81
4W-C	2.18	1.13
4W-D	2.25	3.71
4W-E	2.28	2.07
4W-F	2.29	1.98
4W-G	2.30	1.17
4W-H	4.18	4.27
4W-I	4.28	4.26
4W-J	4.31	4.41
4W-K	4.37	4.21
4W-L	4.38	4.33
4W-M	4.53	5.11
4W-N	4.79	4.48
4W-O	4.91	5.30
4W-P	7.00	6.62
4W-Q	7.41	7.158
4W-R	8.95	8.008
4W-S	10.63	9.168
4W-T	-------	0.525
4W-U	-------	4.921
4W-V	-------	5.708
4W-W	-------	8.157

Table 3.14: The relative energies of the 1/4 Diacetyl/Water clusters are given in kcal/mol for both B3LYP and MP2 optimized geometries.

While the trend of the structures shows that the lowest energy structures have the most water molecules involved in hydrogen bonding with one another, 4W-O, 4W-P, 4W-Q, and 4W-R all have their four water molecules involved in hydrogen bonding interactions with one another. The increase in energy for these structures could be due to the length of the hydrogen bonds or the magnitude of hydrogen bond angles that could be straining the water molecules.

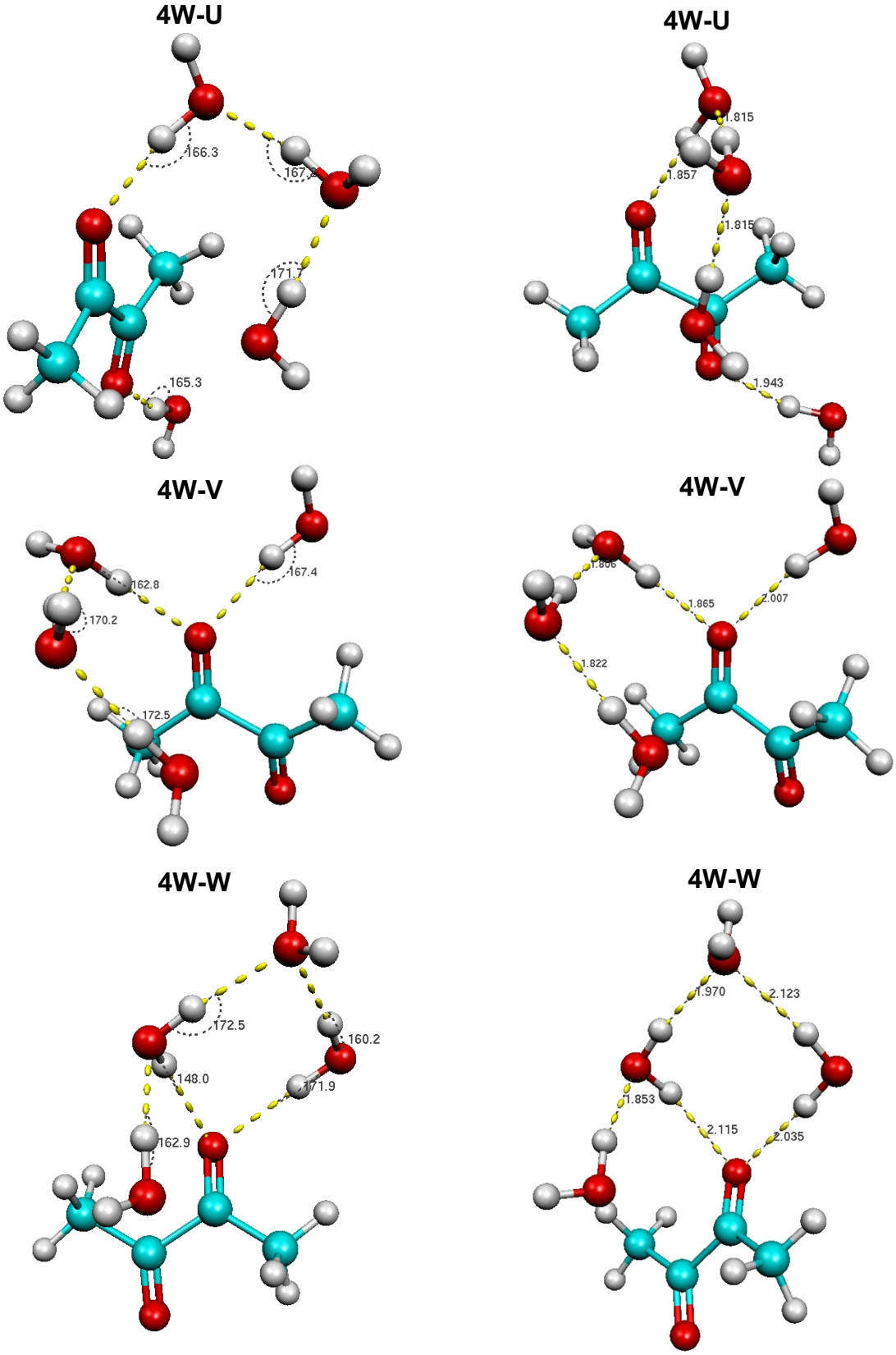

Figure 3.26: The hydrogen bond angles and lengths of 4W-U, 4W-V, and 4W-W are shown.

All of the bond lengths for the hydrogen bonds in the three structures are of a reasonable length. The most notable destabilizing force can be seen in the bond angles of the three structures. The favored hydrogen bonding angle is 180°, yet the bond angles in 4W-U, 4W-V, and 4W-W are more acute than this[50]. In fact, in structure 4W-W, one of the hydrogen bonds has an angle of 148.0°, and this large deviation is likely why this structure has the highest relative energy of the B3LYP optimized structures. These bond angles could also be why the MP2 method did not optimize these structures as the B3LYP method did.

Nevertheless, both the MP2 and B3LYP methods determined the lowest energy structure to be 4W-A. This structure includes the four water molecules involved in hydrogen bond interactions in a rhombus nature. The ordering of the subsequent structures is not agreed upon by the two methods, so as was done with the other complexes, additional methods were used to determine the relative energetics of the lowest energy structures. Due to time constraints and computational cost, the single-point energy calculations were not included in these methods.

Method	4W-A	4W-B	4W-C	4W-D
B3LYP	0.00	3.81	1.13	3.71
B3LYP-D3	0.00	1.91	2.28	2.20
M06-2X	0.00	1.52	1.33	1.44
M06-2X-D3	0.00	1.52	2.78	1.42
MP2	0.00	1.92	2.18	2.25
ω-B97XD	0.00	2.36	2.38	2.36

Table 3.15: The relative energies of the 1/4 Diacetyl/Water clusters are given in kcal/mol for both B3LYP and MP2 optimized geometries. *Denotes a single-point energy computation.

Frequency calculations were desired for both the MP2 and B3LYP optimized structures. However, time constraints the calculations of the MP2 geometries. As a result, only the theoretical for the B3LYP optimized structures are shown and discussed. In the first set of spectra presented, the lowest energy structure appears to have more separation

between the different vibrational modes of the water molecules. The range that highlights these motions of the water molecules are shown in ***Figure 3.28***.

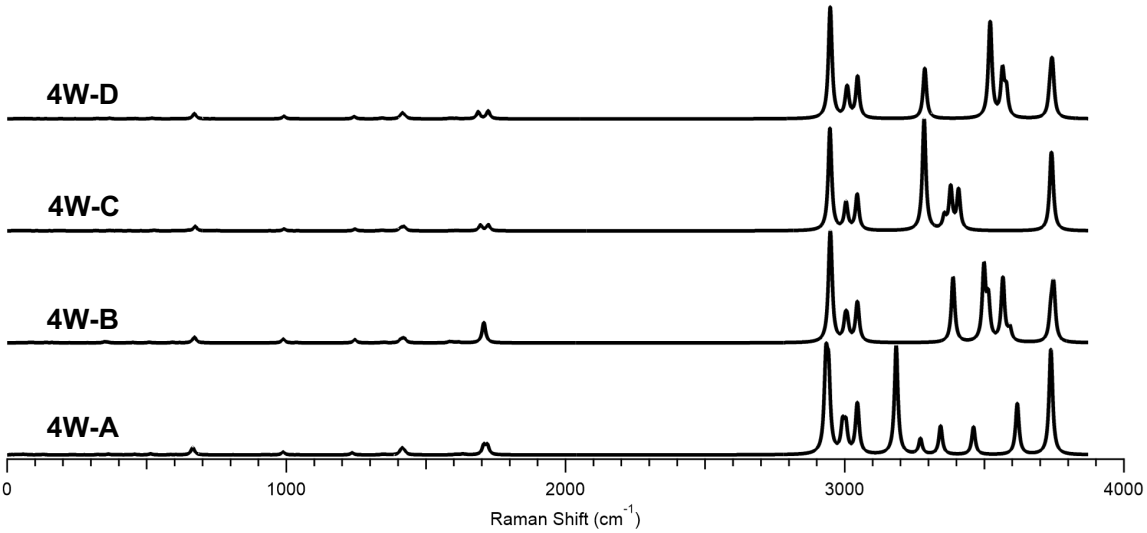

Figure 3.27: The Simulated Raman spectra are shown for the B3LYP optimized structures 4W-A, 4W-B, 4W-C, and 4W-D.

As can be seen in the figure below, there is slight blue shifting for the C-H stretching modes as the energy of the 1/4 Diacetyl/Water structure increases. It is possible that this increase in energy of the vibrational modes associated with the methyl groups is resulting from electrostatic interactions with the oxygen atom of nearby water molecules.

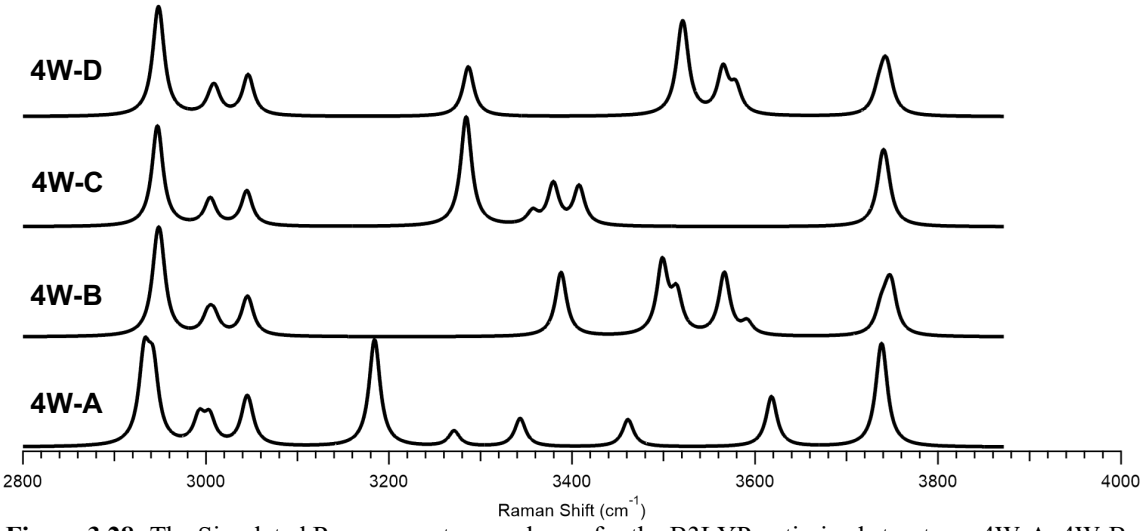

Figure 3.28: The Simulated Raman spectra are shown for the B3LYP optimized structures 4W-A, 4W-B, 4W-C, and 4W-D for the range 2800 to 4000 cm^{-1}.

Overall, the stretching modes of the water molecules are lower in energy for 4W-A than the other three structures. The cyclic arrangement of the water molecules in 4W-A is likely the reason behind this, as each water molecule serves as a donor and acceptor of a hydrogen bond. This especially stabilizing relationship is what leads the stretching motions to be lower in energy for the majority of these vibrational motions.

Of final interest for the simulated spectra generated from the B3LYP optimized structures are the peaks associated with the carbonyl stretching frequencies. As can be seen in the figure below, the largest splitting of the carbonyl stretching motions is seen for 4W-D, whereas 4W-B appears to have negligible splitting (6.51 cm^{-1} between the two peaks).

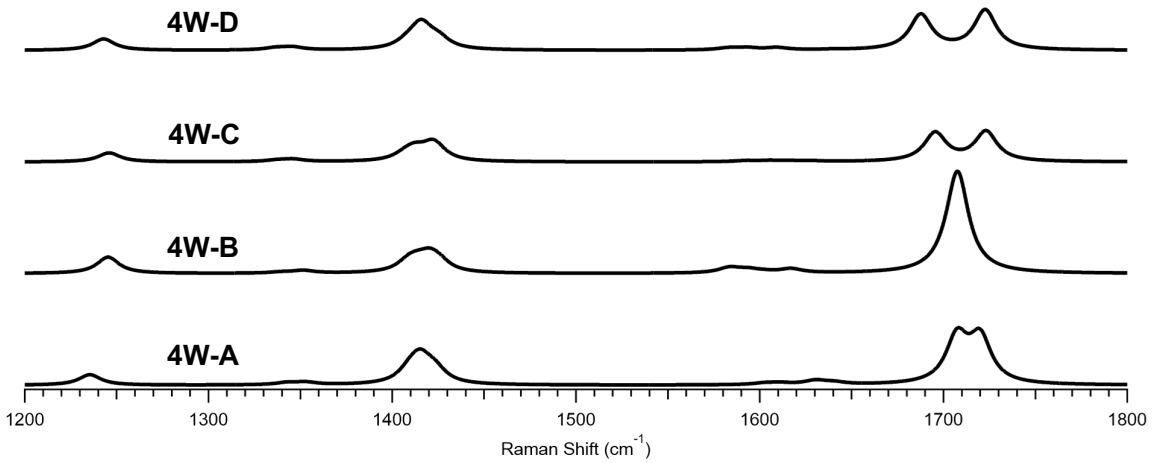

Figure 3.29: The Simulated Raman spectra are shown for the B3LYP optimized structures 4W-A, 4W-B, 4W-C, and 4W-D for the range 1200 to 1800 cm^{-1}.

The carbonyl stretching modes are centered at 1713.68, 1704.40, 1709.33, and 1705.17 cm^{-1} for 4W-A, 4W-B, 4W-C, and 4W-D, respectively. Therefore, the very different arrangements of the four water molecules that these structures propose do not seem to have large effects on the carbonyl stretching motion. However, it is noted that the lowest energy structure 4W-A has the highest energy carbonyl stretching motion. This is likely due to the fact that 4W-A only includes one hydrogen bond to an oxygen of a

carbonyl group, whereas the structures 4W-B and 4W-D, which have the lowest carbonyl stretching frequencies, have two hydrogen bonds involved with the carbonyl groups. The carbonyl stretching frequency is higher than 4W-B and 4W-D in 4W-C because it too only includes one stabilizing hydrogen bond for the carbonyl groups. The exact values of the carbonyl stretching frequencies, as well as other vibrational modes that have been discussed are listed in the table below.

Vibrational Assignment	Vibrational Mode Description	4W-A Freq. (cm^{-1})	4W-B Freq. (cm^{-1})	4W-C Freq. (cm^{-1})	4W-D Freq. (cm^{-1})
v_{51}	HB C=O stretching	1707.38	1701.14	1695.50	1687.63
v_{52}	NB C=O stretching	1719.98	1707.65	1723.15	1722.71
v_{53}	CH_3 umbrella	2932.67	2946.41	2946.68	2946.76
v_{54}	CH_3 umbrella	2942.27	2950.19	2947.09	2949.13
v_{55}	Asymmetric C-H Stretching	2992.60	3002.36	3003.37	3006.03
v_{56}	Asymmetric C-H Stretching	3003.97	3008.75	3005.75	3010.07
v_{57}	Asymmetric C-H Stretching	3043.98	3044.04	3044.49	3045.43
v_{58}	Asymmetric C-H Stretching	3047.27	3047.11	3045.20	3047.02
v_{59}	Symmetric O-H Stretching	3184.29	3388.05	3284.38	3286.72
v_{60}	Asymmetric O-H Stretching	3271.20	3498.70	3356.93	3518.87
v_{61}	Symmetric O-H Stretching	3343.35	3514.39	3379.59	3522.10
v_{62}	Asymmetric O-H Stretching	3461.20	3566.46	3407.76	3565.06
v_{63}	Asymmetric O-H Stretching	3618.07	3591.38	3738.31	3578.95
v_{64}	Asymmetric O-H Stretching	3736.28	3737.60	3739.10	3734.97
v_{65}	Asymmetric O-H Stretching	3737.89	3744.77	3739.90	3741.64
v_{66}	Asymmetric O-H Stretching	3739.91	3749.03	3743.43	3745.58

Table 3.16: The vibrational modes of 4W-A, 4W-B, 4W-C, 4W-D, and 4W-T as determined by the B3LYP method are given.

3.6 1/5 DIACETYL/WATER COMPLEXES

The construction of the clusters with five water molecules followed the procedure dictated for the 1/4 Diacetyl/Water complexes. A total of forty-two input geometries were constructed using seventeen of the output geometries from the 1/4 Diacetyl Water complexes. Like for the other complexes, these input geometries were constructed using *Gaussian 6* software by placing a fifth water molecule in locations that allowed for potential hydrogen bonding or favorable electrostatic interactions. As a result, forty-eight input geometries were constructed for the 1/5 Diacetyl/Water complexes.

As was done for the previous complexes, the goal was to have the input geometries first optimized using the B3LYP method, with the B3LYP-optimized geometries then being used as the input files for the MP2 method. However, due to time constraints, the MP2 calculations could not be completed, and only the results for the B3LYP method are discussed in this section.

The B3LYP optimizations resulted in thirty-nine unique structures, as eight of the initial input geometries either resulted in equivalent structures or were unable to optimize because the arrangement of the atoms was too energetically unfavorable for the B3LYP method to make adjustments to the structure. All of the structures were optimized to the aug-cc-pVTZ basis set with tight convergence. These forty structures are shown in the figure below.

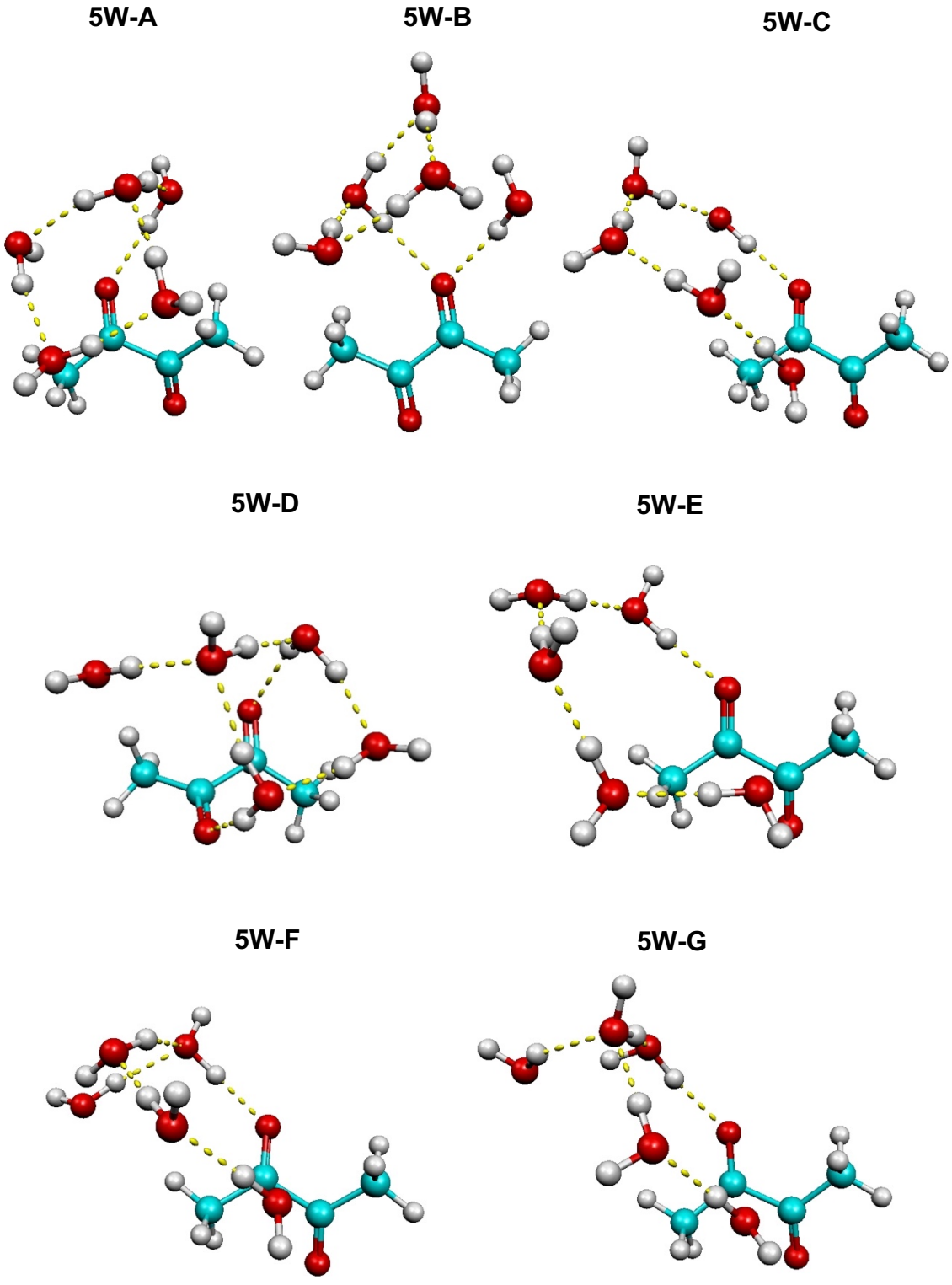
5W-A
5W-B
5W-C
5W-D
5W-E
5W-F
5W-G

5W-H

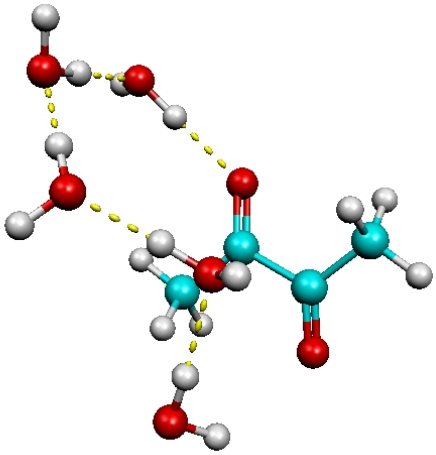

5W-I

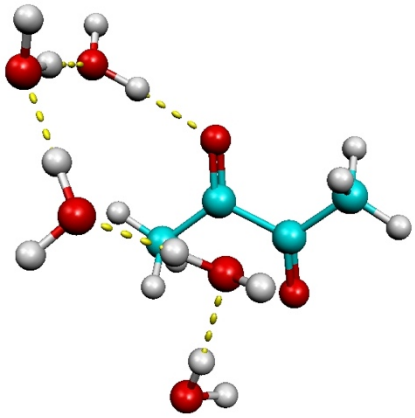

5W-J

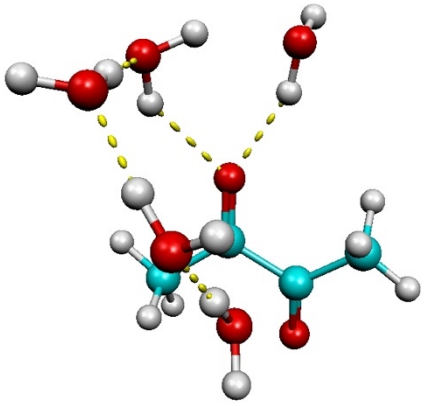

5W-K

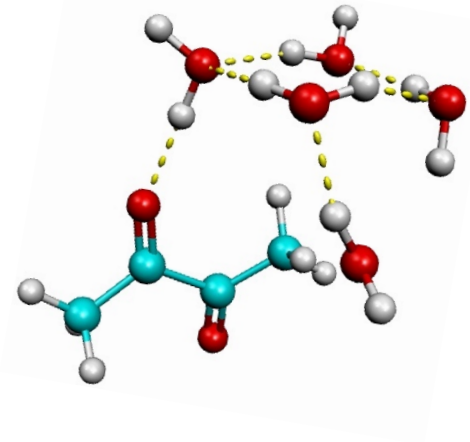

5W-L

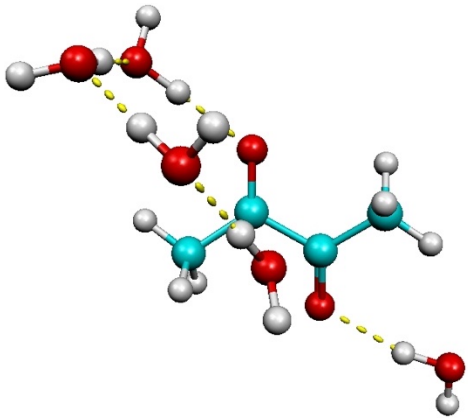

5W-M

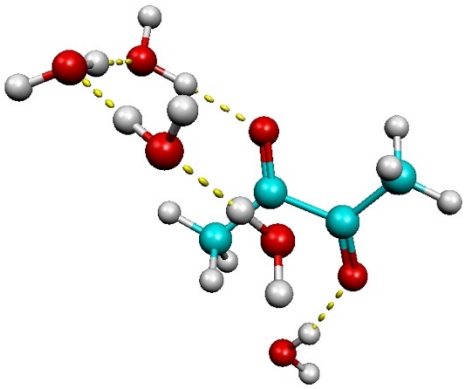

5W-N

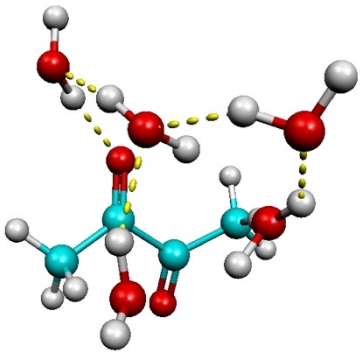

5W-O

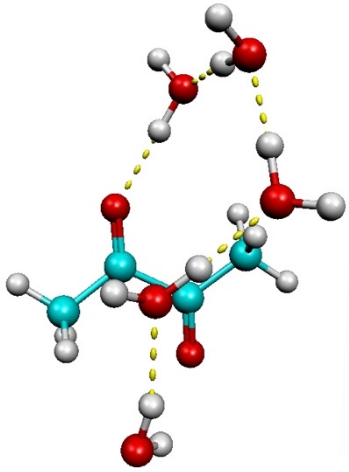

5W-P

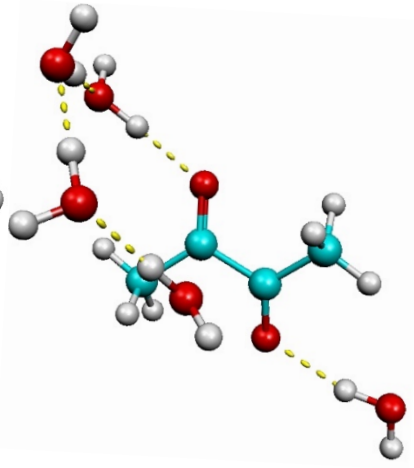

5W-Q

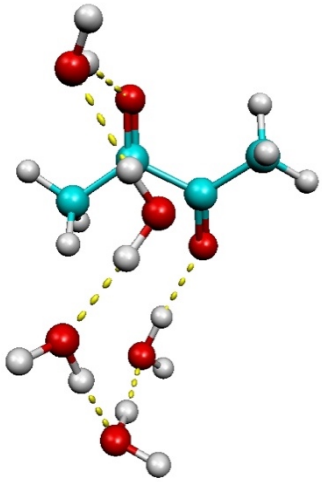

5W-R

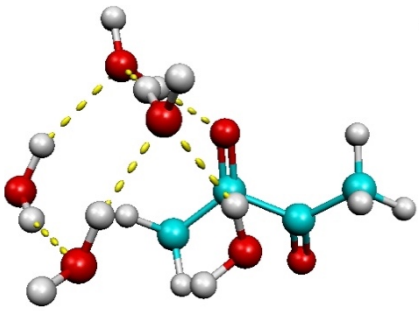

5W-S

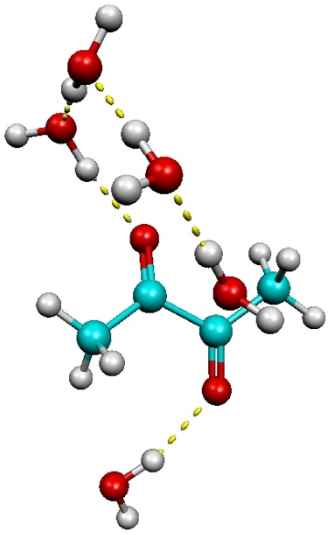

5W-T

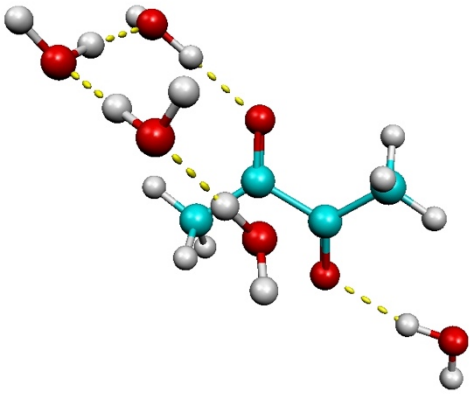

5W-U

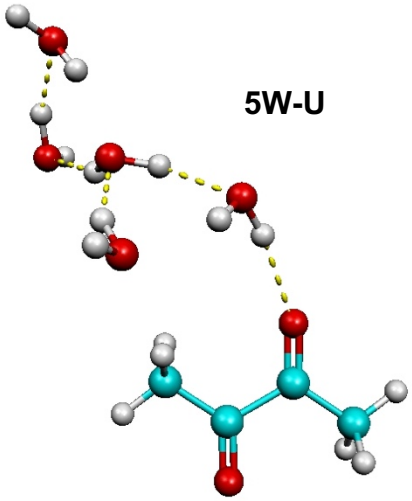

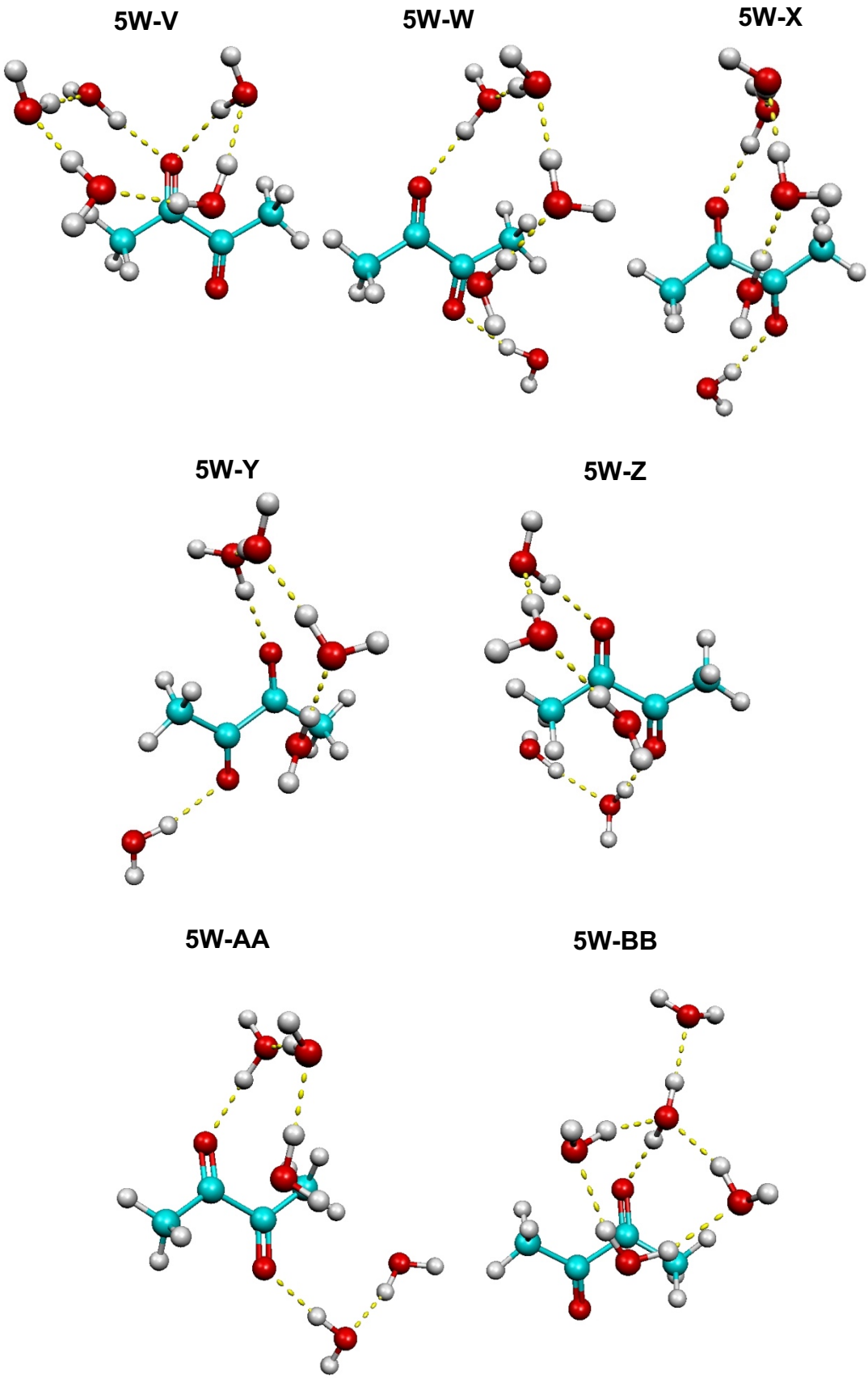
5W-V
5W-W
5W-X
5W-Y
5W-Z
5W-AA
5W-BB

5W-CC

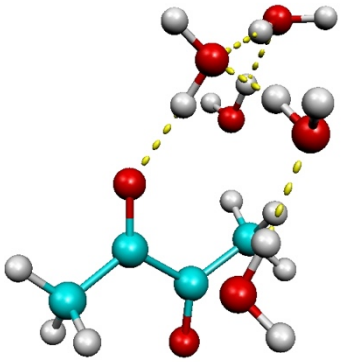

5W-DD

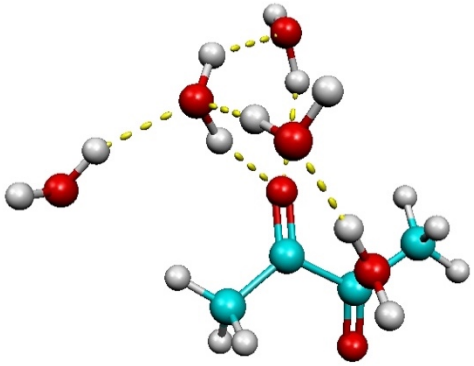

5W-EE

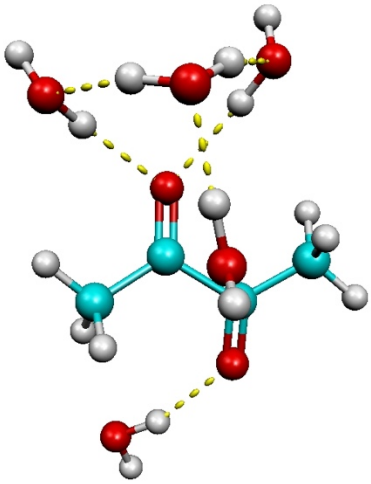

5W-FF

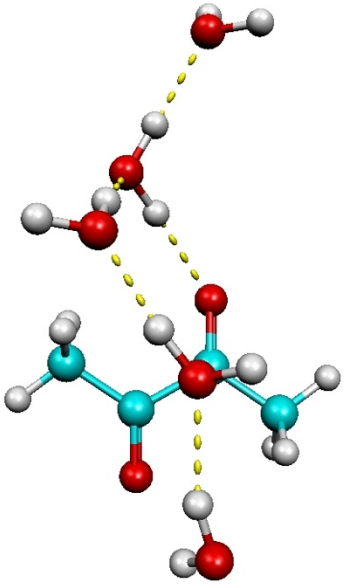

5W-GG

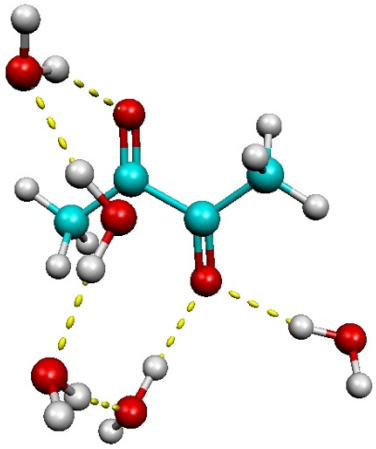

5W-HH

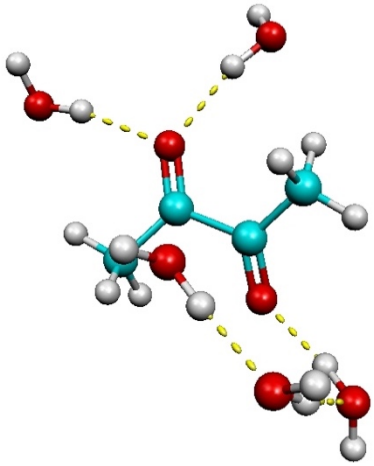

5W-II

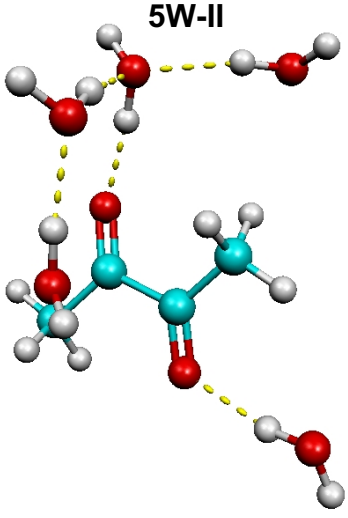

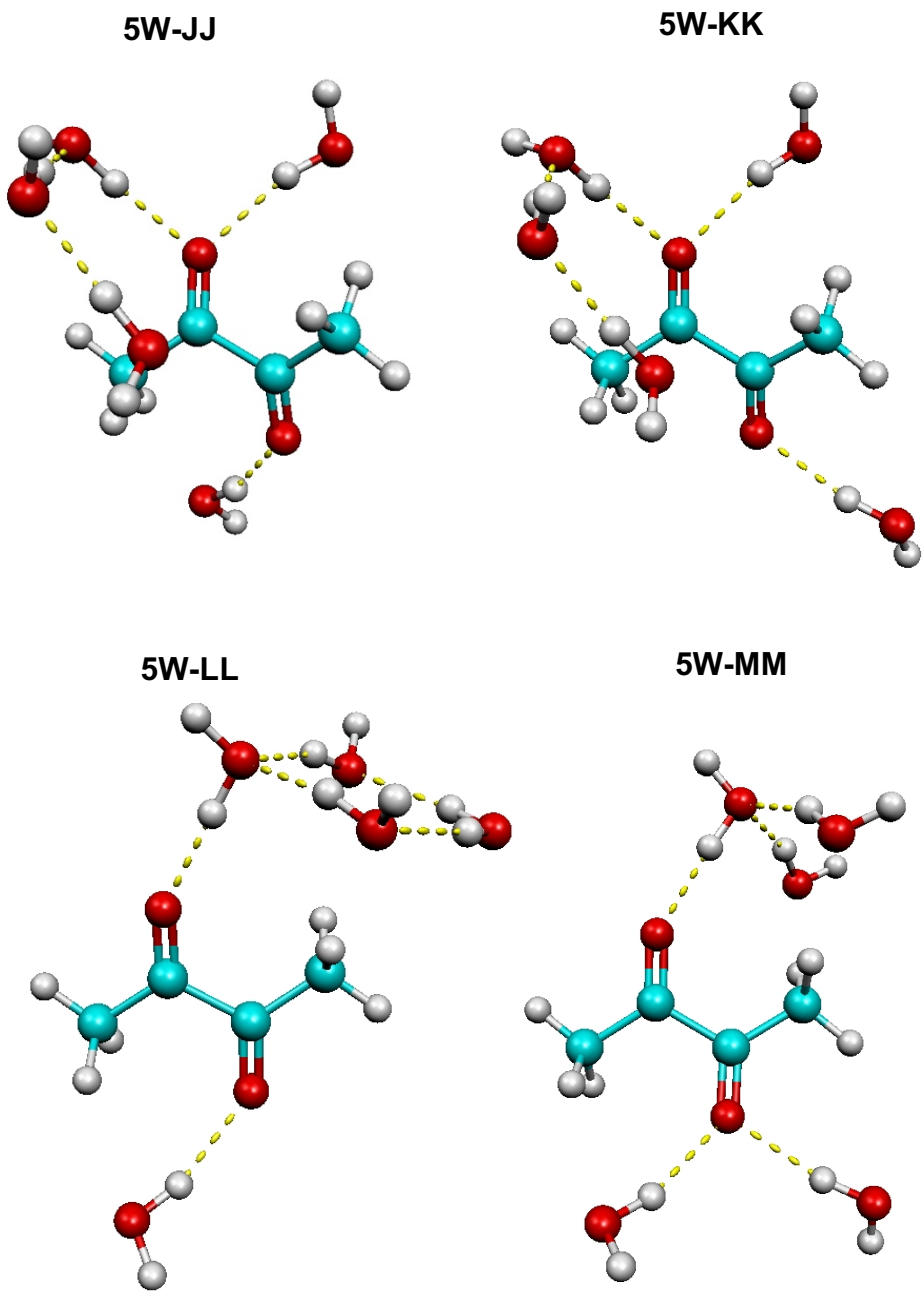

Figure 3.30: The B3LYP optimized structures for 1/5 Diacetyl/Water complexes are shown in order of increasing energy.

Because only one method was able to be used in the optimizations of the five water complexes, the table that contains the relative energy values of the structures only lists the energy in kcal/mol as determined by the B3LYP method.

Structure	Relative Energy (kcal/mol)	Structure	Relative Energy (kcal/mol)
5W-A	0.00	5W-U	4.49
5W-B	0.52	5W-V	4.59
5W-C	1.17	5W-W	4.78
5W-D	1.19	5W-X	4.88
5W-E	1.27	5W-Y	4.96
5W-F	2.02	5W-Z	5.20
5W-G	2.70	5W-AA	5.69
5W-H	2.71	5W-BB	5.81
5W-I	2.76	5W-CC	5.90
5W-J	2.95	5W-DD	6.61
5W-K	3.29	5W-EE	6.72
5W-L	3.41	5W-FF	6.78
5W-M	3.42	5W-GG	7.13
5W-N	2.70	5W-HH	7.94
5W-O	2.71	5W-II	8.25
5W-P	2.76	5W-JJ	8.49
5W-Q	2.95	5W-KK	8.91
5W-R	3.29	5W-LL	9.61
5W-S	3.41	5W-MM	12.93
5W-T	3.42		

Table 3.17: The relative energies of the 1/5 Diacetyl/Water clusters are given in kcal/mol for the B3LYP optimized geometries.

The first five structures predicted by the B3LYP method were then investigated through their simulated Raman spectra. These spectra are shown below.

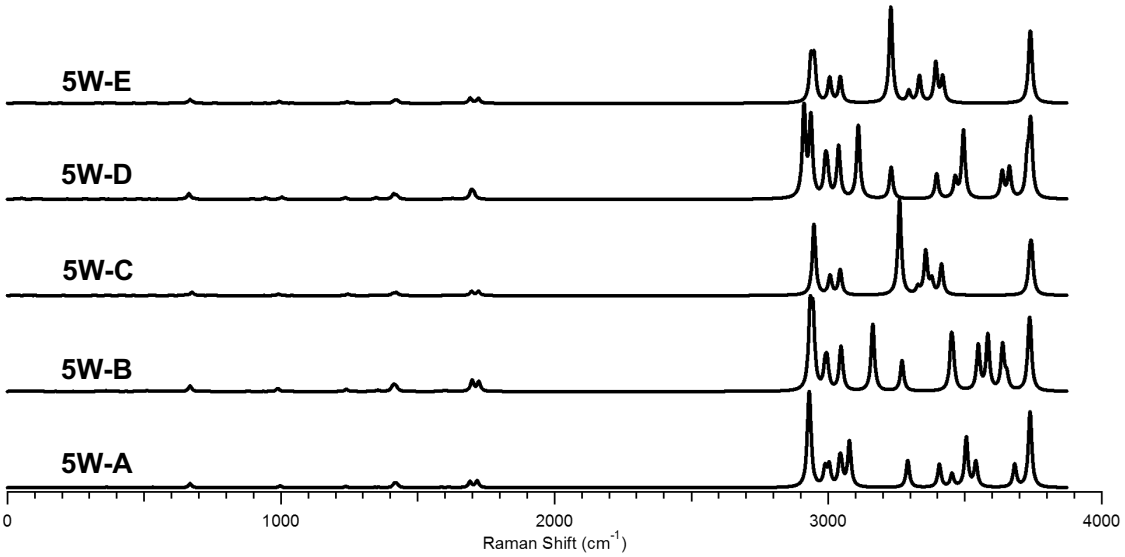

Figure 3.31: The Simulated spectra for B3LYP optimized 1/5 Diacetyl/Water complexes are shown.

In order to visualize the vibrational modes of the methyl groups and the water molecules, the above spectra were investigated between 2800 and 4000 cm^{-1}.

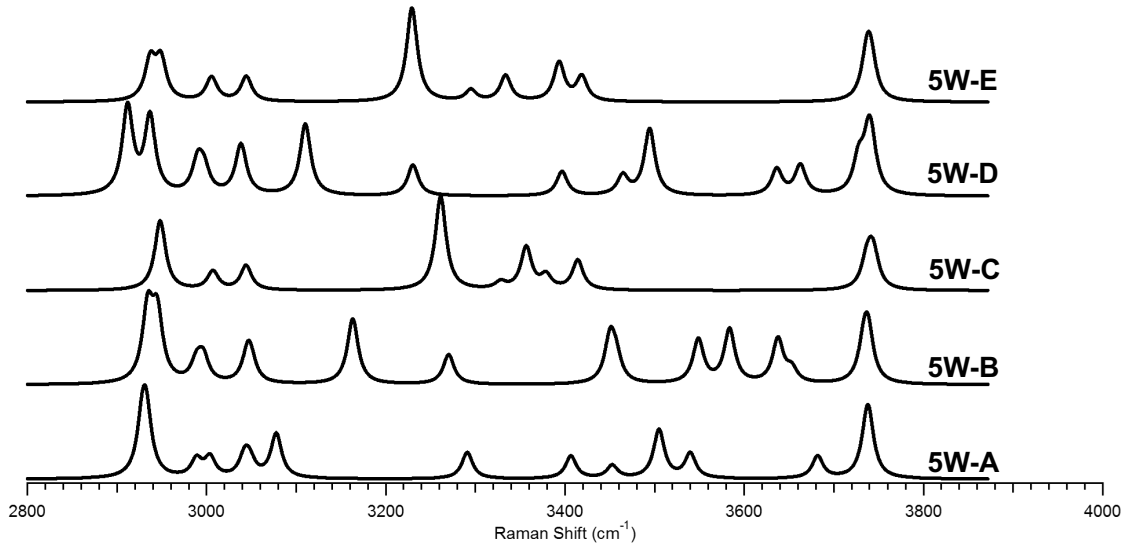

Figure 3.32: The Simulated Raman spectra for B3LYP optimized 1/5 Diacetyl/Water complexes are shown for the range 2800 to 4000 cm^{-1}.

In the final peak of the spectra, there appears to have a blue shift to higher frequency vibrations as the energy of the structure increases. The lowest energy structure must stabilize the motion described here more than the water molecules are stabilized in 5W-B, 5W-C, 5W-D, and 5W-E. Additionally, the 5W-C and 5W-E structures, which are very similar in construction, have similar Raman spectra. The 5W-E structure appears to have a greater range associated with the energies of the stretching motions of the water molecules compared to 5W-C, and these differences could result from the differing orientation of the water molecules in the chain of hydrogen bonds within the two structures. The 5W-A, 5W-B, and 5W-C structures all contain a ring of four water molecules hydrogen bonded to one another, but the variation in the connection point to the diacetyl molecule and the location of the final water molecule appear to prevent these simulated spectra from having as much similarity as the 3W-C and 3W-E spectra do.

When the carbonyl stretching frequencies are investigated further for the five structures, all but 5W-D show splitting of the peak around 1700 cm-1. This structure involves the four-water molecule ring being hydrogen bonded to both of the carbonyl groups, and as such, the energy of the vibrational motion of both oxygens is very similar. In the other four structures, only one carbonyl oxygen serves as a hydrogen bond accepting site, so the energy difference in the vibrational motions of the carbonyl groups is larger.

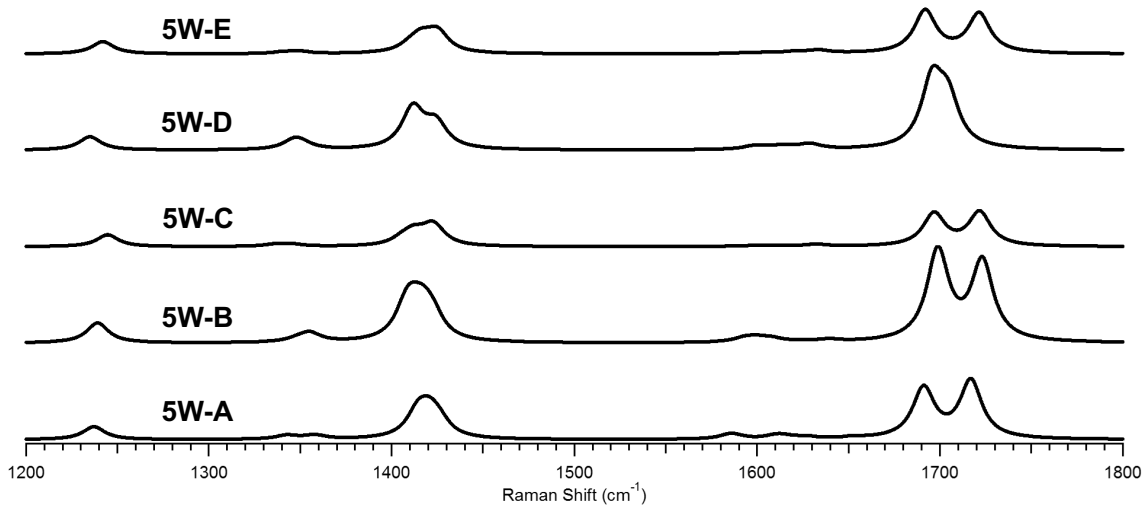

Figure 3.33: The Simulated Raman spectra for B3LYP optimized 1/5 Diacetyl/Water complexes are shown for the range 2800 to 4000 cm^{-1}.

The frequencies of all of the vibrational modes investigated for the five structures are shown in the table below. It should be noted that without additional computational methods or experimental data, the true lowest energy structure is not yet determinable, and therefore the evaluation of the vibrational frequencies of the five structures is incomplete.

Vibrational Assignment	Vibrational Mode Description	5W-A Freq. (cm^{-1})	5W-B Freq. (cm^{-1})	5W-C Freq. (cm^{-1})	5W-D Freq. (cm^{-1})	5W-E Freq. (cm^{-1})
ν_{58}	Asymmetric C=O stretching	1691.03	1698.79	1696.74	1751.74	1695.68
ν_{59}	Symmetric C=O stretching	1716.88	1723.12	1721.68	1760.76	1704.42
ν_{60}	CH_3 umbrella	2928.64	2934.32	2947.55	3008.07	2911.81
ν_{61}	CH_3 umbrella	2932.86	2944.94	2948.57	3033.89	2936.81
ν_{62}	Asymmetric C-H Stretching	2988.77	2988.85	3005.89	3088.86	2990.02
ν_{63}	Asymmetric C-H Stretching	3003.71	2996.35	3008.00	3096.33	2997.25
ν_{64}	Asymmetric C-H Stretching	3042.58	3045.99	3043.60	3138.13	3037.71
ν_{65}	Asymmetric C-H Stretching	3048.24	3049.53	3044.93	3139.6	3039.13
ν_{66}	Symmetric O-H Stretching	3077.74	3163.12	3261.22	3213.04	3110.22
ν_{67}	Asymmetric O-H Stretching	3290.91	3270.17	3328.30	3337.1	3230.31
ν_{68}	Asymmetric O-H Stretching	3406.60	3450.37	3356.74	3508.92	3396.63
ν_{69}	Asymmetric O-H Stretching	3452.69	3456.86	3378.77	3579.05	3464.52
ν_{70}	Symmetric O-H Stretching	3504.90	3548.80	3414.25	3609.98	3494.46
ν_{71}	Asymmetric O-H Stretching	3539.80	3583.64	3736.44	3756.59	3636.38
ν_{72}	Asymmetric O-H Stretching	3681.95	3637.66	3736.76	3783.71	3662.63
ν_{73}	Symmetric O-H Stretching	3735.76	3653.03	3741.75	3850.96	3727.73
ν_{74}	Asymmetric O-H Stretching	3738.18	3733.69	3742.91	3862.31	3738.72
ν_{75}	Asymmetric O-H Stretching	3739.21	3738.25	3745.43	3865.84	3742.13

Table 3.18: The vibrational modes of the B3LYP optimized 1/5 Diacetyl/Water clusters are given.

3.7 TRENDS IN THEORETICAL SPECTRA

The lowest energy structures of the 1/1, 1/2, 1/3, 1/4, and 1/5 Diacetyl/Water structures were compared with their simulated Raman spectra to elicit the effects of increasing water molecules on the vibrational modes of diacetyl and the water molecules themselves. As was done throughout this work, the theoretical Raman spectra is presented for the B3LYP optimized lowest energy structures, as well as the MP2 optimized lowest energy structures. Where there were discrepancies in the determination of the lowest energy structure by the two methods, the ordering of the structures as determined by the MP2 method was maintained. In other words, the structure that was determined to be the lowest energy by the MP2 method is shown in each of the spectra presented. This geometry

is optimized by the B3LYP method in the B3LYP spectra and optimized by the MP2 method in the MP2 spectra.

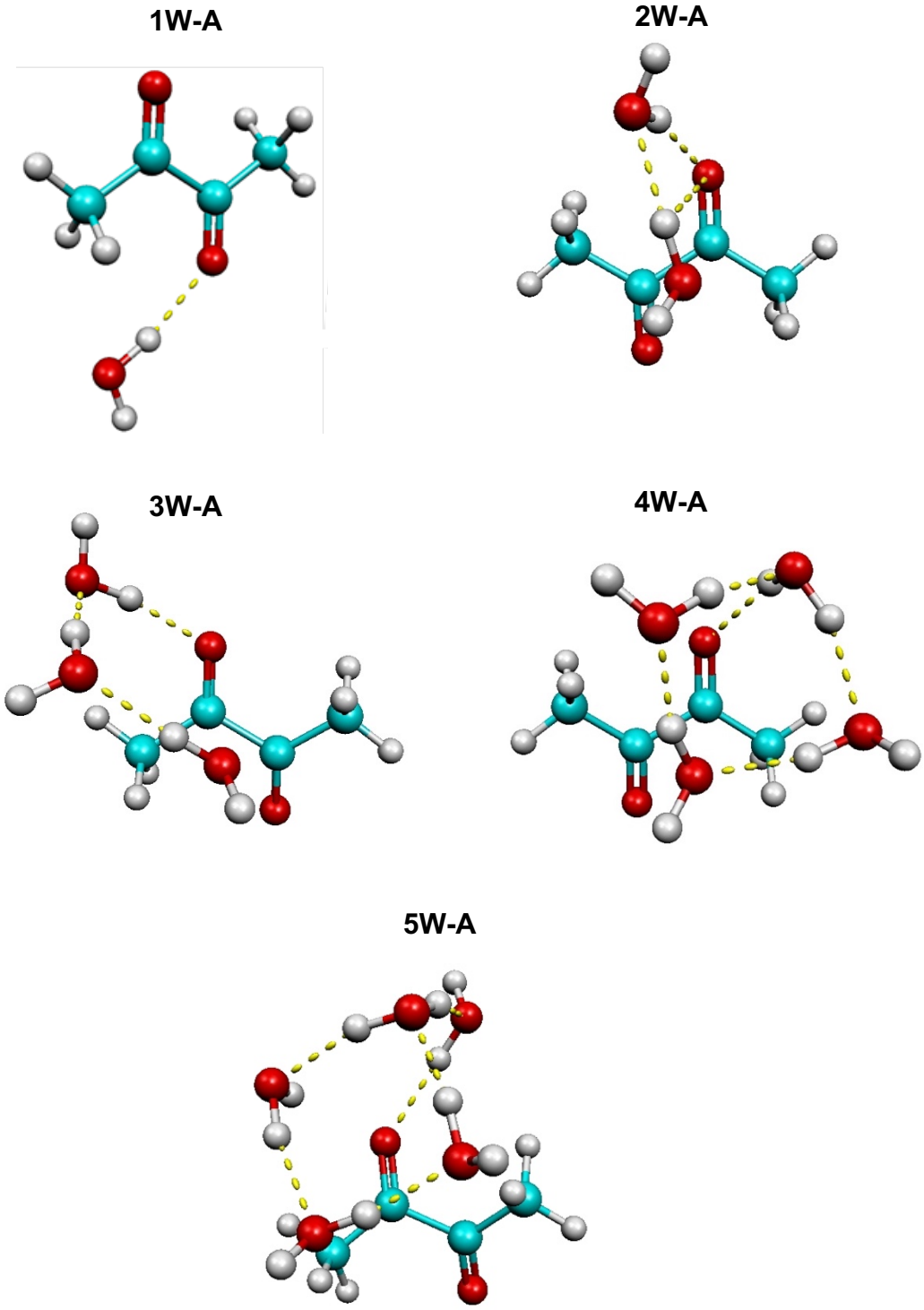

Figure 3.34: The Lowest energy structures for the 1/1 to 1/5 Diacetyl/Water structures are shown. All but the 1/5 complex are MP2 optimized. The 5W-A structure was optimized using the B3LYP method.

As the increasing number of water molecules in the higher order clusters led to an increase in the number of vibrational modes (predicted by the expression of 3n-6 for vibrational modes in a molecule), only the vibrational modes that the complexes shared or general trends in the types of motions were explored. Additionally, due to the inability to finish frequency calculations for the 1/4 Diacetyl/Water complexes and the optimizations for the 1/5 Diacetyl/Water complexes using the MP2 method, the 4W-A and 5W-A structures are omitted from the simulated Raman spectra presented for the MP2 method.

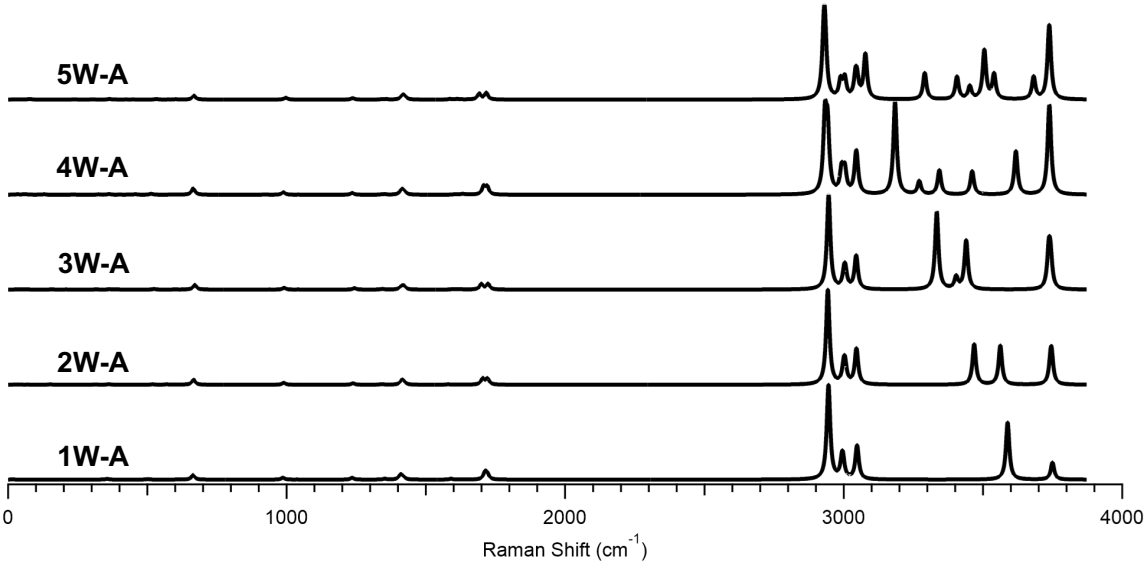

Figure 3.35: The Simulated Raman spectra for the lowest energy structures of B3LYP optimized 1/1 to 1/5 Diacetyl/Water complexes are shown.

The most notable aspect of the spectra of the five structures is the increase in the number of peaks as the number of water molecules in the complexes increases. This increase is expected because the increase in the number of atoms present allows for an additional set of vibrational motions. When the spectra are zoomed in on the range where the methyl groups and water molecules stretch, more trends are visible.

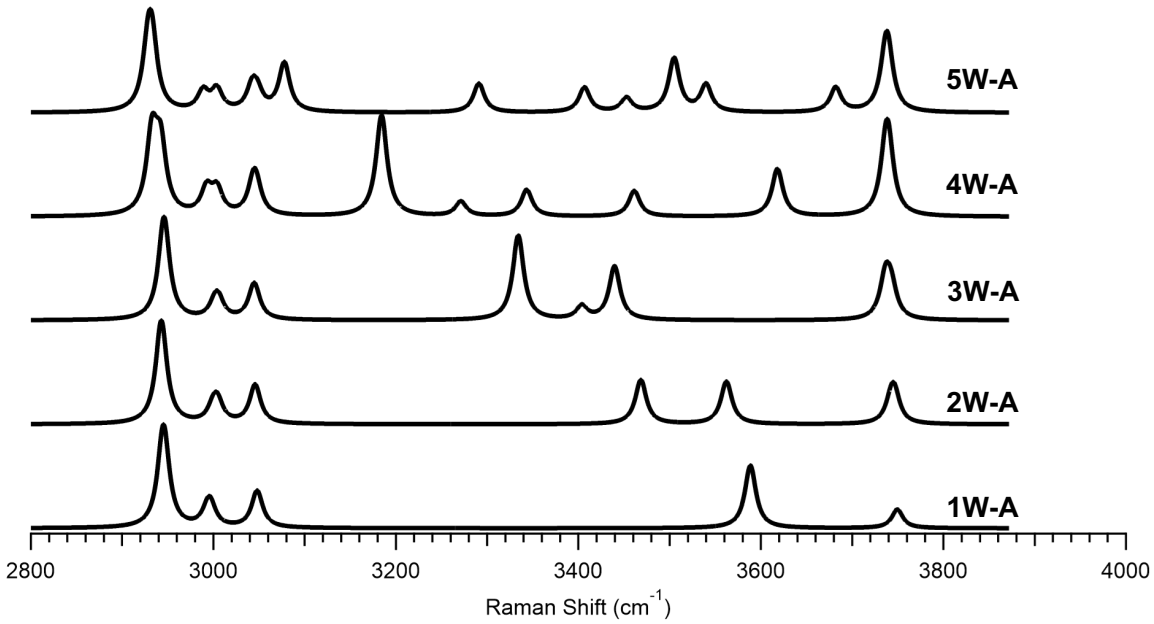

Figure 3.36: The Simulated Raman spectra for the lowest energy structures of B3LYP optimized 1/1 to 1/5 Diacetyl/Water complexes are shown for the range 2800 to 4000 cm^{-1}.

As can be seen in the figure above, the CH_3 umbrella motion that is centered at 2938 cm^{-1} in 1W-A shifts to lower energy as the number of water molecules increases in the complexes. The exact frequencies of this motion are detailed in the table that follows the B3LYP spectra.

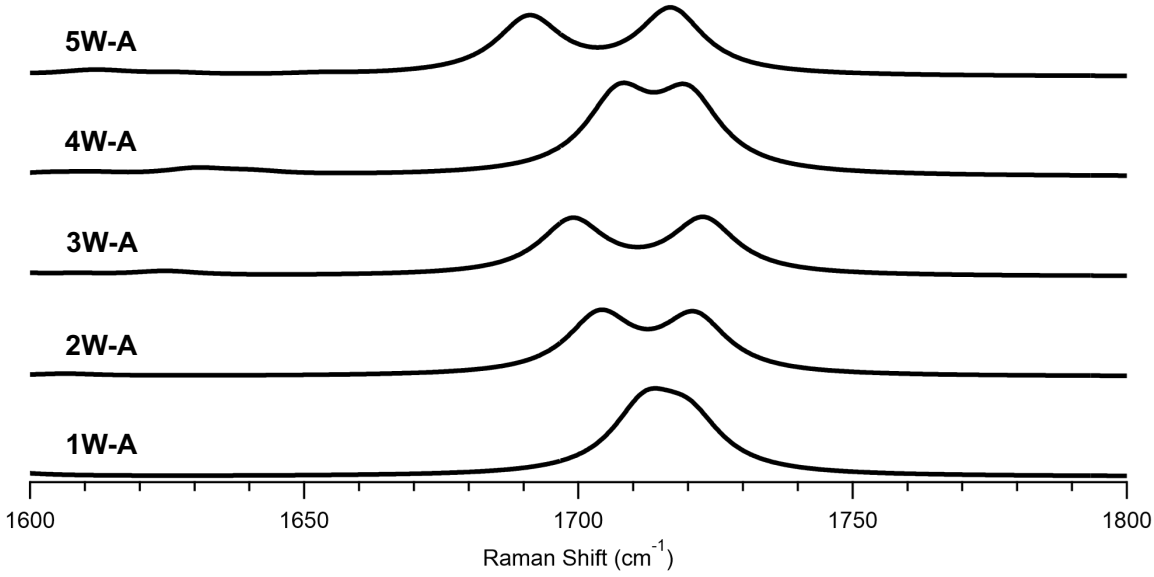

Figure 3.37: The Simulated Raman spectra for the lowest energy structures of B3LYP optimized 1/1 to 1/5 Diacetyl/Water complexes are shown for the range 1200 to 1800 cm^{-1}.

Apart from the 4W-A structure, the carbonyl stretching frequencies appear to have greater splitting and the centers of the vibrational motions appear to shift to lower wavenumbers. The difference in the symmetric and antisymmetric carbonyl stretching motions appears to increase with the greater number of water molecules because only one carbonyl group is hydrogen bonded to the water molecules in each of the structures. Therefore, the stabilization for one carbonyl motion continues to increase, while one carbonyl is largely unaffected. This separation in stabilization causes the increased splitting of the peaks. The vibrational modes associated with the carbonyl group and the rest of the diacetyl molecule are shown in the table below.

Vibrational Mode Description	Diacetyl	1W-A Freq. (cm^{-1})	2W-A Freq. (cm^{-1})	3W-A Freq. (cm^{-1})	4W-A Freq. (cm^{-1})	5W-A Freq. (cm^{-1})
Symmetric C=O Stretch	1721.33	1712.21	1703.91	1698.91	1707.38	1691.03
Asymmetric C=O Stretch	-------	1720.17	1721.18	1722.82	1719.98	1716.88
CH_3 umbrella	2945.21	2944.28	2942.24	2945.35	2932.67	2928.64
CH_3 umbrella	2945.25	2946.31	2943.46	2946.27	2942.27	2932.86
Asymmetric C-H Stretching	2995.69	2993.54	3000.02	3001.56	2992.60	2988.77
Asymmetric C-H Stretching	2995.95	2996.74	3004.66	3005.69	3003.97	3003.71
Asymmetric C-H Stretching	3046.57	3047.45	3045.67	3044.17	3043.98	3042.58
Asymmetric C-H Stretching	3047.20	3049.02	3046.29	3045.71	3047.27	3048.24

Table 3.19: The theoretical frequencies of vibrational modes in B3LYP lowest energy structures are shown.

For the MP2 structures, only 1W-A, 2W-A, and 3W-A could be compared. The first figure presented shows frequencies spanning 0 to 4000 cm^{-1}. The two figures that follow will zoom in on the methyl group and water molecule vibrations, as well as the carbonyl stretching motions predicted in the spectra. In the first figure, the stretching motions of the methyl group appear to be very similar in shape amongst the three complexes.

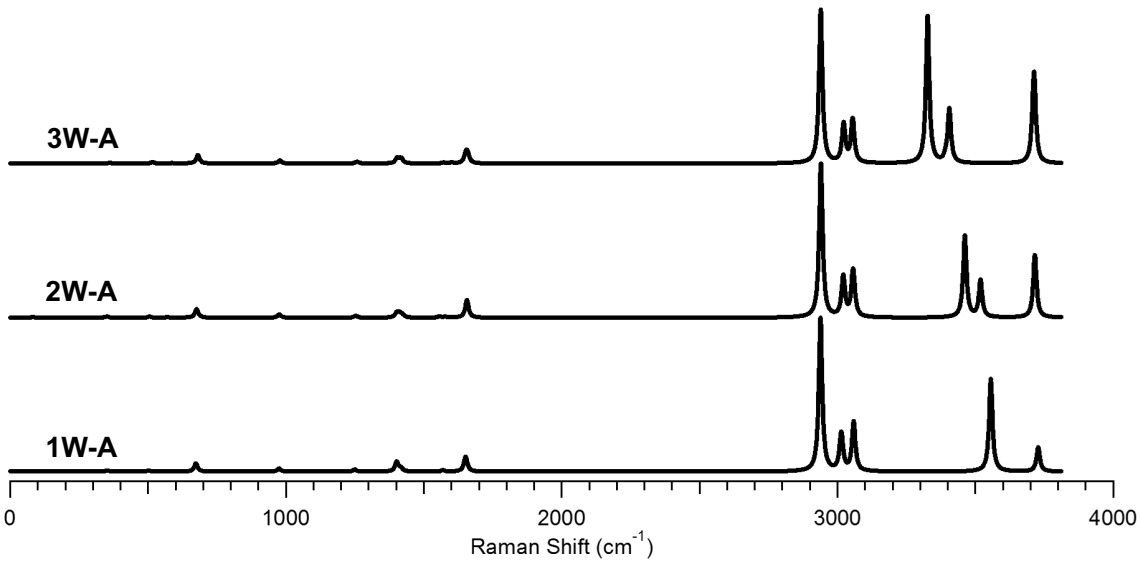

Figure 3.38: The Simulated Raman spectra for the lowest energy structures of MP2 optimized 1/1 to 1/3 Diacetyl/Water complexes are shown.

As can be seen in the figure below, the general shape of the C-H stretching motions remains the same, but the frequency values shift slightly. The first peak after 3000 cm-1 represents the first two asymmetric C-H stretching motions, and as the number of water molecules in the system increases, the frequencies of the two motions increases. The first asymmetric stretch increases from 3011.46 cm^{-1} for 1W-A to 3019.53 cm^{-1} for 2W-A, and finally to 3021.33 cm^{-1} for 3W-A. The second of these asymmetric stretching motions increases from 3015.18 cm^{-1} to 3022.23 cm^{-1} to 3023.12 cm^{-1}. Because the second stretch does not have as large of an increase in energy of the motions as the number of water molecules increases, the separation between these two small peaks increases in range from 1W-A to 2W-A to 3W-A.

Additionally, the spectra shown between 2800 and 4000 cm^{-1} show the red shifting of the symmetric HOH stretching motions as the number of water molecules increases in the complexes. For the 1W-A structure, the symmetric HOH stretching mode occurs at 3555.88 cm^{-1}. For 2W-A, symmetric HOH stretching occurs at 3461.77 cm^{-1}, and for 3W-

A, the symmetric stretching motion is at 3326.79 cm^{-1}. The coordination with additional water molecules appears to be decreasing the energy of symmetric HOH motion significantly.

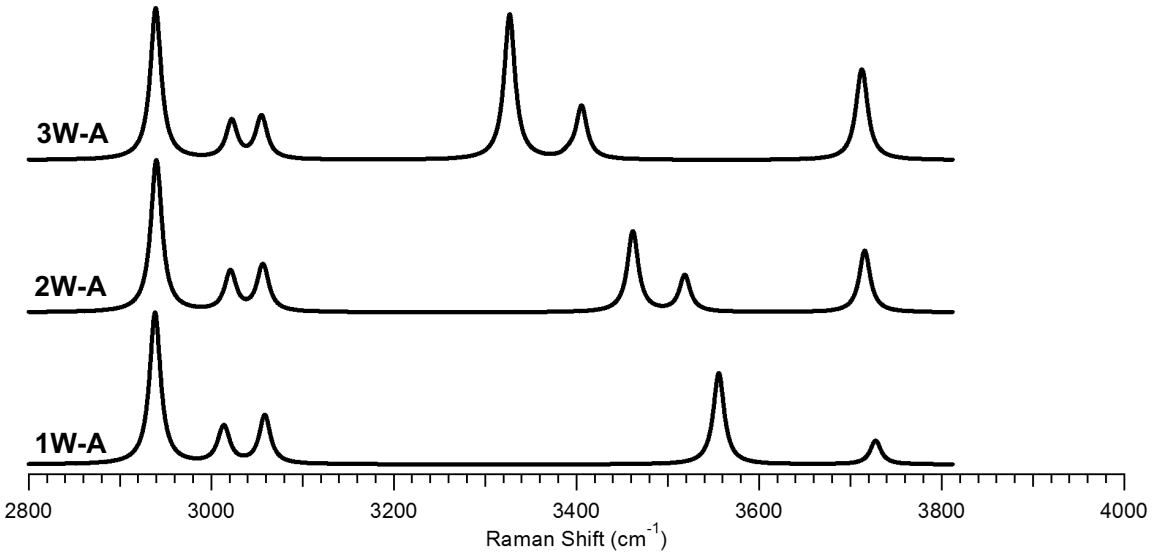

Figure 3.39: The Simulated Raman spectra for the lowest energy structures of MP2 optimized 1/1 to 1/3 Diacetyl/Water complexes are shown for the range 2800 to 4000 cm^{-1}.

When the spectra are focused on the carbonyl stretching frequencies, the trends shown in the B3LYP frequency calculations are not readily visible in the MP2 calculations. The lack of the red shifting trend and increasing separation in the carbonyl stretching peak could result from having only three structures to compare. For example, the broadness of the peak decreases between 1W-A and 2W-A, but it increases between 2W-A and 3W-A. The frequency of the vibrations increases between 1W-A and 2W-A, but decreases between 2W-A and 3W-A. Without comparison to the 4W-A and 5W-A structures, these spectra cannot be explained or analyzed with the scrutiny that was applied to the B3LYP frequency calculations, so further conclusions could be provided by finishing these calculations and experimental studies.

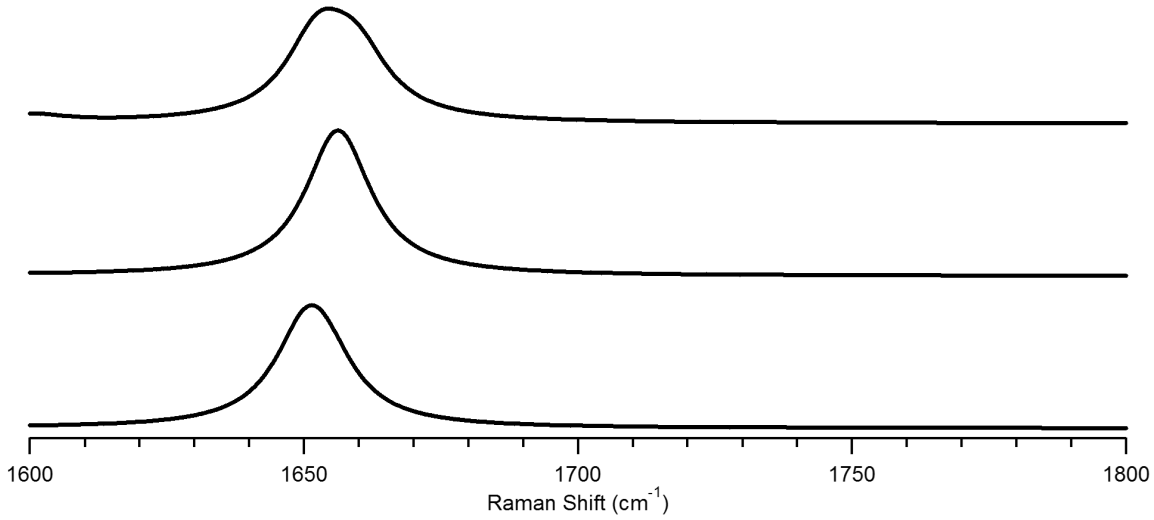

Figure 3.40: The Simulated Raman spectra for the lowest energy structures of MP2 optimized 1/1 to 1/3 Diacetyl/Water complexes are shown for the range 1200 to 1800 cm^{-1}.

The frequency values of the vibrational motions that can be compared to the diacetyl molecule alone are shown in the table below. As is predicted, the MP2 method has much lower calculated values for the C=O stretching motions compared to B3LYP. The determination of the better method of the two would be best understood through comparison to experiment.

Vibrational Mode Description	Diacetyl	1W-A Freq. (cm^{-1})	2W-A Freq. (cm^{-1})	3W-A Freq. (cm^{-1})
Symmetric C=O Stretch	1652.11	1650.42	1655.97	1652.57
Asymmetric C=O Stretch	-------	1653.84	1657.49	1659.60
CH_3 umbrella	2938.31	2937.88	2938.93	2939.18
CH_3 umbrella	-------	2939.07	2940.94	2939.32
Asymmetric C-H Stretching	3014.87	3011.46	3019.53	3021.33
Asymmetric C-H Stretching	-------	3015.18	3022.23	3023.12
Asymmetric C-H Stretching	3057.79	3058.02	3055.06	3053.54
Asymmetric C-H Stretching	-------	3059.79	3058.61	3056.39

Table 3.20: The theoretical frequencies of vibrational modes in MP2 lowest energy structures are shown.

CHAPTER 4: SUMMARY AND FUTURE WORK

4.1 SUMMARY

Through the optimizations of Diacetyl/Water complexes that ranged from one to five water molecules, the simulated Raman spectra and the diacetyl and water interactions could be explored. While neither the MP2 nor the single-point energy calculations for the higher order complexes could be finished in time to present this work, the completion and analysis of the 1/2 Diacetyl/Water complexes alone revealed information not discussed in the work done by Dargent, et. al. For example, a new structure, 2W-J, was optimized in this work that was not shown in previous articles, and the structure that Dargent, et. al. found and identified as "π_like_π_like_trans" could not be found using the B3LYP or MP2 methods[44]. This inability to optimize the structure despite repeated attempts was a result of the higher theory being used presently in this work. This higher theory is also beneficial in the instances that the results in this thesis agreed with results obtained by Dargent, et. al, as the higher theory would help to confirm the findings. Therefore, advancement in the field has been made despite shortcomings of the higher order calculations.

In addition to the spectroscopic trends that are described in the previous section, this research showed that multiple methods are needed for the detection and optimization of clusters that involve the noncovalent interactions at play. Neither the B3LYP method nor MP2 method could detect every possible structure on their own. Often, the two methods even disagreed on the energetics of the structures when they optimized very similar input geometries. As a result, this research showed the relevance of using multiple methods, and even ones beyond the "gold standard" of a rCCSD(T) single-point energy calculation to elicit the true lowest energy structure. The addition of experimental data to this research would likely show an advantage between either the ab initio methods, like MP2, or the

DFT methods, like B3LYP, in determining these lowest energy structures, but in the absence of this data, the procedure of using multiple methods proved beneficial.

4.2 FUTURE WORK

The most pertinent information that could be obtained in future work would be experimental data for diacetyl and water mixtures of varying concentrations. Additionally, the gas-phase Raman spectra would be especially useful, as the interest in these complexes was rooted in the use of diacetyl as a flavor additive in e-cigarettes. Due to time constraints and the restrictions of the COVID-19 pandemic, this experimental data could not be obtained, but the addition of this information would be simple to obtain with the vacuum pumped cell that is being constructed by Ashley Williams.

Additionally, future work could finish the calculations that could not be completed in time for this thesis. The maintenance that was done on Maple, the supercomputer provided by the Mississippi Center for Supercomputing Research (MCSR), delayed and terminated calculations that were meant to contribute to this work. Because the final calculations presented in this thesis are the most computationally expensive, this delay was detrimental to obtaining information about the 1/4 and 1/5 Diacetyl/Water complexes. However, the procedure for the calculations and presentation of the information that would be provided are well understood, so these calculations could be finished readily given more time. These calculations could then include the addition of multiple diacetyl molecules or more water molecules in the complexes to see whether dimerization or other intermolecular interactions are also present in the diacetyl and water mixtures.

Finally, as the interest in diacetyl stems from its use in flavoring in e-cigarettes, it would be useful to determine the interactions that diacetyl has with other gases, such as

oxygen, nitrogen, and carbon dioxide, that are prevalent in respiratory exchange. These interactions could help to determine the molecular interactions that occur when the organic molecule is inhaled. Additionally, the molecule could be investigated in conjunction with methanol and ethanol to see the combined effects of e-cigarette and alcohol use. These calculations could follow the procedure outlined in this thesis. The addition of experiment for each of these potential avenues would add to the information that could be gathered, as would experimental data in this thesis.

REFERENCES:

1. Hubbs, Ann F., et. al. *Toxicologic Pathology* **2008** *36* (2): 330-344. https://doi-org.umiss.idm.oclc.org/10.1177/0192623307312694
2. Harber, P. Diacetyl-induced lung disease. *Toxicological Reviews*. **2006** *25* (4):261-272. doi: 10.2165/00139709-200625040-00006
3. Wondrak, Georg T., et. al. *Biochemical Pharmacology* **2002** *63* (3): 361-373. https://doi-org.umiss.idm.oclc.org/10.1016/S0006-2952(01)00915-7
4. Luisa T. M. Profeta, Robert L. Sams, Timothy J. Johnson, and Stephen D. Williams *The Journal of Physical Chemistry A* **2011** 115 (35), 9886-9900 DOI: 10.1021/jp204532x
5. Dargent, D., Zins, E.L., Madebène, B. *et al.* Topological insights into the 1/1 diacetyl/water complex gained using a new methodological approach. *J Mol Model* 21, 214 (2015). https://doi.org/10.1007/s00894-015-2751-9
6. Miguel Rodríguez Mellado J. Correlations between chemical reactivity and mutagenic activity against S. typhimurium TA100 for α-dicarbonyl compounds as a proof of the mutagenic mechanism. *Mutation Research/Fundamental and Molecular Mechanisms of Mutagenesis*. **1994** *304* (2): 261-264. doi: 10.1016/0027-5107(94)90218-6.
7. Miller, A. G. Assessment of protein function following cross-linking by α-dicarbonyls. *Annals of the New York Academy of Sciences*. **2005** *1043* (1): 195-200. doi: 10.1196/annals.1333.024.
8. Kovacic P, Cooksy AL (2005) Role of diacetyl metabolite in alcohol toxicity and addiction via electron transfer and oxidative stress. *Arch Toxicol* 79:123–128 doi:10.1007/s00204-004-0602-z
9. Stoner GD, Shimkin MB, Kniazeff AJ, Weisburger JH, Weisburger EK, Gori GB (1973) Test for carcinogenicity of food additives and chemotherapeutic agents by the pulmonary tumor response in Strain A mice. *Cancer Res* 33:3069–3085.
10. Ikan R (ed) (1996) The Maillard reaction. Consequences for the chemical and life sciences. New York: Wiley, pp 132, 137
11. Kreiss, K. e. a. (2002). "Clinical Bronchiolitis Obliterans in Workers at a Microwave-Popcorn Plant." *The New England Journal of Medicine* **347**(5): 330-338.
12. Hubbs, Ann F., et. al. *Toxicology and Applied Pharmacology* **2002** *185* (2): 128-135. https://doi-org.umiss.idm.oclc.org/10.1006/taap.2002.9525
13. Kanwal, R. Evaluation of flavorings-related lung disease risk at six microwave popcorn plants. *Journal of Occupational and Environmental Medicine.* **2006** *48* (2):149-157. doi: 10.1097/01.jom.0000194152. 48728.fb.
14. Zaccone, E. J. e. a. (2015). "Diacetyl and 2,3-pentanedione exposure of human cultured airway epithelial cells: Ion transport effects and metabolism of butter flavoring agents." *Toxicology and Applied Pharmacology* **289**: 542-549.
15. Fedan, J. S. e. a. (2006). "Popcorn worker's lung: In vitro exposure to diacetyl, an ingredient in microwave popcorn butter flavoring, increases reactivity to methacholine." *Toxicology and Applied Pharmacology* **215**: 17-22.
16. Allen, J. G. e. a. (2016). "Flavoring Chemicals in E-Cigarettes: Diacetyl, 2,3-Pentanedione, and Acetoin in a Sample of 51 Products, Including Fruit-, Candy-,

and Cocktail-Flavored E-Cigarettes." *Environmental Health Perspectives* **124**(6): 733-739.
17. Grace Kong, PhD, Meghan E. Morean, PhD, Dana A. Cavallo, PhD, Deepa R. Camenga, MD, Suchitra Krishnan-Sarin, PhD, Reasons for Electronic Cigarette Experimentation and Discontinuation Among Adolescents and Young Adults, *Nicotine & Tobacco Research*, Volume 17, Issue 7, July 2015, Pages 847–854, https://doi-org.umiss.idm.oclc.org/10.1093/ntr/ntu257
18. Wang TW, Neff LJ, Park-Lee E, Ren C, Cullen KA, King BA. E-cigarette Use Among Middle and High School Students — United States, 2020. MMWR Morb Mortal Wkly Rep 2020; 69: 1310–1312. DOI: http://dx.doi.org/10.15585/mmwr.mm6937e1
19. Engel, Thomas, Philip Reid, and Warren Hehre. *Physical Chemistry*. 3rd ed. Boston: Pearson, 2013. Print.
20. Klein, David R. *Organic Chemistry*. 3rd ed. Hoboken, NJ: Wiley, 2017.
21. Sienerth, Karl D., Granger, Jill N., Granger, Robert M. *Instrumental Analysis: Revised Edition*. United Kingdom: Oxford University Press, 2017.
22. Meissler, Gary L., Paul J. Fischer, and Donald A. Tarr. *Inorganic Chemistry*. 5th ed. Boston: Pearson, 2014. Print.
23. Raman, C., Krishnan, K. A New Type of Secondary Radiation. *Nature* 121, 501–502 (1928). https://doi.org/10.1038/121501c0
24. Bumbrah, G. S. and Sharma, R. M. "Raman spectroscopy- Basic principle, instrumentation and selected applications for the characterization of drugs of abuse." *Egyptian Journal of Forensic Sciences* **2016** *6* (3): 209-215. https://doi.org/10.1016/j.ejfs.2015.06.001
25. Clifford Dykstra, Gernot Frenking, Kwang Kim, and Gustavo Scuseria. *Theory and Applications of Computational Chemistry: The First Forty Years*. Amsterdam: Elsevier Science, 2005.
26. E. Schrödinger, *Ann. Phys. (Leipzig)*, **1926**, *79*, 361, 489, 734; **1926**, *80*, 437; **1926** *81*, 109; *Naturwissenshaften*, **1926**, *14*, 664; *Phys. Rev.*, **1926**. *28*, 1049.
27. Baseden, Kyle A. and Jesse W. Tye. "Introduction to Density Functional Theory: Calculations by Hand on the Helium Atom." *Journal of Chemical Education* 91 (2014): 2116-2123.
28. Feiguin, Adrian E. "The Hartree-Fock Method." *Phys 5870: Modern Computational Methods in Solids*, Northeastern University, 2009.
29. Hohenberg, P.; Walter, K. Inhomogeneous electron gas *Phys. Rev.* **1964**, 136, B864–B871
30. Cohen, Aron J., Paula Mori-Sánchez, and Weitao Yang. *Science* **2008** *321*(5890), 792-794. DOI: 10.1126/science.1158722
31. Aron J. Cohen, Paula Mori-Sánchez, and Weitao Yang. *Chemical Reviews* **2012** *112* (1), 289-320. DOI: 10.1021/cr200107z
32. Julian Tirado-Rives and William L. Jorgensen. *Journal of Chemical Theory and Computation* **2008** *4* (2), 297-306. DOI: 10.1021/ct700248k
33. Yuemin Liu, Yucheng Liu, August A. Gallo, Kathleen D. Knierim, Eric R. Taylor, Nianfeng Tzeng. *Journal of Molecular Structure* **2015**, 223-228. https://doi.org/10.1016/j.molstruc.2014.12.028.

34. Katherine L. Munroe, David H. Magers, and Nathan I. Hammer. *The Journal of Physical Chemistry B* **2011** *115* (23), 7699-7707 DOI: 10.1021/jp203840w
35. "Precomputed Vibrational Scaling Factors." *Computational Chemistry Comparison and Benchmark DataBase*, National Institute of Standards and Technology, 2013, cccbdb.nist.gov/vibscalejust.asp.
36. M. Darvish Ganji, S. M. Hosseini-khan, and Z. Amini-tabarc. *Phys. Chem. Chem. Phys.*, 2015, **17**, 2504-2511
37. S. Grimme , J. Antony , S. Ehrlich and H. Krieg , *J. Chem. Phys.*, 2010, **132** , 154104
38. Ying Wang, et. al. *Proceedings of the National Academy of Sciences of the United States of America*, **2018** *115* (41): 10257-10262.
39. Yan Zhao and Donald G. Truhlar A*cc. Chem. Res.* **2008**, 41, 2, 157–167
40. Luke W. Bertels, Joonho Lee, and Martin Head-Gordon. *The Journal of Physical Chemistry Letters* **2019** *10* (15), 4170-4176 DOI: 10.1021/acs.jpclett.9b01641
41. Jan Gerit Brandenburg, et. al. *J. Chem. Phys.* **148**, 064104 (2018); https://doi.org/10.1063/1.5012601
42. Jeng-Da Chai and Martin Head-Gordon. *Phys. Chem. Chem. Phys.*, 2008, **10**, 6615-6620
43. Andrew Mahler, John J. Determan, and Angela K. Wilson. *J. Chem. Phys.* **151**, 064110 (2019)
44. Dargent, D., Zins, E.L., Madebène, B. *et al.* Energy, structure and topological characterization of the isomers of the 1/2 diacetyl/water complex. *Theoretical Chemistry Accounts* 135, 2 (2016). https://doi.org/10.1007/s00894-015-2751-9
45. Dimitrios G. Liakos and Frank Neese. *J. Chem. Theory Comput.* 2015, 11, 9, 4054–4063
46. Péter R. Nagy and Mihály Kállay. *J. Chem. Theory Comput.* 2019, 15, 10, 5275–5298
47. Jørgensen, P., and Simons, J. *Second Quantization-Based Methods in Quantum Chemistry*. New York: Academic Press, 1981.
48. Luisa T. M. Profeta, Robert L. Sams, Timothy J. Johnson, and Stephen D. Williams. *The Journal of Physical Chemistry A* **2011** *115* (35), 9886-9900 DOI: 10.1021/jp204532x
49. J. R. Durig, S. E. Hannum, and S. C. Brown. *The Journal of Physical Chemistry* **1975** *75* (13), 1946-1956. DOI: 10.1021/j100682a008
50. D. Herschlag and M. M. Pinney. Hydrogen Bonds: Simple after All? *Biochemistry* **2018** *57* (24), 3338-3352. DOI: 10.1021/acs.biochem.8b00217
51. G. A. Verville, H. K. Byrd, A. Kamischke, S. A. Smith, D. H. Magers, N. I. Hammer, "Raman Spectroscopic and Quantum Chemical Investigation of the Effects of Tri-methylamine N-oxide (TMAO) on Hydrated Guanidinium and Hydrogen-Bonded Water Networks," *Journal of Raman Spectroscopy* (2021). DOI: 10.1002/jrs.6061